Valorization of lignin as an active material for electrochemical energy storage

Auteur : Natalis, Vincent
Promoteur(s) : Richel, Aurore; Vertruyen, Benedicte
Faculté : Faculté des Sciences
Diplôme : Master en sciences chimiques, à finalité approfondie
Année académique : 2017-2018
URI/URL : http://hdl.handle.net/2268.2/8506
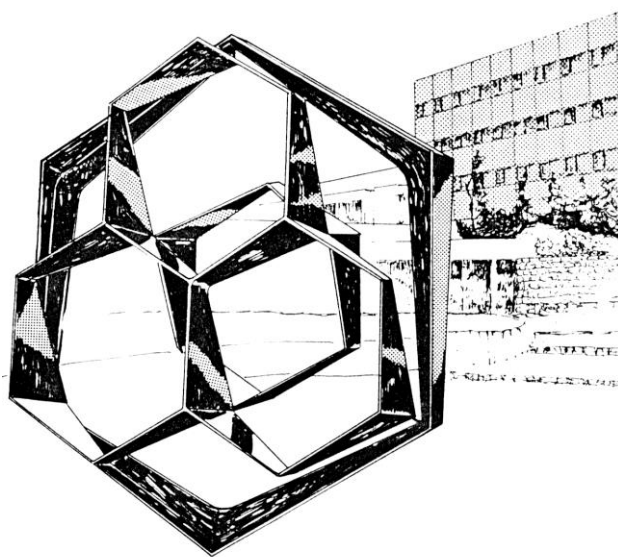
FACULTE DES SCIENCES
Département de Chimie

Biomasse et Technologies Vertes (GABTx-Uliège) – Pr. Richel
GreenMat (ULiège) – Pr. Vertruyen

Valorization of lignin as an active material for electrochemical energy storage

Année académique 2017-2018

Dissertation présentée par
Vincent Natalis
en vue de l'obtention du diplôme de
Master en Sciences Chimiques

Acknowledgments

First and foremost, I would like to warmly thank my two promoters, Ms. Richel and Vertuyen, who provided a helpful guidance throughout the whole master thesis. Their work was essential, precise, concise and kind, and their help available at all times. Thank you !

A big thanks goes to the team of the laboratory of Biomass and Green Technologies, with whom I spent these 5 months: Alex, Isabelle (for her kind remarks!), Sophie, Maroua, Quentin, Christel, Romolo and Lionel.

An immense thank you to the big heads that helped me think and overthink, write and rewrite every little piece of data: Thibaut & Thibaut, Lauris, and, of course, the future Pope of Lignin, whose time I stole way too much - Thomas !

A huge thanks to Thibaut L., Mathilde and Antoine for their help in laboratory experiments.

A special thanks to Elias for the nice pictures he helped me with.

A double thanks to Caroline and Anthony, who helped me for all Greenmat-related experiments.

I also thank the people who helped me proof-read this piece: Johana, Françoise, Louis the nightly owl, my parents and André. This work is also theirs.

Abstract

Lignin is one of the three major architectural biopolymers of lignocellulosic biomass, and the largest available feedstock of natural aromatic polymer on Earth. Its valorization in second-generation biorefineries remains a challenge. Among possible uses, lignin can be carbonized to create porous carbons, which are useful as supercapacitors, a kind of capacitor that also displays battery-like properties. Recent studies show lignin could also be exploited as a bio-sourced, redox-active material in batteries thanks to its numerous quinone-like moieties. Still, we lack fundamental pieces of knowledge about lignin, such as the impact of pretreatment type on lignin structure, molecular weight fractionation, organic solvent solubility or electrochemical properties. Moreover, to the best of our knowledge, no research has been conducted on the use of soda-extracted lignin in batteries.

In this master thesis, illustrated in **fig. 1**, we fractionated soda-extracted lignin samples from three sources (softwood, hardwood, herbaceous), characterized them by Fourier transform infrared (FTIR) spectroscopy, high pressure size exclusion chromatography (HPSEC), nuclear
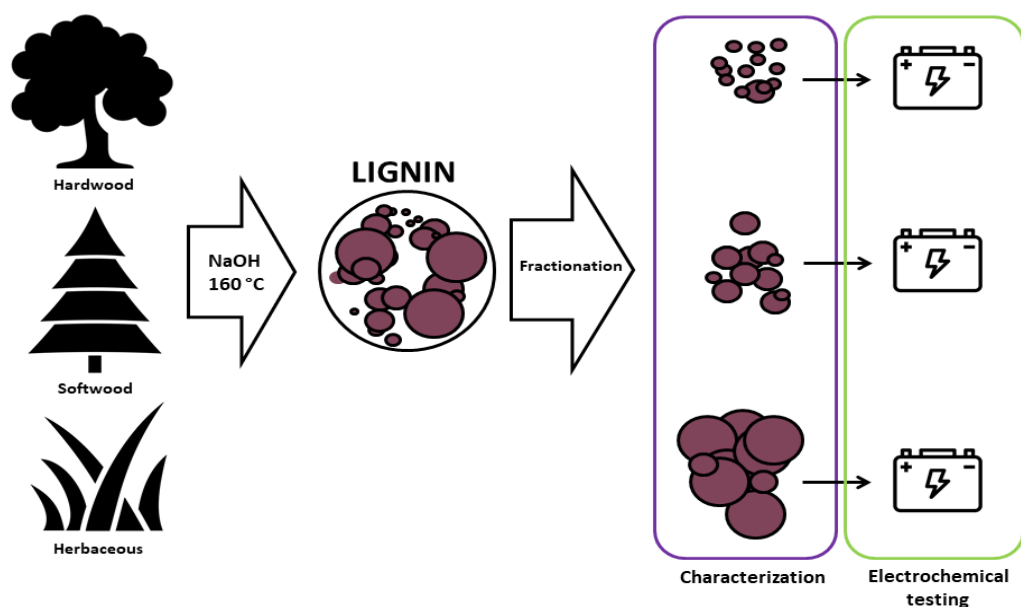
Figure 1 Visual scheme of the whole master thesis. Brown dots: Lignin molecules. Source for symbols: [72]–[74]

magnetic resonance (NMR) and scanning electron microscopy (SEM). We linked their characteristics to their electrochemical capacity performances, measured by cyclic voltammetry (CV). Our results showed that organic solvent fractionation and pH-driven fractionation created a range of molecular weight-separated fractions of smaller polydispersity. All fractions had unique relative abundances of oxygenated functionalities. Soda-extracted lignin exhibited a ~16 mAh/g capacity. This showed that soda-extracted samples are as capacitive as Kraft-extracted samples reported in literature. Furthermore, our softwood samples displayed capacities 4 and 8 times higher than herbaceous and hardwood lignins, respectively.

La lignine est un des trois principaux biopolymères structurants de la biomasse lignocellulosique. C'est le plus grand réservoir naturel de polymères aromatiques sur Terre. Dans les bioraffineries de seconde génération, sa valorisation reste un challenge. Une des applications de la lignine est sa carbonisation en noir de carbone poreux, utilisé comme supercondasteur, un type de condensateur qui présente aussi des propriétés de batterie. Des études récentes montrent que la lignine pourrait aussi être utilisée comme matériau oxydoréducteur dans les batteries, du fait de sa haute teneur en fonctions quinone. Pourtant, nous manquons toujours de données fondamentales sur la lignine, comme, notamment, l'impact du type de prétraitement sur sa structure, son fractionnement par masse molaire, sa solubilité dans les solvants organiques et ses propriétés électrochimiques. De plus, d'après nos recherches bibliographiques, il n'existe aucune étude sur l'utilisation de la lignine extraite à la soude dans des batteries.

*Dans ce mémoire, illustré en **fig. 1**, nous avons fractionné des échantillons de lignine provenant de trois sources (résineux, feuillu, herbacée) selon leur masse molaire, les avons caractérisés par FTIR, HP-SEC, RMN et SEM, puis avons mis en lien ces caractéristiques avec leurs performances électrochimiques, mesurées par CV. Nos résultats montrent que le fractionnement par solvant organique et le fractionnement par pH ont créé une série de fractions de faible polydispersisté, séparées selon leur masse molaire. Toutes les fractions avaient des abondances relatives uniques de fonctionnalités oxygénées. La lignine extraite à la soude avait une capacitance de 16 mAh/g, ce qui met en évidence le fait que les échantillons extraits à la soude sont aussi capacitifs que les lignines issues du procédé Kraft décrites dans la littérature. De plus, nos échantillons de résineux avaient des capacitances 4 et 8 fois plus élevées que, respectivement, ceux d'herbacée et de feuillu.*

Table of Contents

Table of figures

Table of tables

1. Introduction

Electrochemical storage demand is rapidly growing, encouraged, among many applications, by the recent development of electric cars, portable electronic devices and housing solar panels. This growth seems incompatible with the growing desire for a more sustainable, environment-friendly society [1]. This society paradigm advocates, for example, for the reduction of pollution associated with the mining of precious metals. One of these metals is lithium, which is used in lithium-ion batteries, the most common type of electronic devices batteries [2]. Sustainable electrical energy storage is thus a highly desirable issue. Could biobased molecules efficiently store large amounts of electrical energy?

Lignin (**fig. 2**) is the second most abundant natural biopolymer on Earth, and the most abundant aromatic polymer. Its production is plentiful and undervalued, since it is mostly burnt in the paper production process [3]. The complex structure and the production of lignin are explored in section 2.1. In section 2.2, we describe two important points of battery development: the combination of battery and capacitors in hybrid materials, called supercapacitors, and the use of biomolecules in the fabrication of aforesaid supercapacitors. In section 2.3, we unfold the fact that (a) lignin is already used to manufacture porous carbon, a type of supercapacitor and that (b) the quinone-like moieties of pristine lignin are redox-active and can reversibly store electrons, making it a suitable candidate for electrochemical storage.
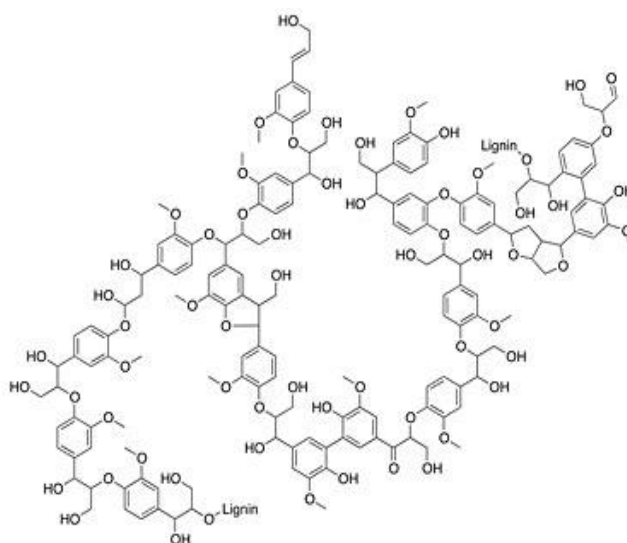
Figure 2 Schematic representation of a molecule of lignin. The figure highlights the diverse number of linkages and the reticulation of the biopolymer [75].

2. State of the art

2.1. What is lignin?

All terrestrial vascular plants, except algae and mosses, contain lignin. This kind of biomass is called lignocellulosic biomass. It is composed of three architectural biopolymers: cellulose, hemicellulose and lignin. **Fig. 3** depicts the spatial arrangement of the three polymers in the secondary wall of cell plants [4].

Cellulose is the major polymeric component of all plants. Its presence ranges from woody plants, with 45% of cellulose in mass, to cotton, which contains up to 95% of cellulose in mass. The polymer is made of D-glucose units linked by β-1,4 bonds. Its structure is generally crystalline because of the many intra- and interfibrillar hydrogen bonds (though some amorphous cellulosic fibers can be encountered). This causes cellulose to be almost completely insoluble in organic solvents. The degree of polymerization of cellulose can greatly vary, ranging from a dozen of units to several thousands.
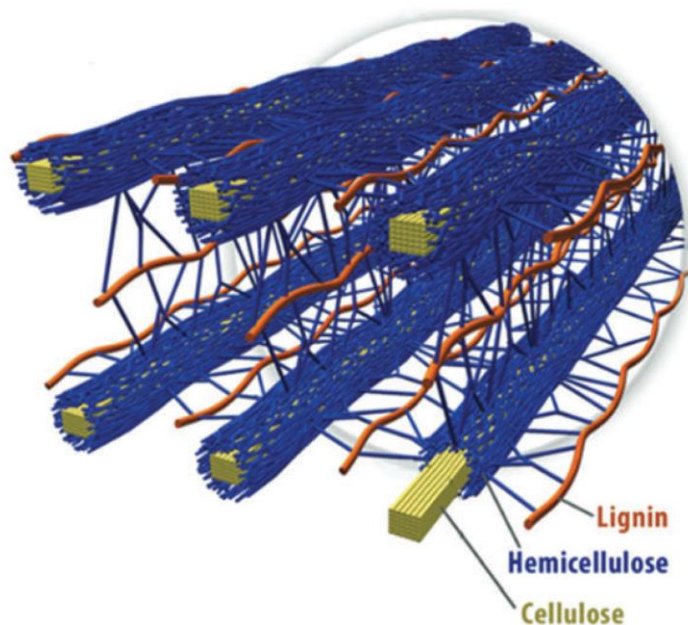
Figure 3 The 3D structure of lignocellulosic biomass [4].

Hemicellulose is a heteropolymer. The main monomeric unit is glucose, but other monomers include xylose, mannose, galactose, rhamnose and arabinose. They are linked by β-1,4 bonds. The complexity of monomeric units and structural linkages requires many enzymes and/or many selective chemical reagents to fully degrade the molecule [5].

Lignin is a crosslinked heteropolymer. It is composed of phenylpropane units linked by ether bonds. These bonds are, for the most, β-aryl ether (β-O-4) bonds, but several other are possible (**tab. 1**). Lignin has a different structure in herbaceous plants, in hardwood and in softwood. There are three monomeric units that radically polymerize into lignin: *p*-hydroxyphenyl alcohol (also called "H" unit), guaicyl alcohol (G) and syringyl alcohol (S) (**fig. 4**). They bind together in multiple ways and produce complex bonds. These first paragraphs are translated and adapted from one of our previous works [6].

Table 1 Distribution percentage of possible linkages in softwood lignin [5].

Linkages	Dimer structure	Distribution percentage [%]
β-O-4	Phenylpropane β-aryl ether	45–50
5-5	Biphenyl and dibenzodioxocin	18–25
β-5	Phenylcoumaran	9–12
α-O-4	Phenylpropane α-aryl ether	6–8
β-1	1,2-Diaryl propane	7–10
4-O-5	Diaryl ether	4–8
β-β	β-β linked structures	0–3

The three biopolymers are embedded to together toform a tight matrix. Lignin acts as glue between cellulose-hemicellulose fibrils (**fig. 3**) and represents 15 to 40% of total plant mass. The role of lignin is to make the structure water-insoluble and mechanically resistant. Its complex structure also acts as a natural barrier against biological and chemical attacks. Lignin is not a well-defined molecule; it is a broad label used to describe a structurally variable polymer. Each extracted lignin differs in relative H:G:S ratio (**tab. 2**), in structure, in bonding patterns (**tab. 1**), in remaining inorganic salts content… Moreover, on the cellular level, environmental and developmental factors induce different structure production between different parts of a plant [7]. Lignin production in plants can vary in quantity up to a few percent between years, depending on seasonal conditions. This variability makes it difficult for industries to rely on lignin for high-value applications: the production is too variable [8], though some solutions can be found (**see section 2.3**).
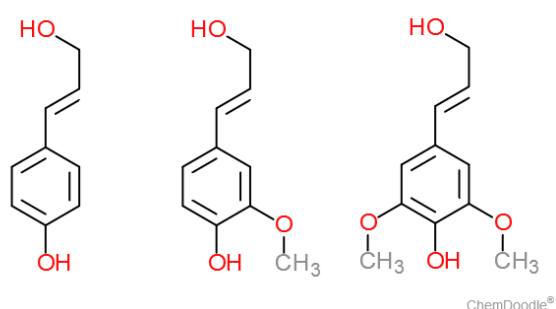
Figure 5 The three monomeric alcohols that polymerize into lignin. From left to right: *p*-hydroxyphenyl (abbreviated H) , coniferyl G and synapil S. Molecules drawn with ChemDoodle ©.
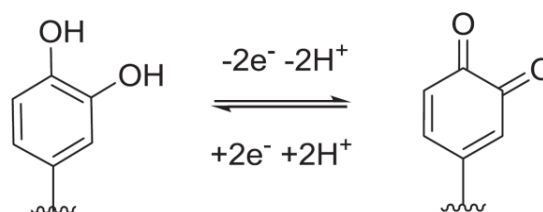
Figure 4 The reversible electrochemical reaction between hydroxyquinone (on the left) and quinone (on the right) [9].

However, extractions processes such as highly acidic or alkaline pretreatments (see section **2.1.2.2**) can make up for this disparity. Or, as we will see in **section 2.3**, some chemical transformations can turn lignin into a more valuable product and hence get rid of its inherent structural discrepancy. The electrochemically active moieties of lignin are its hydroquinone-like functions [9], [10].As can be seen in **fig. 4**, an end-chain quinone can reversibly accept two electrons, turning itself into a hydroxyquinone and vice versa, which is the reason why lignin can be used as a charge storage molecule. The H monomer (**fig. 5**) only has one phenolic hydroxyl on its aromatic ring, thus it cannot undergo the redox reaction.

Conversely, the redox reaction can be achieved in G and S monomers, which bear 1 and 2 methoxy moieties on their aromatic ring, respectively. In lignin cyclic voltammetry measurements, the S group has a potential of 0.35V and the G group has a potential of 0.55V [9] and thus electrochemical properties depend on G and S quantities of the extracted lignin. In reference papers [9], [11], [12], the 0.55V guaiacyl group contribution to charge storage is higher than the S one, and thus, one can hypothesize that the higher the G relative proportion, the better. According to H:G:S quantifications (**tab. 2**) [13], softwood provides the highest G content and consequently, one could can legitimately assume softwoods should exhibit the highest charge storage performance.

Table 2 Schematic representation of H, G, S monomeric units contents. In grey, softwood lignin seems to be the best candidate for electrochemical applications, since it has the highest G content (G being the most redox active monomer). Tick: significant presence. Low: low presence. O: no significant presence [13].

	Softwood	Hardwood	Herbaceous
H	Low	O	✓
S	O	✓	✓
G	✓	✓	✓

2.1.1. Lignin is produced in paper mills and biorefineries

Around the world, every year, carbon gets trapped in biomass and the quantity of biomass increases. Estimations of the natural worldwide production of lignin in biomass range from 0.5 to 3.6 BT (billion tons) annually. Projections show the US could reach 1.2 BT of commercial biomass production by 2060, and that the European Union could produce up commercial biomass to 300 MT by 2030 [14].

Lignin valorization is impacted by lignin production. The main source of lignin in the world is the paper industry, which separates cellulose and lignin, then uses cellulose to craft paper.

17

Lignin is undesirable because it is responsible for the yellowing of paper [15]. The lignin is often burnt on site to produce heat and to retrieve the chemicals used to separate the biopolymers (NaOH, sulfites, etc.). Lignin can also come out of biorefineries, which are aimed at valorizing agricultural and forest waste (chopped wood, leftover crops, …) by producing chemicals out of the left-alone lignocellulosic biomass of these two industries [16].

2.1.1.1. The paper industry produces 50 MT/y of underutilized lignin via two main processes

The industries that use the greatest amounts of wood every year are the wood industry and the paper industry. The latter is the only one which tries to separate the three components of wood. The paper industries produce 50 million tons of lignin every year, less than 2% of which are commercialized – the other 98% are burnt on-site or pressed into pellets designed to be burnt [17], [18]. Among the four main lignin extraction processes, 1100 kT of commercial lignin are produced each year. The 2 most common extraction processes are the Kraft and the Sulfite processes [16].

The Sulfite process produces 1000 kT of lignin every year. In the sulfite process, cellulose and lignin are separated by sulfite (SO_3^{2-}) or bisulfite (HSO_3^-) anions, which depolymerize lignin ether bonds. The resulting lignosulfonates are very different from native lignin: they contain a lot of sulfonate functionalities, which make them highly soluble in water. Carbohydrates (i.e. cellulose and hemicelluloses) are not totally removed, which means lignosulfonates need further purification before being put to use [19]. The Kraft process produces 87 kT of lignin every year. The lignocellulosic biomass is heated to temperatures above 150°C together with Na_2S and NaOH, producing *in situ* hydrogenosulfide anions (HS^-), which depolymerize lignin by breaking its ether bonds. The resulting lignin is recovered in an aqueous solution called black liquor. The so-called "Kraft lignin" is soluble in alkaline media, contains considerable quantities of sulfur-bearing moieties and has a smaller molar mass [18], [19]. The two next processes, in terms of lignin production quantities, are the **alkaline** (5-10 kT per year) and the **organosolv** (3 kT per year) [18]. They are described in the following section.

2.1.1.2 Biorefineries employ a wide variety of pretreatments to maximize lignocellulosic biomass valorization

Pretreatments are physical, physico-chemical, chemical or biological processes applied to lignocellulosic biomass to separate biomass into cellulose, hemicelluloses and lignin (**fig. 6**). Biorefineries are usually aiming at cellulose fermentation, and thus at maximizing cellulose accessibility to cellulase (i.e. the enzyme that depolymerizes cellulose into glucose), with only little consideration for a valorizing and reliable lignin production. Still, the recent trend of high-value molecules production from lignin has shown the need for robust and diverse separation techniques of the three biopolymers. In our case, we need a sound, selective lignin separation. Among the numerous and creative methods that exist to separate the three biopolymers, the following are all the ones that are specifically aimed at removing and isolating lignin from lignocellulosic biomass. This list is thus non-exhaustive, since some other methods are more performing at increasing cellulose accessibility rather than lignin separation. It shows the vast array of possible methods to get lignin out of plants, and gives background information on the method we chose for this master thesis. For an extensive review, we suggest the work of Kumar and Sharma [13].
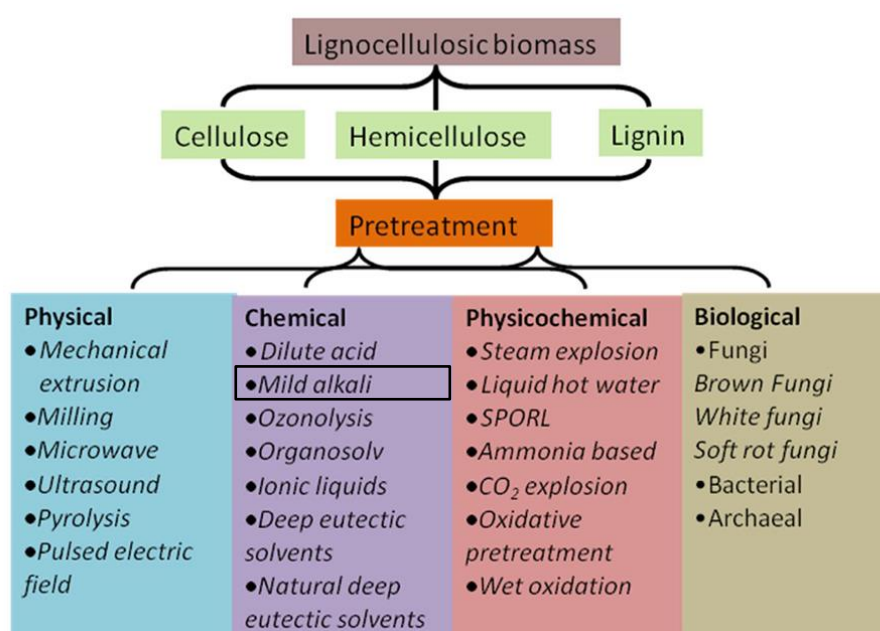
Figure 6 Overview of all available biorefinery pretreatments to separate lignin, hemicelluloses and cellulose. SPORL: Sulfite Pretreatment to Overcome Recalcitrance of Lignocellulose [18].

Oxidation

Wet oxidation

Wet oxidation consists in bringing together lignocellulosic biomass, water and oxygen in a pressured (>120 psi) vessel, and heating the mixture at >120°C. A liquid and a solid fraction are retrieved: the liquid fraction contains lignin and broken down hemicelluloses, while the solid fraction contains a higher percentage of cellulose [20]. This process can be improved by alkaline or acid treatment[21].

H_2O_2

H_2O_2 is commonly used in association with an alkaline reagent, to oxidize the three polymers. Lignin is the most reactive of the three; it is thus selectively affected and can dissolve up to 50%. Conditions and costs are comparable to other methods [22].

Ozonolysis

Ozone induces degradation of lignin in mild conditions, and has a specific affinity for aromatic rings. It depolymerizes lignin by breaking aromatic rings into carboxylic acids. The structure of lignin is hugely altered. However, ozone is an expensive molecule, both energetically and financially, and its use remains marginal [23].

Acidic pretreatment

Application of strong or dilute acids (H_2SO_4, HCl, HNO_3, H_3PO_4) induces lignin degradation and solubilization, as well as hemicellulose partial or total destruction. Temperatures up to 100-200 °C can be used. Long and precise optimizations often have to be sought [24].

Organosolv

In general, an organosolv pretreatment involves a mixture of water, organic solvent and mineral acid – typically H_2SO_4. A variety of organosolv processes exist: water/ethanol, water/formic acid, water/methanol/NaOH, water/acetic acid, water/butanol, water/acetone, to name but a few. Organosolv processes generate very pure lignin, with less than 1% in weight of carbohydrates. It is gaining increasing attention in the biorefinery field of research. As alcohols, organic acids and ketones can be derived from biomass, the solvent need of the refinery could be met by its own production, forming a more environmentally responsible closed loop [25].

Ammoniac recycle percolation (ARP)

In this process, lignocellulosic biomass is subjected to aqueous ammonia (10-15%) at temperatures between 150 and 170°C. Ammonia breaks down carbohydrates-lignin bonds and intramolecular lignin bond. Lignin is thus in the liquid phase, which contains the ammoniac. The liquid phase is then evaporated to be recycled. Lignin is isolated by washing. It is partially depolymerized [26].

Room temperature ionic liquids and deep eutectic solvents

Ionic liquids are a relatively new class of solvents, made out of cations and anions only (typically imidazolium salts), with low melting points and low vapor pressure. Some authors report quasi-total dissolution of lignocellulosic biomass in ionic liquids, allowing a selective precipitation of lignin and hemicelluloses with the right anti-solvent. High-purity high-molecular weight lignins are obtained: no co-precipitated inorganic salts, no sulfur in the lignin, and no acids or bases are needed to carry out the process. Still, ionic liquids are expensive and need very precise optimization parameters, which are sometimes difficult to replicate from literature [18].

Alkaline

There are three commonly used alkaline reagents to carry out this pretreatment: dilute NaOH (most common, most efficient), KOH and $Ca(OH)_2$ (less efficient but cheaper). They depolymerize hemicelluloses and lignin and increase cellulose accessibility. The method is simple and can be used at temperatures between 100°C and 200°C. Some lignin ether and ester bonds are cleaved and lignin is solubilized in the process. It is then recovered by acidification of the liquid phase [24], [27], [28]. This implies that the produced lignin is sulfur-free since no sulfur is used, compared to Kraft lignin or lignosulfonates, which do contain sulfur. Still, the alkaline-treated lignin needs further purification of the inorganic salts introduced by neutralization of the base by the acid.

We chose this pretreatment for this master thesis for the simplicity of the reaction, the availability of the alkaline-resistant reactor in the laboratory, low cost of the reagents and the possibility of getting "pure" lignin (sulfur-free and salt-free after purification).

2.1.2. Lignin can be valorized in both low value and high value applications

Lignin is, as for now, mainly used as a fuel in the paper industry and in biorefineries. It is a low-grade fuel (21.13 MJ/kg) compared to gasoline (47.3 MJ/kg) or ethanol (29.7 MJ/kg) because of its high oxygen content and over functionalization [29][30]. It has the upside of being produced in the process and thus of being available on site. However, projections show that the development of biorefineries that process agricultural and forestry wastes will generate 60% more lignin than needed for energy production. Moreover, lignin has numerous higher value applications (**fig. 7**). A non-exhaustive list is proposed herein.
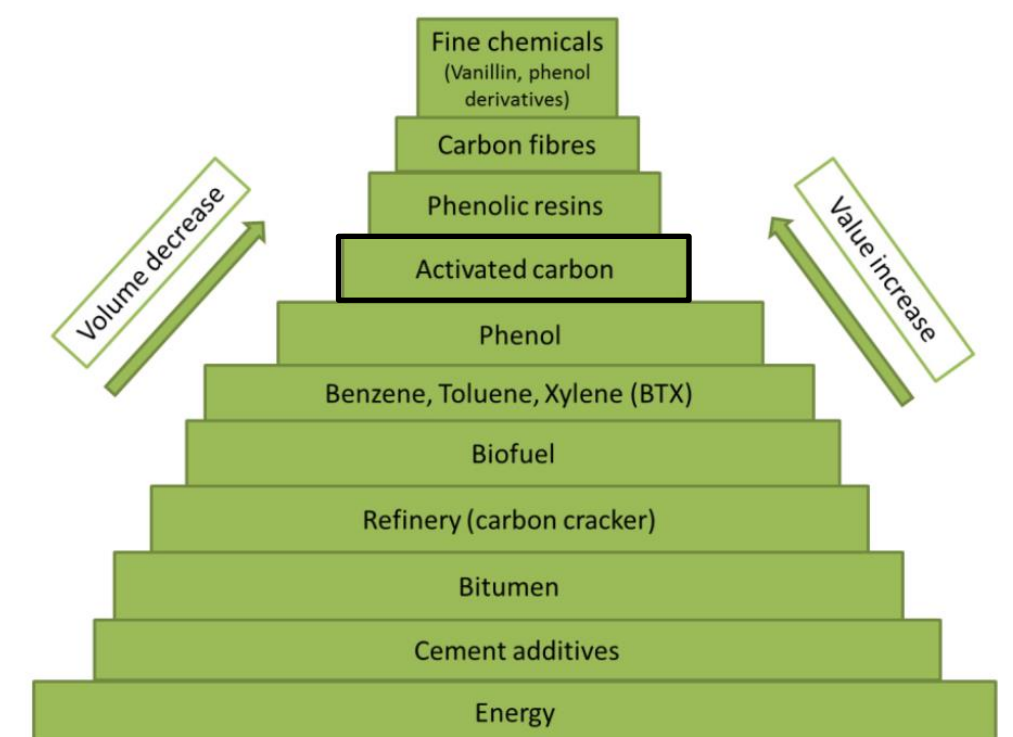
Figure 7 Schematic representation of possible valorizations for lignin, arranged by volume and value. Framed in black, an application that will be further explained in **section 2.3** [31].

Materials

- Lignosulfonates, i.e., lignin produced by the sulfite process (see **section 2.1.2.2**) are already used in cement production as dispersant. The modified cement requires less water in the mixture and displays improved mechanical properties [31].

- Carbon fibers are usually produced by the transformation of polyacrylonitrile (PAN); recent studies show that 45 to 60% of steel car structure could be replaced by carbon fiber. PAN is too expensive to be the precursor to carbon fibers. Lignin could replace PAN as precursor. Carbonization of lignin has exhibited significant improvements in recent years, and lignin could thus be a suitable precursor candidate for automotive structural carbon fibers [32].

Chemistry: polymer, agriculture, fine chemicals

- Lignosulfonates are used as dispersants in foams, elastomers and resins [19].

- Lignosulfonates are promising non-toxic slow-release fertilizers. Lignin acts as a matrix that slowly opens up to release N- and P-doped chemicals [16].

- The Borregaard biorefinery, in Norway, produces vanillin (4-hydroxy-3-méthoxybenzaldehyde) from lignin (**fig. 8**, 4th colum). Vanillin is the most used flavoring agent worldwide [20].
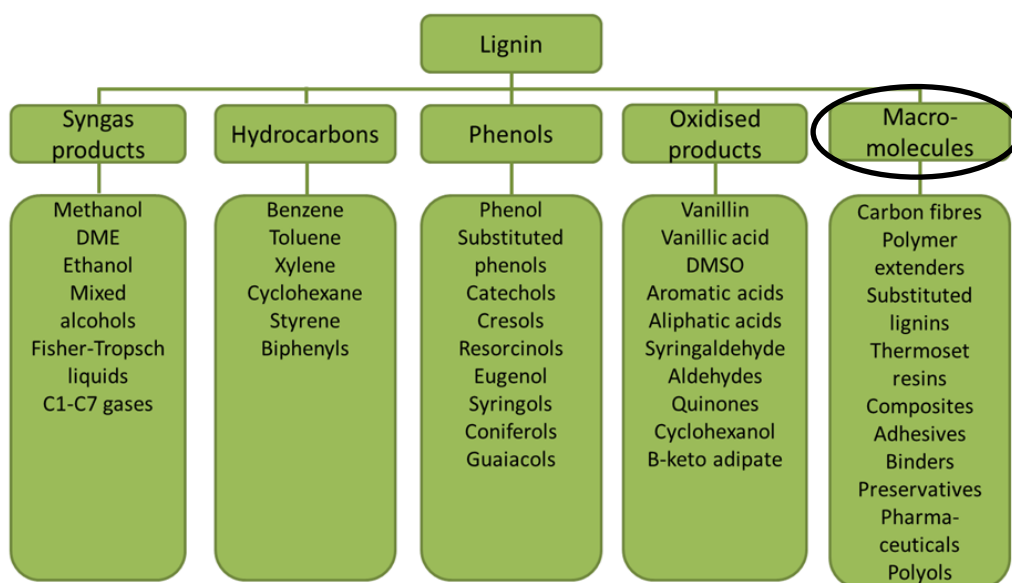
Figure 8 Schematic representation of the possible ways to valorize lignin. In black, we circled the application we are aiming at: the valorization of lignin as a biopolymer [31].

- Lignin can be used in polyurethane blends as co-monomer thanks to its numerous hydroxyl functions [18].

- Parkhust and coworkers demonstrated in 1982 that lignin could be hydrocracked into pure phenol (20%) and benzene (14%). Lignin being nowadays worth 110$/T and phenol worth ~1000$/T [33], this low yield could soon become attractive, considering that aromatics coming from petrol are decreasing [16]. Aromatic aldehydes such as syringaldehyde can also be produced in the process [21].

- Benzene-Toluene-Xylenes (BTX) can be obtained from lignin, but the process is far from efficient. Catalysis and purification are still challenging [19].

Energy storage

This is the subject of this master thesis. Lignin can be valorized either by carbonization to produce porous carbon (**fig. 8**), or by mixing non-carbonized lignin with said porous carbon. See **section 2.3.** for the development on this subject.

The valorization of lignin has gained renewed interest over the last decade because of three factors.

(a) Genetic bioengineering: researchers were able to manufacture mutants with less recalcitrant lignin, hence easier to extract at lower costs and higher purity [19].

(b) Advances in analytical/computational chemistry : new techniques include advances in time of flight – second ion mass spectrometry (TOF-SIMS), atomic force microscopy (AFM), function-detecting antibodies, high performance liquid chromatography (HPLC) and anti-stokes Raman scattering (ARS) [34].

(c) Optimization of pretreatment methods [18].

2.1.3. Lignin can be fractionated according to molecular weight or surface moieties

Lignin is usually fractionated for two reasons: (a) to diminish the polydispersity of the polymer and (b) to retrieve fractions with different physico-chemical properties. Some fragments may be fitter for certain applications than other, due to aggregation or surface phenomena. Three methods are commonly used.

Ultrafiltration

A continuous flow of solubilized lignin in alkaline water passes onto a cylindrical membrane with a specific cut-off. This membrane discriminates particles according to their hydrodynamic volume; the small particles, low molecular weight lignin and inorganic salts go through the membrane, while the remaining high molecular weight lignin stays in a self-looped tube to re-enter the membrane compartment to be filtered again. Different cut-offs can be used to isolate different molecular weights. Care should be taken for the absolute molecular weight of the separated lignin: ultrafiltration is based on hydrodynamic volume, and biases can be induced by the aggregation of lignin in different solvent conditions [35]. See **section 5.5** for details.

pH fractionation

Different lignins precipitate at different pH. By adjusting pH at different values, one can retrieve distinct fractions. The method is simple, straightforward, and only requires water and acid; but it does not guarantee molecular weight separation, since many factors (charge, hydrophilic/hydrophobic moieties, oxygen content, sulfur content for lignosulfonates/Kraft lignin) can be accounted for differentiated precipitation [36].

Solvent fractionation

Organic solvents can be used to separate lignin according to its solubility in these solvents. Fractionation can be conducted either in parallel or sequentially. In the first case, a number of samples of pristine lignin are dissolved in the corresponding number of solvents, and each sample gets separated in two fractions, soluble and insoluble. In the second case, one given sample is mixed in solvent A. The insoluble part is filtered off, and then mixed in a solvent B, and so on. Multiple narrower molecular weight, functionally-enriched fractions are thus retrieved from one sample [37], [38].

2.2. Electrochemical storage : capacitors and biomolecules

On the market, two very different technologies are used to store electrical charge: batteries and capacitors. Batteries rely on electrochemically active substances which accept electrons from an outer source during charge then release electrons during discharge. Capacitors store electrical energy in an electric field between two surfaces. Batteries have slow kinetics since a chemical reaction has to take place. Therefore, they can store a lot of energy but lack power because they charge and discharge at slow rates. On the contrary, capacitors have high power – they can liberate their electrical charge in less than a second – but they are not able to store a lot of energy. In between these two extremes lie the supercapacitors, which display both battery-like and capacitor-like features. They are often displayed in Ragone plots (**fig. 9**),
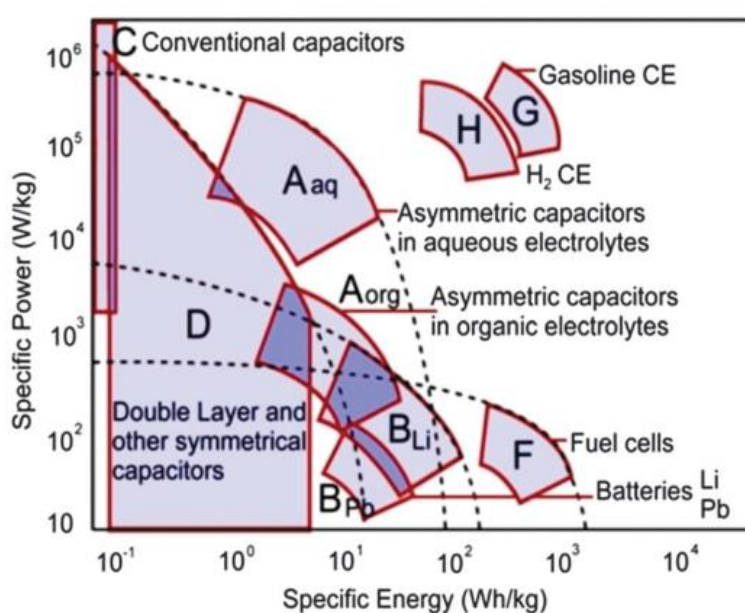
Figure 9 Ragone plot, displaying the specific power as a function of specific energy. Gasoline combustion engine (CE) and H_2 combustion engine (CE) should be considered apart, because they consume fuel and do not store it [39].

which show specific power against specific energy. They are two types of supercapacitors: electric double-layer capacitors (EDLC) and electrochemical supercapacitors (ESC). EDLCs consist of high-surface carbon, which can store charge in the electrical double layer induced by the electric field created when a voltage potential is applied. ESCs rely on electroactive molecules linked to an electrode, which can undergo redox reactions at this electrolyte-electrode interface – this phenomenon is called pseudocapacitance [39].

Wang et al. have recently reviewed bio-based molecules used in electrochemical storage [2]. Bio-molecules are environmentally friendly, biocompatible, sustainable, flexible and chemically diverse. Two types of biomolecules can be interesting in the context of energy storage: pteridines and quinones (**fig. 10**). Pteridines are directly involved in the plant energy storage mechanisms. They are electron shuttles that can be cycled thousands of times without losing efficiency. Quinones moieties are very common in plant molecules. They are often part of structural molecule.
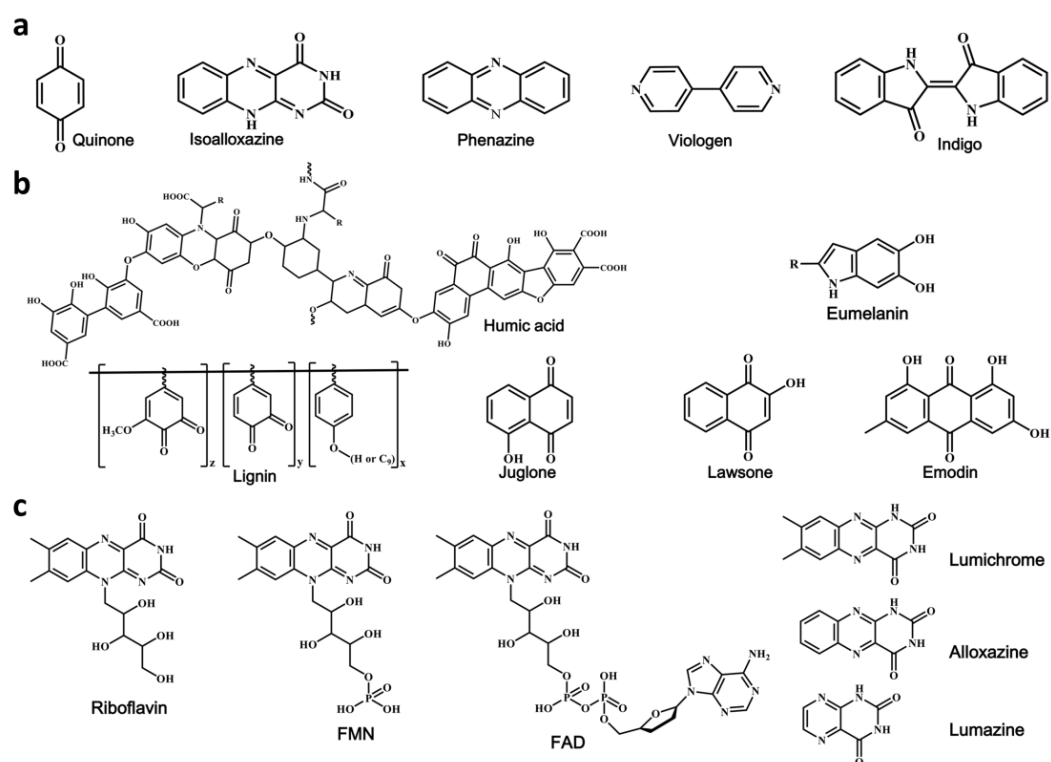
Figure 10 Array of biomolecules that are being investigated for their electrochemical storage potential. (a) and (b): quinones (c): pteridines [2].

- Pteridines: many biomolecules possess a pteridine-like moiety (**fig. 10**). The isoalloxazine part of pteridine is redox-active. Riboflavin, flavin mononucleotide (FMN) and flavin adenine nucleotide (FAD) have already been tested in redox flow batteries, i.e., batteries with liquid reservoirs as active materials, connected to a central reservoir separated in two by a semi-permeable membrane. As such, flavins exhibit a specific capacity of [100-200] mAh/g. Park et al. [40] also tailored the flavins to be more effective by removing inactive parts of the molecule to keep the isoalloxazine cores. Lumichrome, alloxazine and lumazine were synthesized by this method. They all reached >200 mAh/g specific capacity values. A major advantage of flavins is their versatility: addition of a lateral group can change the solubility, and solubility is a crucial parameter in redox flow batteries.

- *Quinones*: Many biomolecules have a quinone-like moiety (**fig. 10**). Quinone is redox-active and can be reversibly transformed into hydroxyquinone (**fig. 5**) [11]. Lignin possesses quinone motifs and has been investigated. Other molecules have also been investigated too, like tannins. Tannins contain 5000 times more phenol per gram than lignin because of their smaller, more condensed structure. Combined with a conductive polymer like polypyrrole (Ppy), tannins can reach 370 F/g for 1 A/g current and 195 F/g for 25 A/g current – these values, compared to lignin, are outstanding [10]. However, their smaller structure means that tannins do not have a satisfactory cycling stability: they slowly dissolve in the electrolyte. To make more stable electrodes, microchannels that are naturally present in carbonized wood can be used as good biosourced templates [12]. A tannin/pyrrole mixture was successfully polymerized *in situ,* i.e., inside the microchannels of the carbonized wood. The polymerization appeared to be very homogeneous judging from electronic microscopy results. Carbonized wood also served as a good natural current collector.

According to Guo and coworkers [10], other good candidates include: melanin, which assembles into nanoparticles; juglone and lawsone, mixed with Ppy for conductivity; and humic acids, which displays poor cycling rate but good storage results.

2.3. Lignin in energy storage

The first part of this section is a review of the use of lignin in porous carbons supercapacitors; the emphasis on method development, capacitive performance, cyclability and originality of the synthesis method. Then, **section 2.3.2** reviews four articles that are the basis for this master thesis: the use of pristine lignin mixed with porous carbon. Porous carbon acts as an electrical double layer capacitor, and lignin acts as a battery-type storage, making the final material a supercapacitor [39], that is, an electrode with both capacitive/non-faradaic contributions from porous carbon, and battery/faradaic contributions from pristine lignin.

2.3.1. Carbonization of biomass creates capacitive porous carbons

In order to get rid of fossil fuels, we need to replace many materials by bio-sourced materials and technologies by sustainable technologies; supercapacitors (see **section 2.2**) could advantageously use porous carbons to accommodate this transition. Porous carbon is a broad term that can describe rather different materials. In general, porous carbons are pure carbon powders, often containing graphitic sheets, with a high surface area (> 500 m²/g) due to their intrinsic porosity. These carbons can be synthesized from biomass by carbonization under inert atmosphere followed by activation, usually with KOH [41]. It should be noted that these two steps often take place at the same time as the precursor can be mixed with KOH before carbonization. Furthermore, biomass-based porous carbons are precursor-sustainable, widely tunable, cheap and easy to make. The capacitive property of porous carbons relies on electrical double layer capacitance: quick charge, quick discharge, but little stored energy. In general, the higher the surface area, the larger the specific capacitance [42]–[44]. Activation is the key to have good electrochemical performance: tests without activation show non-activated porous carbons are way less capacitive than their activated counterparts [45]. Although this review focuses on alkaline activators, there are many activator agents, among which KOH, NaOH, H_3PO_4 and $ZnCl_2$ [46]. Often, carbonization and activation take place at the same time, because the activating agent is also the reactant used to extract lignin from its lignocellulosic matrix [47].

2.3.1.1. Carbonization of lignocellulosic biomass creates capacitive porous carbons

Biomass precursors have recently been reviewed by Tang et al. [2]. Cellulose carbonizes as well as hemicelluloses and lignin, producing partially graphitic porous carbon. Many precursors have been tested, among which orange peels, coconut shells, pomelo and litchi peels, rice husk, soy beans, bamboo and human hair (**fig. 11**). Ojha and coworkers [45] compared KOH-activated and non-activated precursors in terms of electrode performances. The precursors were starch (glucosidic polymer), and two lignocellulosic candidates: jute, a herbaceous plant, and rice husk, the hard shell or rice grains. Activation was supposed to create pores, oxygenated surface functionalities and random defects which would increase conductivity. It was confirmed that the activation of jute and rice husk produced amorphous multilayer carbon sheets, with few surface functionalities (**fig. 12**).

Cyclic voltammetry measurements showed much higher specific capacitance for activated materials than for non-activated ones, thus showing that activation creates materials with

Material	C (mAh/g)	I (A/g)
Citrus peel	140	0,1
Litchi shell	499	0,5
Bamboo	550	0,5
Olive stone	670	0,1
Human hair	700	0,05
Pomelo peel	750	0,2
Soybeans	758	0,2
Banana peel	800	0,1
Wheat straw	920	0,1
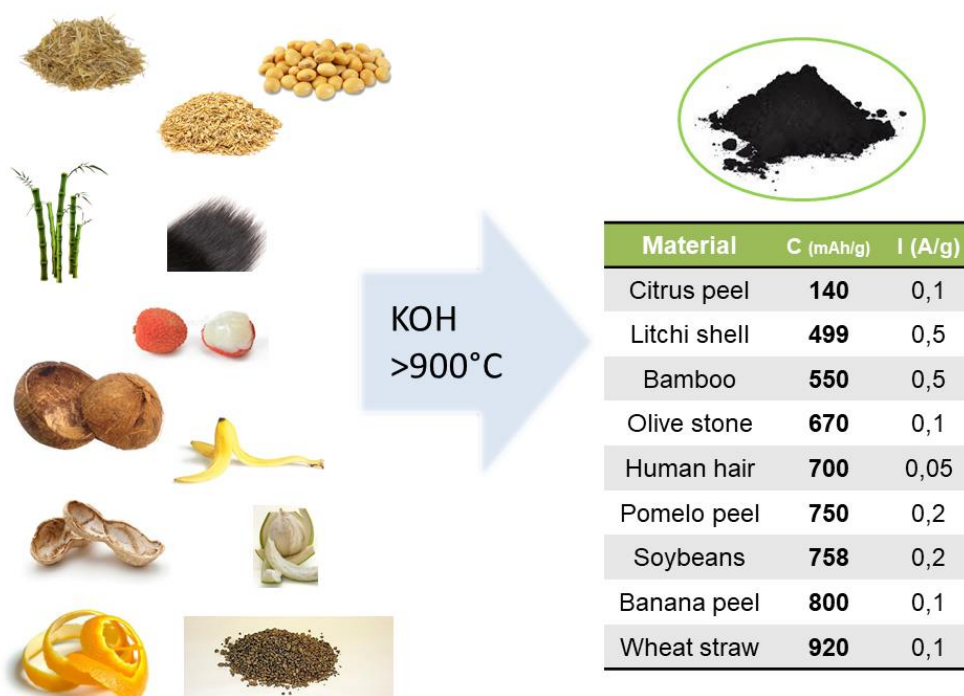
Figure 11 Adapted from table 1 in Tang et al, 2017 [2]. C: specific capacitance density, I: current density. KOH: activator. Sources for pictures: [76]–[84].

higher specific surfaces. This higher charge was also caused by a higher number of surface functionalities. Activated carbon from jute had the highest specific capacitance: 476 F/g (at 0.2 A/g) and 200 F/g (at 10 A/g), which was hypothesized to be caused by the higher lignin content of the precursor (%lignin in dry jute: 26%; dry rice husk: 16%). The electrolyte was aqueous H_2SO_4, 0.5M. The authors compared the results for jute and rice husk to those of starch, which did not contain lignin. They concluded that starch produced activated carbon with low conductivity compared to the two others, and that "*synergistic effect of lignin and cellulose in the biomass is the key factor for high specific capacitance*".

We just explained two examples of lignocellulosic biomass carbonization. Now, let us focus on the carbonization of lignin on its own, separated from cellulose and hemicellulose. Since lignin already contains aromatics, research teams expected it to create more capacitive graphitic porous carbon. The next section is a short review of important articles.
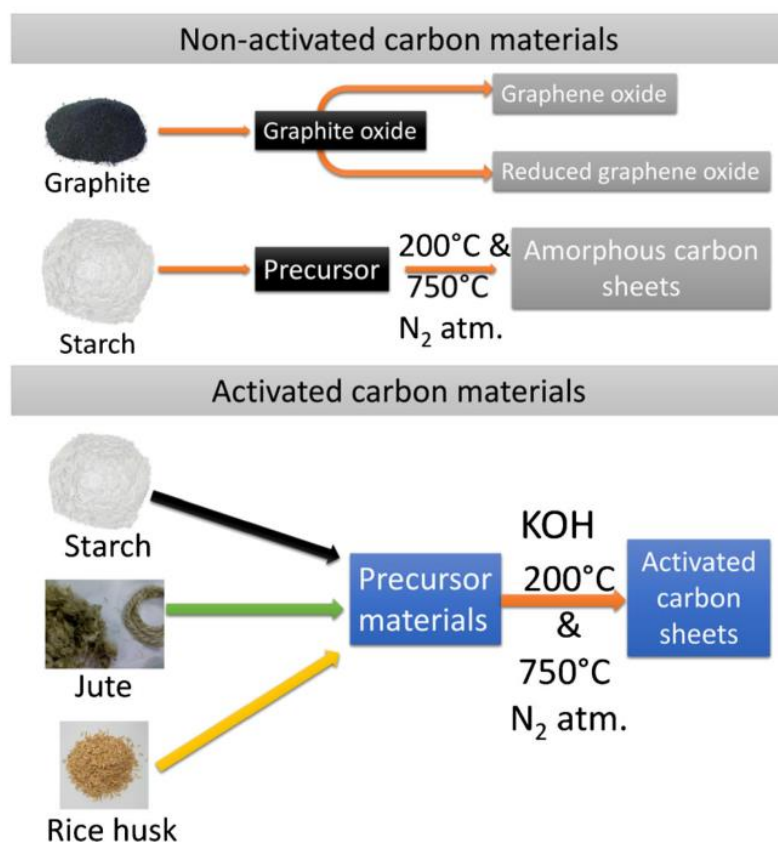
Figure 12 Comparison between non-activated carbon materials and activated carbon materials. Starch was used as cellulosic material, jute and rice husk as lignocellulosic materials [45].

.

2.3.1.2. Carbonization of pristine lignin creates capacitive porous carbons

In addition to exhibiting good electrochemical performances, electrodes obtained by lignin carbonization have another major advantage. As mentioned in **section 2.1.**, natural lignin production is highly variable – in structure, relative H:G:S contents, and purity – and this carbonization smoothens this lignin disparity, making lignin use more robust, reliable, and less industrially risky. However, as lignin is carbonized above 700°C, experiments are often conducted between 700°C and 2400°C. This requires large amounts of energy [37].

Carbonized lignin has remarkable capacitive properties

Hu and coworkers [48] synthesized carbon nanoplates by simultaneous carbonization and alkaline (NaOH or KOH) activation of alkaline-extracted lignin. The simplicity of the method lies in the same reactant (NaOH or KOH) being used for extraction and porous carbon activation. NaOH vs. KOH activation efficiency was studied. The synthesized carbons were described as graphite-like circular nanoplates, 10-25 nm in diameter, separated by amorphous carbon clusters. Brunaueur-Emmet-Teller (BET), SEM and transmission electron microscopy (TEM) analysis allowed to conclude that the micro- and mesostructures were slit-like, and that the aggregated nanoplates resembled graphene structure with its typical π-π stacking. Raman spectrometry showed that increases in temperature and in impregnation time led to a broadening of micropores into mesopores, beneficial for high surface area. On the contrary, increase of base concentration boosted the carving of mesopores into micropores. For the electrochemical properties, NaOH-activated carbons performed better than KOH-activated carbons : 248 F/g (at 20 mV/s) for NaOH and 149 F/g (at 20 mV/s) for KOH, as well as 95% and 92% resilience, respectively, after 5000 cycles. The electrolyte was not mentioned.

Klose and coworkers [46] synthesized porous activated carbon in a two-step process (**fig. 13**). First, Kraft lignin was carbonized with KOH as activating agent, then it was washed to remove any side-products. As for structure, the team noticed that (a) the pore volume increased with KOH concentration, which was demonstrated by BET data and that (b) the

carbon produced was not very graphitized, even mainly amorphous. Amorphousness was assessed by Raman disorganized (D)/graphitic (G) peaks ratio analysis. A thorough analysis of x-ray photoelectron spectroscopy (XPS) data was conducted: the team investigated the influence of surface and sub-surface heteroatoms oxygen and sulfur. The authors noted that the oxygen 7%-presence on the surface increased capacitive performance because oxygenated functionalities displayed pseudocapacitance. However, oxygen presence decreased electrical conductivity. Sulfur introduced by the Kraft extraction process was absent on the surface, but present at ~10% beneath it. Authors hypothesized that it increased carbon conductivity by doping.

For electrochemical properties, galvanostatic charge-discharge analysis revealed a specific capacitance of 231 F/g (at 1 A/g) and 203 F/g (at 10 A/g). The electrolyte was the ionic liquid 1-ethyl-3-methylimidazolium tetrafluoroborate ($EMIBF_4$), which showed viscosity problems but induced good capacitance values. The cycling rate dropped by 50% after 10.000 cycles,

Figure 13 Schematic path of the transformations of carbon. CO_2 is trapped in lignocellulosic biomass, lignin is extracted, carbonized and used as supercapacitor. In the Ragone graph on the right, C is the specific capacitance density and I the applied current density. The graph shows that the smaller the current, the higher the capacity, which is the expectedanswer from an electric double layer capacitor [46].

which was supposedly caused by either the decomposition of the ionic liquid electrolyte at a too high voltage window (3V) or because of the partial degradation of oxygen-bearing surface functionalities. Ionic liquids thus seem promising but in need of optimization for cycling stability. It should be noted that, in addition to voltage degradation, oxygen-bearing and sulfur-bearing surface functionalities have been shown to catalyze electrolyte degradation [46].

Liu and coworkers [8] synthesized carbon nanosheets by ice templating softwood alkali lignin. An aqueous suspension of lignin was immersed in liquid nitrogen, creating lignin sheets, which were then carbonized at 900°C for 6h (**fig. 14**). The authors wanted to determine the influence of precursor lignin concentration on the reaction. It was observed that the lower the lignin concentration in the suspension, the better the electrochemical properties. When the concentration diminished, the produced carbon was more graphitized; and when concentration increased, the size of the carbon nanosheets increased but the specific area decreased. These carbonized nanosheets were partially graphitized. Higher lignin suspension concentration also increased oxygen presence on the surface, enhancing pseudocapacitance. The authors insisted on the absence of activating agent for the synthesis: with no byproduct, the method possesses reduced environmental impact. The only reactant was lignin itself. They hypothesized that the <2 nm micropores were caused by the escape of CO_2 and H_2O gases during carbonization, and that these spontaneously created gases could suffice to create small micropores and advantageously replace KOH activation.
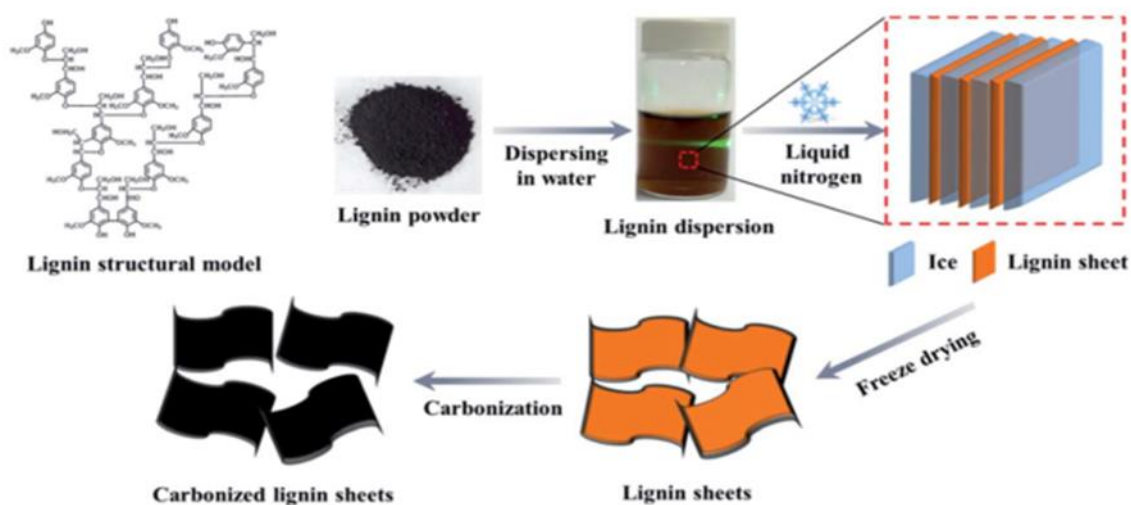
Figure 14 Schematic synthesis of carbonized lignin sheets. Lignin is dispersed in an alkaline solution, frozen with liquid nitrogen, freeze dried and carbonized [44]

34

The electrochemical performances were 281 F/g (at 0.5 A/g) and 103 F/g (at 20 A/g). Stability reached 91% resilience after 5.000 cycles. The electrolyte was aqueous H_2SO_4, 1M.

Tran and coworkers [44] synthesized a porous activated carbon (**fig. 15**) by mixing graphene oxide (GO) and organosolv hardwood lignin in a suspension. Then, they simultaneously reduced the GO and carbonized/activated lignin into porous carbon. The idea was to use lignin as a spacer between reduced GO (rGO) sheets, which, because of their graphene structure, had a tendency to stack up with π-π bonding. This π-π bonding taking place between rGO and lignin matrix also ensured good stability and suppressed the need for a carbon-lignin bindern but was too strong and needed to be decreased. To do so, the authors tested proportions of 0 to 85% of lignin in their suspension, and found out that specific surface increased from 19 m² to 1280 m² in specific surface area. The flexibility of the casted films was intermediate between brittle lignin and flexible graphene. Optimization showed that the 85:15 lignin:GO ratio is best, creating a wide carbon matrix with dispersed, loosely stacked graphene sheets. In accordance with literary hypotheses, increased KOH concentration caused more etching of the porous electrode, creating more and more slit pores (~1 nm). The electrochemical performances displayed were 200 F/g (at 20 mV/s) and 160 F/g (at 1 V/s). The electrolyte was aqueous H_2SO_4 1M.

Figure 15 Schematic synthesis of the carbonized lignin-embedded rGO sheets [8].
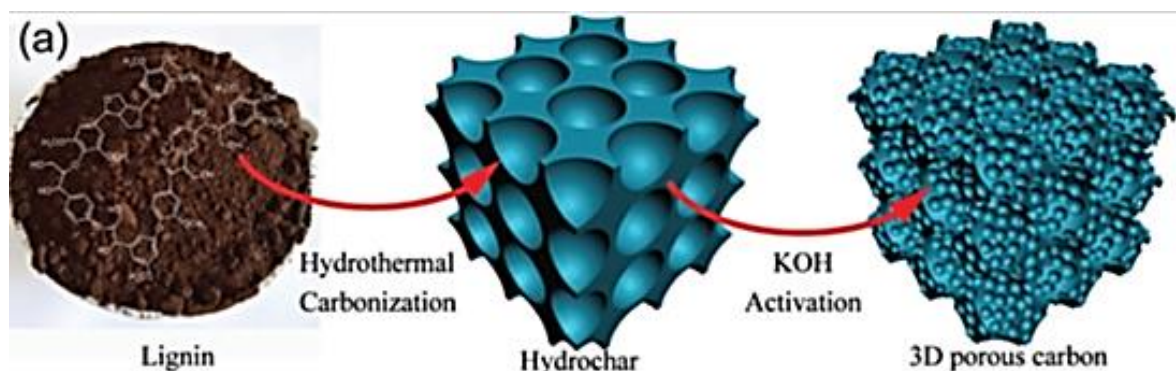
Figure 16 Schematic synthesis of hierarchical porous carbon. The two "red arrow" steps take place at the same time: KOH is mixed with lignin during hydrothermal carbonization [41]

Guo and coworkers [41] used lignin coming from enzymatic hydrolysis to create hierarchical 3D porous carbon without template. Template casting is the standard way of producing hierarchical porous carbon. Their new method consisted of a hydrothermal carbonization followed by high-temperature KOH activation (**fig. 16**). Their work showed that increasing KOH concentration increased surface area, but decreased yield, since more carbon had been etched off by the activating KOH. The electrode was tested in two electrolytes: KOH 6M, and an ionic liquid, 1-ethyl-3-methylimidazolium bis(trifluoromethylsulfonyl)imide (EMIMTFSI). They reached a good specific capacitance, even at high currents: 420 F/g (at 0.1 A/g) and 284 F/g (at 100 A/g) in KOH; 218 F/g (at 1 A/g) and 159 F/g (at 50 A/g) in the ionic liquid. After 5000 cycles, the electrode showed 99% capability retention in KOH and 90% retention in the ionic liquid. Impedance measurements showed that the ionic liquid was more resistive (4.2 ohms vs. 1.39 ohms in the KOH system), thus causing a decrease in the overall specific capacitance. The researchers also hypothesized that pore size was a major factor for ionic liquid use, as the solvent ions could hinder one another in nanopores. Guo also furthered the point of Hu about pore size: the specific capacitance is directly impacted by the ratio size of pores/size of the electrolyte.
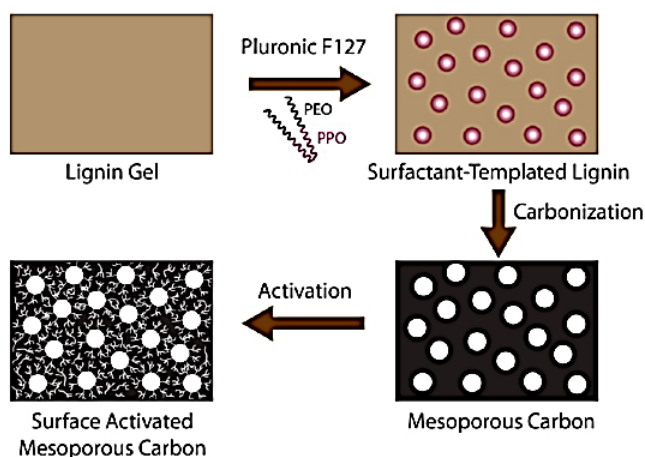
Figure 17 Schematic synthesis of F-127 templated porous activated carbon [51].
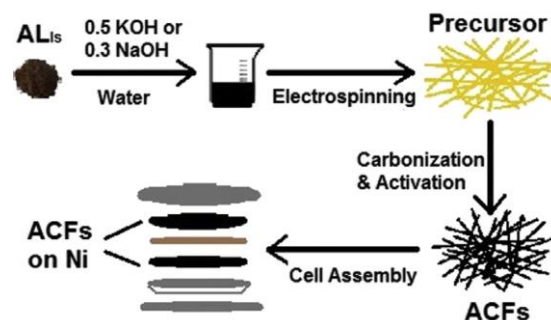
Figure 18 Schematic synthesis of electrospun carbonized lignin fibers, as well as cell assembly for electrochemical tests. AL: alkaline-extracted lignin. ACF: activated carbon fiber [49].

Two research teams synthesized activated carbon fibers by electrospinning alkaline solutions of lignin (**fig. 17**), producing highly packed mats of carbon nanofibers with high specific area (>500 m²/g). Electrochemical performance were 64 F/g at 0.5 A/g, 90% retention after 6000 cycles [49] and 196 F/g at 0.5 A/g, 95% retention after 5000 cycles [50] in 6M NaOH electrolyte [49], [50].

Using poly(ethylene oxide) (PEO)/poly(propylene oxide) PPO copolymers and triblock polymer surfactant F127 as templates, the authors synthesized a mesoporous activated carbon from pre-cross-linked lignin with KOH, at 1000°C (**fig. 18**). Results showed 97 F/g results at 0.1 A/g [51].

Chen et al. [52] implemented the same method as Dipendu et al. [51] with a twist: the addition of nickel oxide particles. NiO was another candidate to electrode manufacturing. The low conductivity, poor stability, but excellent specific capacitance of NiO was complementary to the characteristics of carbon: high conductivity, good stability, but mediocre specific capacitance compared to transition metals. The resulting material was a mix of hierarchical porous carbon and NiO nanoparticles, with good performance: 880 F/g at 1 A/g, with 93.7% capability retention after 1000 cycles.

Carbonized lignin is a good battery electrode

Lithium-ion batteries electrodes are usually made out of graphite. During charge, lithium ions migrate toward the graphitic anode, and insert themselves in between the graphene layers of graphite [39]. At charge, the ions migrate back to the other electrode.

Tenhaeff and coworkers [53] proposed to use the porous activated carbon created from lignin carbonization to build an anode for lithium-ion batteries, taking advantage of the capacitive properties and graphitic structure of lignin-derived porous carbon. Lignin was extracted via Alcell pretreatment (organosolv treatment, see **section 2.1.1.2**.), melted into fibers and carbonized at >1000°C. The resulting nano-crystalline fiber network was tested in a cell against a lithium counter electrode in a conventional lithium ion battery electrolyte, 1.2 M $LiPF_6$ in ethylene carbonate/dimethyl carbonate. The Coulombic efficiency measured were over 99.9% and comparable to conventional lithium-ion battery performances [39].

Other types of batteries could be enhanced by lignin use. Zhang et al. [17] used the same carbonization-activation reaction than others in **section 2.3.1.2.**, but with lithium-selenium battery. The hydrothermal pretreatement with alkaline activation remains, but selenium is added in the process to be encapsulated in the porous carbon. It is mentioned that both Li-S and Li-Se batteries could benefit from the hierarchical porous carbon structure to avoid the loss by solubilization of polyselenide and polysulfide which are a major hurdle to battery optimization. No clear value for an optimized battery or proto-battery was reported.

2.3.2. Non-carbonized lignin is used synergistically with porous carbon to create supercapacitors

Carbonizing lignin at >900°C to produce carbonaceous materials is a process that requires massive amounts of energy and yields are often very low (<10%) [48]. This low yield is caused by the creation of pores driven by alkaline etching and thus removal of material from a "block" of lignin [55]. Using pristine lignin instead of carbonized lignin as one of the main ingredient of the electric charges storage system would therefore be a very attractive alternative. This approach has been pioneered by Chalewaert-umpon and coworkers in two recent publications [9], [11]: they used pristine lignin as redox-active molecule, instead of transforming it into porous carbon.

In the first work [9], Kraft lignin was blended with activated carbon and polyvinylidene fluoride (PVDF) as binder, in order to combine electrical double layer capacitance (non-faradaic capacitance) from the activated carbon, and pseudocapacitance (faradaic capacitance) from the lignin molecules (**fig. 19**). The two effects supposedly combined to increase the total specific capacity. The activated carbon was also used to counteract the isolating nature of lignin, which would have hampered its performance as electrode. By simple mixing of the two powders, the authors reached a reasonable 80 mAh/g with a non-optimized system. They
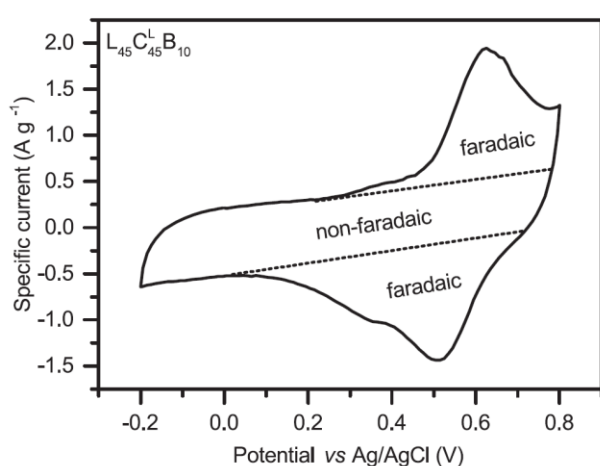
Figure 19 CV curve of the lignin-porous carbon mixture. Non-faradaic capacitive contribution comes from the porous carbon. Faradaic, pseudocapacitive contribution comes from lignin [9].
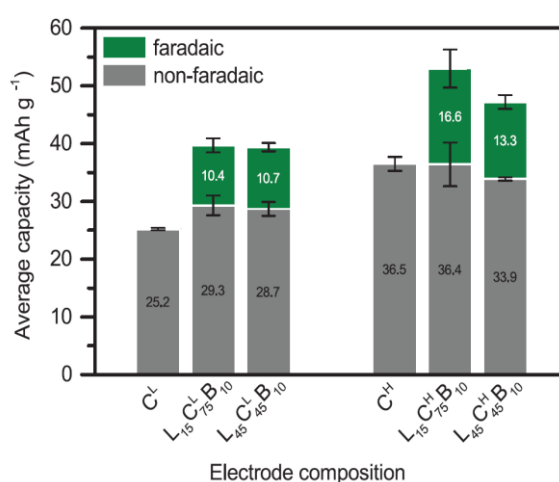
Figure 20 Faradaic and non-faradaic contributions from different lignin:carbon ratios. The best results appeared at 15:75:10 lignin:carbon:binder ratio [9].

also noticed that (a) the specific capacity increased with acidic electrolyte ($HClO_4$) concentration, which was expected from a proton-dependent reaction (see **section 2.1**) and that (b) the best most performing electrode had a ratio of 15:75:10 lignin:carbon:binder, both in faradaic and non-faradaic capacity (**fig. 20**). This indicated that complex interactions between lignin and the porous carbon were in place. These interactions depended on insulation, electrolyte penetration and lignin-carbon microstructure. Stability was estimated at 100% after 100 cycles by galvanostatic charge/discharge. Impedance measurements confirmed the major role of lignin microstructure, because it impacted drastically the electrode performance. Lignin and porous carbon being both bio-sourced, this study opened the path toward a totally bio-sourced battery.

The second article from Chaleawlert-umpon and coworkers [11] built on the results of the first article: the main change was the use of glyoxal instead of PVDF as binder. Glyoxal is bio-sourced and biodegradable, while PVDF is not. In addition, glyoxal is known to cross-link different strands of lignin, which could increase the electrode stability. The authors investigated the best order to mix the three constituents of the electrode, as well as the temperature treatment for the electrode fabrication. They found out that glyoxal ought to be added after the mixing of carbon and lignin, because cross-linking before the mixing produced small particles of aggregated lignin that were too insulating (**fig. 21**). On the contrary, when cross-linked after mixing, lignin was dispersed across the entire carbon surface, increasing electrochemical properties, i.e. conductivity and capacity. Yet, they did
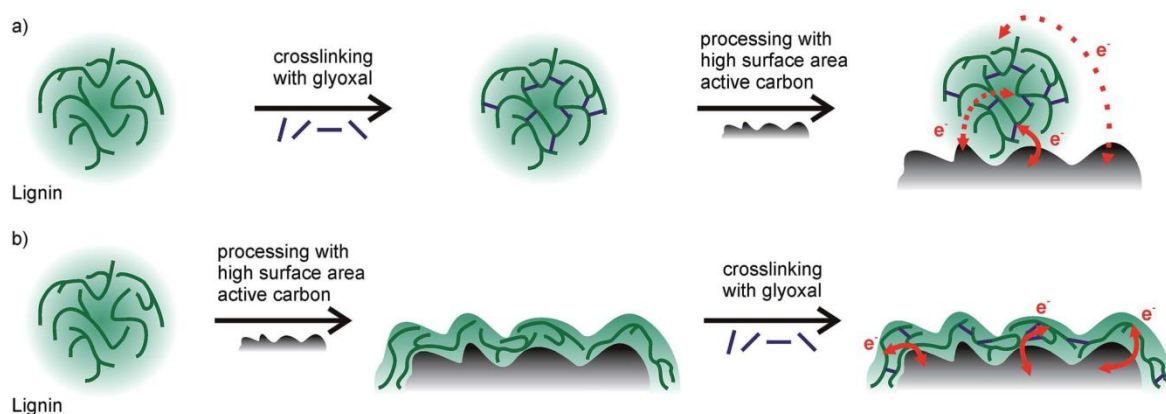
Figure 21 Visual representation of the expected microstructure of lignin, glyoxal and carbon. The difference between (a) and (b) is the order of mixing of the three reagents [11].

not reach higher specific capacity than in the first article (80 mAh/g). The temperature treatment investigation showed that cross-linking was maximum at 80°C, but that 60°C was preferable because at 80°C, phenolic –OH would tended to react together and polymerize, which is undesired since they are the redox-active moieties of the molecule.
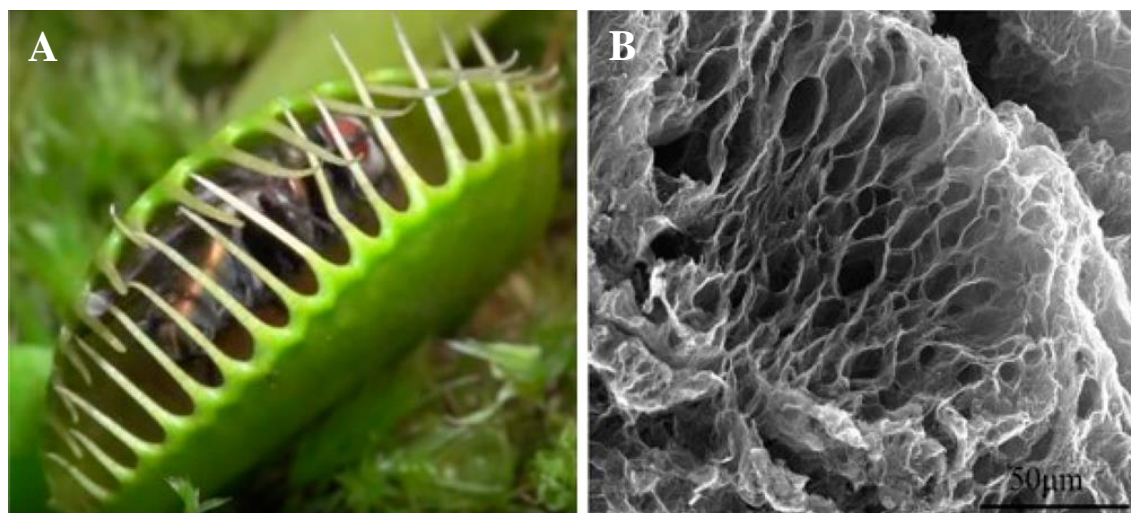
Figure 22 (a) Picture of a Venus flytrap [55] (b) SEM picture of a closed graphene cage . Lignin is supposed to be engulfed in the graphene pore. The legend on the picture says 50 μm [55].

Geng and coworkers [55] approached electrode improvement with an original solution: biomimetic mimicry of a Venus flytrap, the carnivorous plant seen **in fig 22A.** The problems that this study tried to tackle were that (a) lignin is an insulator, thus a poor current collector and that (b) lignosulfonates, the sulfonated version of lignin, quickly dissolve when immerged in an aqueous solution. The proposed solution was to create a 2D graphene plane, to add lignosulfonate onto it, then by reduction, close the plane on itself like a flytrap, so that lignin would still be accessible to the electrolyte but unable to escape the graphene cage (**fig. 22B**). The aromatics of lignin were expected to guarantee that it would be solidly π-π linked to the graphene. SEM pictures (**fig. 22B**) showed promising results and cyclic voltammetry showed reasonable specific capacitance values: 226 F/g (at 0.8 A/g) and 166 F/g (at 2 A/g). The cycling stability, which was the expected main improvement, was 88% after 15.000 cycles. The authors also studied the importance of electrode mass loading. At higher loadings, the thickness of the lignin film increased, and as lignin is insulating, it just decreased the accessibility of the lignin connected to graphene beneath it and decreased the overall specific capacitance.

A parallel between redox-active bio-sourced phenolic compounds: tannins are more capacitive than lignin, but less stable

Mukhopadhyay et al. [12] published a pioneering study which focuses on tannins (**fig. 23**), small polyphenolic molecules that make up 12 to 16% of bark mass. They can be extracted in the same way as lignin and contain, comparatively, 5000 times more phenol per gram than lignin. The authors synthesized a mixed polypyrrole (Ppy)-tannin electrode, that polymerized inside carbonized wood, taking advantage of the natural channel-like structure of carbonized woody fibers. SEM analysis showed uniform tannin/Ppy layers and demonstrated that the thinnest electrodes were the most performing. The carbonized wood also played the role of electron "percolation" pathway and enhanced conductivity. The specific capacitance values were excellent: 370 F/g (at 0.5 A/g) down to 196 F/g (at 25 A/g); and they were comparable to lignin-Ppy electrodes (**tab. 3**). However, the cycling stability was poor because tannins, compared to lignin, are extremely soluble in water, and started dissolving immediately in the 1M $HClO_4$ electrolyte.
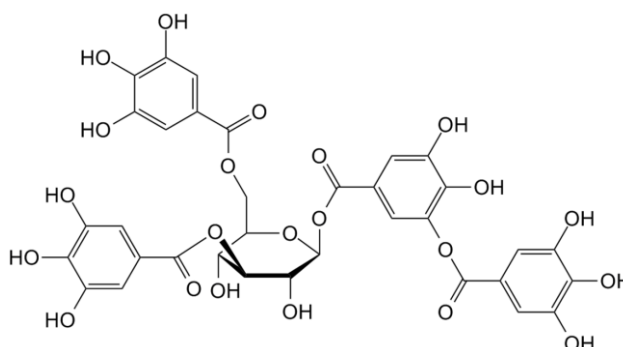
Figure 23 Schematic representation of a tannin molecule [12]

Table 3 Comparison of the capacitive performances of three electrodes: Ppy alone, L/Ppy: lignin combined with Ppy and T/Ppy: tannins combined with Ppy. Results show tannins are two times more capacitive than lignin [12].

Current (A/g)	0.5	1	5	10	25
Ppy alone (F/g)	94	88	80	72	7
L/Ppy (F/g)	151	145	129	123	108
T/Ppy (F/g)	370	278	220	205	196

2.4. State of the art: a summary

Section 2.1 explained what lignin was: a natural reticulate heteropolymer made from 3 phenylpropane alcohols, labeled G, H and S (**fig. 24**). Lignin could be extracted by a number of chemical treatments. Among them, we chose the alkaline pretreatment for this master thesis. Lignin is already valorized in the polymer and material industries, and, more recently, was used in electrochemical storage. Lignin is very polydisperse and needs to be fractionated for some applications. Methods like ultrafiltration, organic solvents fractionation and pH fractionation can achieve that. In section 2.2, we explained what a supercapacitor was and how biomolecules were used in batteries and capacitors.

In section 2.3, we explained that lignin was a redox-active molecule that had already shown to be an interesting active material for batteries when associated with other polymers or when transformed into porous carbons. Lignin to porous carbon conversion included diverse processes such as alkaline-activated hydrothermal carbonization, polymer templating and electrospinning. Lastly, recent studies reported the use of lignin in association with porous carbon, to add a pseudocapacitive property to the specific capacitance of porous carbon

In summary, lignin can be used as a precursor to electrode material (porous carbon) and as a battery redox-active molecule thanks to its unique aromatic reticulate structure. As for now, lignin is mainly valorized in low-value applications, but these electrochemical properties pave the way towards the valorization of lignin in complex systems such as supercapacitors. What hinders its advances in technical applications is a lack of fundamental knowledge about the structure of lignin, its properties and its possible transformations.
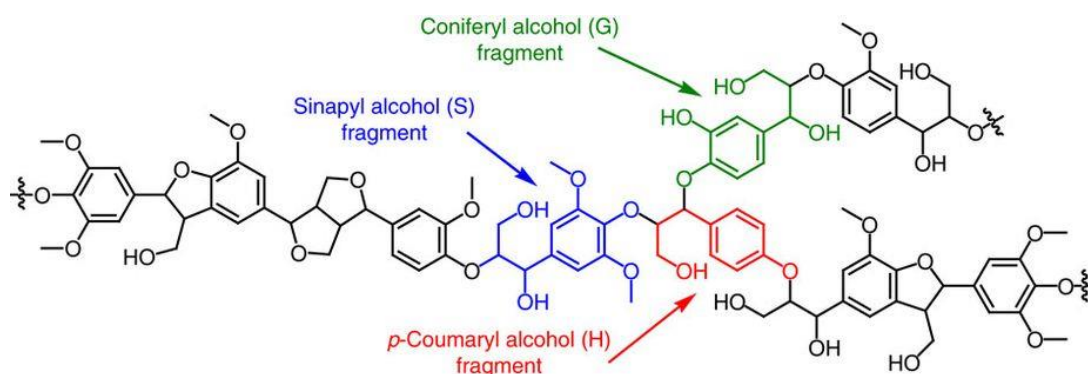
Figure 24 Schematic representation of a lignin fragment. The three monolignols that constitute the polymer are highlighted [85].

3. Objectives

The two articles of Chalewaert-umpon and coworkers [9], [11] open a new research field in the chemistry of lignin: the use of lignin as redox-active molecule to increase the faradaic storage of supercapacitors. Their pioneering works establish a proof-of-concept, as well as some first benchmarks such as optimal temperature and ideal mixing order of the reactants [11]. Still, the literature lacks fundamental knowledge about multiple facets of lignin, such as the links between structure and electrochemical properties, or the links between solubility, molecular weight and functionality content. This lack hinders the rationalization of experimental results and consequently, the advances needed to improve those results. The objective of this work is to build up on Chalewaert-umpon's results, with a specific focus on the influence of molecular weight and chemical moieties of lignin on its electrochemical performances. We also wanted to observe if the alkaline pretreatment would cause different electrochemical performance than Chalewaert-umpon's Kraft sulfur-containing lignin.

To investigate the influence of molecular weight and chemical moieties on these performances, we chose to fractionate lignin. Three methods were chosen: pH fractionation, acetone/water mixtures and successive organic solvent dissolutions. The obtained fractions were characterized by HPSEC, FTIR, NMR, SEM, Klason method for lignin impurities dosage and electrochemically tested by CV.

By corollary, other major fields of research for lignin were addressed and furthered, such as (a) the solubility of lignin in organic solvents, and in different pH conditions, (b) the search for a suitable molecular weight analysis for lignin and (c) the difficulty of lignin chemical moieties characterization due to its intrinsic heterogeneity.

4. Materials and methods

Materials

Three different lignins were analyzed in this master thesis: Douglas pine (DPL), Beech (BL) and Herbaceous (HL). **Douglas pine** (*Pseudotsuga menziesii L.*) chips were obtained from a milled sample harvested in Gembloux Agro Bio Tech's campus. Chips were between 1 and 5 cm in length and 1-5 mm wide. **Beech** (F*agus Salvatica L.*) chips were obtained from trees cut on January 31, 2016, located in the most southern part of Belgium and ball milled to 4-mm wide particles. Protobind^TM P1000 lignin was a commercial mixed wheat straw/Sarkanda grass soda lignin bought from Green Value S.A.

All chemicals were obtained from either Sigma-Aldrich or VWR and used as received.

Lignin Extraction

Lignin was extracted from either Douglas Pine (samples labeled D1 or D2) or Beech (labeled H1). The dry milled pieces of wood were introduced in a 5050 Parr reactor, along with NaOH 3% (w:v), with a ratio 1:10 sample:solvent (w:v). The mixture was heated at 160°C for 30 minutes. Solid residue and black liquor were separated by centrifugation (10.000 RPM, 7 minutes). The lignin was precipitated out the black liquor by bringing the pH to 2 using concentrated H_2SO_4. The lignin was separated from the solution by centrifugation (10,000 RPM, JA-10, 7 minutes).

Dialysis

The black, gooey solid was then transferred to dialysis tubes (cut-off 1 kDa), then immersed in demineralized water. The dialysis was monitored by conduction measurement. Water was replaced by fresh demineralized water as soon as conductivity exceeded 200 µS/cm. Dialysis lasted between 3 and 5 days, depending on salt content and tube length. Dialysis was stopped when conductivity was under 10 µS/cm for at least 3 hours straight. The samples were then frozen and lyophilized.

Ball-milling

A total of 5 g of lignin were added in a ceramic-coated titanium vessel, together with 2 drops of ethanol. It was ball-milled 3 times 36h, for a total of 108h per sample. After 36h and 72h, 1 gram of lignin was removed and stocked for further analysis.

Polymeric Sonication

Lignin was mixed with solvent (aqueous NaOH 5% (w:v)) with a 1:10 ratio (w:v and submitted to a 12-mm wide sonication probe at 35% amplitude for 45 minutes. The slurry mixture was precipitated at pH = 2 using concentrated H_2SO_4, and centrifuged at 1100 g for 7 minutes, followed by washing to remove Na_2SO_4 salts.

HPSEC

HPSEC solvent was prepared by mixing 6.9 g of NaH_2PO_4 with 3.2 g of NaOH in 1 liter of deionized **water**. pH was then brought to 12 with dropwise addition of NaOH 6M. The solution was filtered on a porosity 3 filtering crucible with a porosity of 100-140 μm and sonicated for 15 minutes to degas. The standards were sodium polystyrenesulfonate beads of 1000, 4000, 16000, 32000 Da. The column was a TSK Gel G3000 PWXL eluted at 0.9 mL/min in a Waters 2695 equipment. A total of 9 mg of lignin in 3 mL of solvent were magnetically stirred for at least 48 hours, then filtrated on 0.45 μm nylon syringe filters. The elution flow was 0.9 mL/minute.

HPLC-SEC solvent was 0.5% (w:v) LiBr in **N,N-dimethylformamide** (**DMF**). LiCl had a disaggregating role. Polystyrene standards were made by dissolving 15 mg of polystyrene beads in the eluent. Standards included 1kDa, 2kDa, 3 kDa, 10 kDa, 20 kDa and 30 kDa . The column was a Styragel HR3 THF placed on a Agilent Technologies 1200 series. In this case, 9 mg of acetylated lignin (see "Lignin acetylation") or pristine lignin in 3 mL of solvent were magnetically stirred for at least 2 hours, and then filtrated on 0.45 μm nylon syringe filters. The elution flow was 0.4 mL/minute.

Fractionation

Lignin was either submitted to fractionation by pH, fractionation by acetone/water mixtures or fractionation by organic solvents. Fractionation by **pH** [36] was performed by dissolving 5g of lignin in 200 mL of NaOH 5% (w (g): v (mL)) and magnetically stirring for 1 hour. pH was then brought to 8 by slow and careful adding of concentrated H_2SO_4 and NaOH 6M when the value of pH = 8 was exceeded. The precipitate was separated from the solution by centrifugation (7 minutes, 1100 g), then washed with 50°C acidified water (deionized water acidified to pH=2 by concentrated H_2SO_4) to remove inorganic salts. The solid was then frozen and lyophilized. The same protocol was applied at pH=5 and pH=2. Fractionation by **acetone/water mixtures** [38] was done as follows: 5g of lignin were magnetically stirred in 100 mL of a mixture 60:40 acetone:water (v:v) for at least two hours. The mixture was filtered on ceramic porosity 2 filters and washed two times with the solvent. The filtrate was rotary evaporated and freeze dried. The solid residue was submitted to the same protocol but with a 30:70 acetone:water (v:v) mixture. Fractionation by **organic solvents** [37] was performed as follows: 5g of lignin were dissolved in 100 mL of an organic solvent and magnetically stirred for at least two hours. The mixture was filtered on ceramic porosity 2 filters. The solid residue was washed two times with 15 mL of the organic solvent, and then was used with another organic solvent. The filtrate was rotary evaporated, the solid residue washed off with 10-20 mL of deionized water and freeze dried. The organic solvent sequence was: ethyl acetate, methyl ethyl ketone, methanol, acetone and dioxane:water 95:5 (v:v) .

Lignin Acetylation [56]

To 1 g of lignin mixed in 23 mL of acetic anhydrous, we carefully added 2.3 mL of acetyl bromide. The mixture was magnetically mixed for 24 hours. Then, 30 mL of ethanol were added to quench the reaction and the solvent removed by rotary evaporation. Next, 30 mL of ethanol were twice added and evaporated, to remove the solvent entirely. The solid residue was either kept as such or submitted to purification. For **purification**, 10 mL of $CHCl_3$ were added to 0.5 g of acetylated lignin. Once the lignin was dissolved, the solution was washed twice with 20 mL of deionized water and the organic phase was dried with Na_2SO_4. The dried $CHCl_3$ solution was added dropwise to 150 mL of dry diethyl ether. Gelatinous drops of lignin started to precipitate. After at least 12 hours, the diethyl ether was rotary evaporated and the remaining solid was weighted.

Klason determination of sugars

A sample of 100 mg lignin was mixed with 3 mL of 72% H_2SO_4 agitated with a vortex for 30 seconds and placed in a 30°C bath for 60 minutes. 84 mL of water were added to drop the acid concentration to 4%. The mixture was then heated for one hour at 121 °C in an autoclave, then let to cool down and filtered. The filtrate contained acid-soluble lignin and carbohydrates, while the solid contained inorganics salts and acid-insoluble lignin. To dose **acid-insoluble lignin** and **inorganics**, the solid residue was put in a dry, weighted crucible and dried at 105°C for at least 4 hours. The sample was then weighted, put in an oven at 550°C for 4 hours, let to cool in a desiccant and weighted again. The difference between non-carbonized and carbonized samples gave insoluble lignin content, and the remaining solid inorganics content. **Acid-soluble lignin** was dosed by UV spectrometry. 3 mL of filtrate were diluted until absorbance at 205 nm was between 0.2 and 0.7. Each sample was analyzed twice. To quantify **carbohydrates**, 20 mL of the filtrate were slowly neutralized with $CaCO_3$ to pH = 5-6. Slowness was required to avoid foam formation. The sample was thoroughly mixed and let to settle. The pH of the filtrate was about 7. The sample was centrifuged at 10.000 RPM for 7 minutes and the supernatant was isolated.

Fourier Transform Infrared (FTIR)

The dry sample of lignin was placed on the FTIR crystal. High quality spectra could only be obtained when deposit quantities were >200 mg. The machine was flushed with nitrogen gas and background compensated. Resolution was 4 cm^{-1}. Spectrum manipulations included baseline correction and normalization, as well as hand peak picking. The spectrometer was a Brücker Vertex 70.

^{31}P NMR dosage of hydroxyls

The reactive mixture was prepared as such: 12,8 µL of 30°C pre-heated cyclohexanol, 1 mL of DMF, 1.2 mL of deuteriated chloroform, 1 mL of pyridine (dried by addition of 10g of NaOH beforehand) and 11.5 mg of chromium acetylacetonate were mixed in a 4 mL-vial. Lignin was dried overnight in a 40°C oven. We mixed 20 mg of dried lignin with 500 µL of reaction mixture and 100 µL of phosphitylatingte agent 2-chloro-4,4,5,5-tetramethyl-1,3,2-

dioxapholane (TMDP). The mixture was agitated and vortexed at room temperature, and centrifuged if a solid residue could still be seen. Up to 1600 scans were taken to generate one spectrum.

Electrode films fabrication

Lignin films were prepared by mixing lignin, activated carbon (80 m²/g) and polyvinylidene fluoride (PVDF) in weight ratio 15:85:10. The powder was suspended in N-methyl-2-pyrrolidone (NMP), which was added drop wise to obtain viscous slurry. The mixture was spread with a 120 μm casting knife on either pure copper foil or fluorine doped tin oxide (FTO) glass and dried at 100°C under vacuum for one night. A 1cm by 1cm square was then cut off and tested as such in cyclic voltammetry.

SEM

SEM was performed on both lignin-carbon films and on pristine lignin powders. The film sample or powder sample was first sprayed with gold to make it conductive. This was done in 60 seconds at 30 mV on a Bal-Tec device. The electronic microscope was a ESEM Philips XL-30 FEG. The secondary electrons detector was used. The electrical tension was 15 kV.

CV

Cyclic voltammetry was performed in a three-electrode cell in H_2SO_4 with a standard calomel electrode for reference. The potential was swept from -0.2 to 0.8 V at 5 mV/s. The reported spectra were the third iteration of the experience, to ensure the system was stabilized.

Schiff test

A sample of lignin (10 mg) was dissolved in 2 mL of methanol. The, 0.5 mL of Schiff's reagent was added. The test was considered positive if any red-pink coloration appeared up until two minutes. Otherwise, the test was considered negative.

5. Results and discussion

5.1. Extraction and purification

5.1.1. Extraction yields are lower than expected

The extraction yields are summarized in **tab. 4**. The dry percentage of retrieved lignin falls around 10%, which is lower than the usual yield (20-30%) [28]. This loss can probably be attributed to low molecular weight lignin losses during dialysis, because the weight measurement was done after dialysis, not before. The cut-off of the dialysis is 1000 Da, which leaves out all smaller lignin fragments.

Table 4 Extraction yields and relative proportion of lignin in dry sample retrieved. DPL: douglas pine lignin. BL: beech lignin. These figures of the 4th column come from unpublished results of the Biomass and Green Technology laboratory.

	Attempt	Yield (%)	Lignin in dry sample (%)	Relative lignin proportion retrieved from dry sample (%)
DPL	1	**9.5**	30.6	**31.0**
	2	**11.7**	30.6	**38.2**
BL	1	**9.2**	21.6	**42.6**

5.1.2. The Klason method shows the dialyzed lignins are >97% pure

The purpose of the Klason method is to determine proportions of carbohydrates, lignin and inorganic salts in a biomass sample. It is mostly appropriate for lignin-rich samples, while other methods like Fibertech are more suitable for carbohydrate-rich samples. In this case, the

Klason method will indicate whether the lignin samples are pure or not, and if dialysis yielded sufficiently pure lignin. Inorganic salts contamination could greatly influence the electrochemical tests results because (a) many inorganic salts are redox-active and (b) the ionic content of the lignin could dissolve in the electrolyte, and influence the ion mobility in the test cell. The detailed methods for calculating these results on the basis of GC-MS (carbohydrates), acid soluble lignin (UV) and inorganic salts (carbonization), as well as error calculation, can be found in **Appendix I**. The lignin samples used in the following analysis are thus >97% pure (**tab. 5, fig. 25**). The dialysis method seems to be efficient, though very time consuming.
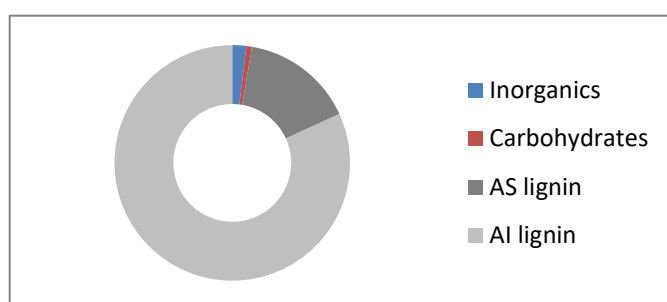
Figure 25 Visual representation of Klason method results. A: acid soluble. AI: acid insoluble.

Table 5 Klason method results. All figures are in percentages and have been normalized to sum up to 100%. DPL: douglas pine lignin. BL: beech lignin. HL: herbaceous lignin

	Carbohydrates	Inorganic salts	Total impurities	Acid soluble lignin	Acid insoluble lignin	Total lignin
DPL	0.77	1.92	**2.62**	15.5	81.81	**97.38**
BL	0.82	2.05	**2.87**	12.8	84.56	**97.63**
HL	0.71	2.03	**2.74**	16.5	80.76	**97.26**

5.2. Fractions proportions are indicators of functionality content

A schematic view of the three fractionations, as well as the labeling of the different fractions is displayed in **fig. 26, fig. 27 and fig. 28**. To help with fraction identification and labeling, a non-attached supplementary "Table of abbreviations" sheet has been included in this master thesis.

5.2.1. pH fractions proportions indicate proportions of carboxylic acids and phenols in the fractions

A sample of 5 g of lignin was dissolved in water, alkalized to pH = 12 by concentrated NaOH. The pH was then brought to pH = 8, pH = 5 then pH = 2 with concentrated H_2SO_4. See **fig. 26** for a visual representation.
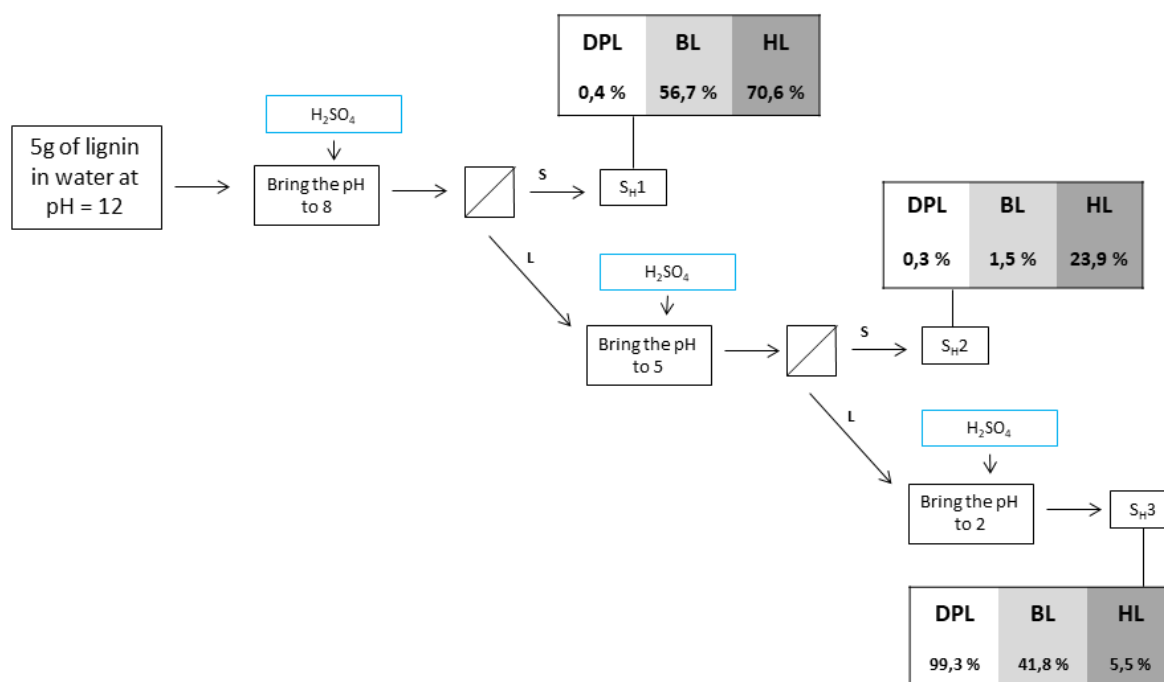
Figure 26 Schematic representation of the pH fractionation methods, as well as fraction proportions results. The % figures are mass percentages of the lignin introduced at the beginning of the fractionation.

DPL did not precipitate until pH = 2. BL precipitated out of the solution at pH = 8 and pH = 2, but not at pH = 5. HL mostly precipitated at pH = 8 and pH = 5, and not much at pH = 2. We rationalized these very different behaviors by evaluating

the quantities of acido-basic active moieties in lignin. The two main functionalities that were affected by pH were carboxylic acids (pKa = 4-5 [57]) and phenols (pKa = 9-10 [57])[1]. At pH = 12, we assumed all these functionalities were deprotonated, hence negatively charged and soluble in water. The addition of H^+ brought the pH to 8, protonating and neutralizing phenol functions, leading to a decrease in solubility. Similarly, when the pH was brought to 2, the carboxylic acids were protonated and neutralized, causing a decrease in solubility. We inferred that DPL contained large amounts of carboxylic acids, which kept the molecule soluble up at pH = 8 and 5 because the pH was still above their pKa (4-5). At pH =2, they were neutralized and the lignin precipitated. These carboxylic acids were numerous enough to keep the lignin soluble until pH = 2. On the contrary, HL mostly precipitated at pH = 8 and 5, and not at pH = 2. We concluded that HL contained comparatively larger amounts of phenols, and fewer carboxylic acids. This hypothesis was corroborated by NMR data. Looking at SA1, SA2 and SA3, we calculated that the ratio of phenolic alcoholic hydroxyls to acid carboxylic hydroxyls were respectively 6:1, 2.3:1 and 1.8:1 (**tab. 6**). This means that SH3 contained proportionally a lot more carboxylic acids than SH1, which confirmed our hypothesis.

Table 6 Relative fraction proportions for DPL, BL and HL. Line 4: percentage of lignin that was recovered, in total, out of the 5 grams we inputted. RL: retrieved lignin. On the right: phenol:carboxylic acid ratios for HL, coming from NMR data (**section 5.6**)

	DPL (%)	**BL** (%)	**HL** (%)	**HL** P:CA
SH1	0.4	56.7	70.6	6:1
SH2	0.3	1.5	23.9	2,3:1
SH3	99.3	41.8	5.5	1,8:1

---

[1] Aliphatic alcohols were not taken into account since their pKa was higher than 12 (pKa = 16-17 [57])

The interpretation of BL results was more complicated, since half of the sample precipitated at pH = 8 and half at pH = 2, and almost no precipitate at pH = 5. A possible explanation could be that HL possessed two distinct sets of lignins, one set containing many phenols, the other containing many carboxylic acids. This hypothesis could be confirmed by ^{31}P NMR, which doses each type of hydroxyl function (aliphatic or aromatic alcohol, acid), by measuring the quantities of each type of hydroxyl in fractions SH1 and SH3, data which were unfortunately not acquired.

5.2.2 Organic solvent fractions proportions were difficult to analyze because of complex lignin solubility

The second type of fractionation was organic solvent fractionation. A sample of lignin was dissolved in ethyl acetate. The solid residue and the ethyl acetate were separated by filtration and the ethyl acetate evaporated to recover the first lignin fraction, F1 (see **fig. 27** for a visual representation). The solid residue was dissolved in the second solvent, methyl ethyl ketone (MEK), and so forth in methanol, acetone, and dioxane:water (95:5), creating fractions F2, F3, F3bis, F4 and INS, the insoluble fraction. F3bis was the acetone-soluble lignin, which was, in mass, insignificant compared to the other fractions. The analysis of this fraction would have been too costly in pristine lignin: a few grams of pristine lignin would have been necessary to isolate a few milligrams of F3bis. F3bis was thus discarded in the characterizations and the following analyses of this master thesis. The proportions of each fraction are displayed in **fig. 27**. The third type of fractionation was acetone/water fractionation. The process was the same as organic solvent fractionation, only the solvents were acetone/water mixtures. The first was acetone:water 60:40 and the second acetone:water 30:70, creating three fractions: SA1, SA2 and SA3, the latter being the insoluble fraction. The proportions of each fraction are displayed in the visual scheme **fig. 28**. Unlike pH fractionation, organic solvent and acetone/water fractionations could not be explained with simple acido-basic considerations: the solubility of lignin in organic solvents can only be assessed by evaluating the non-covalent interactions it can form with the solvent molecules. These interactions are summed up in a theory that describes the solubility of polymers in organic solvents: Hansen solubility parameters theory. This theory will be used throughout this master thesis to infer structural pieces of information from solubility observations.
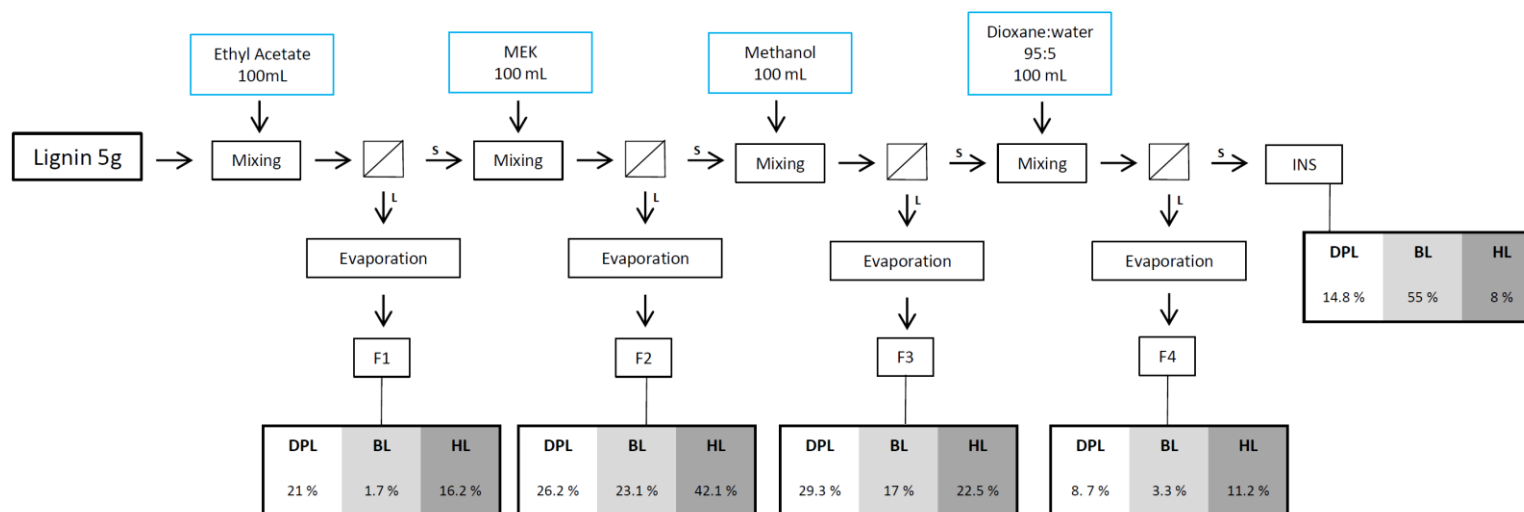
Figure 27 Schematic representation of the organic solvent fractionation, as well as the fraction proportions for each type of lignin.
S: solid. L: liquid. Dashed box: filtration. The % figures are mass percentages of the lignin introduced at the beginning of the fractionation.
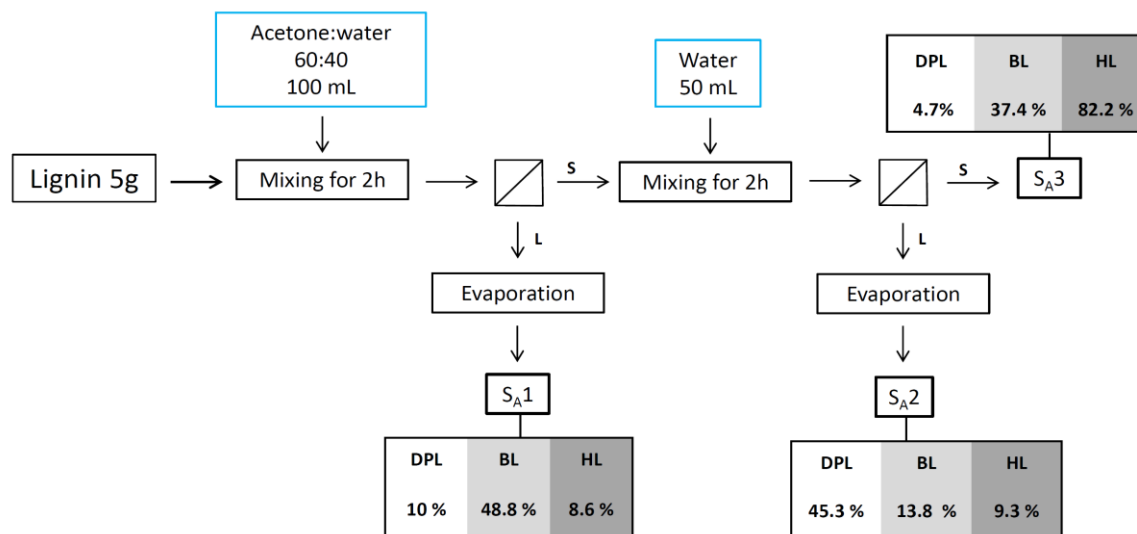
Figure 28 Schematic representation of the acetone/water fractionation, as well as the fraction proportions for each type of lignin. S: solid. L: liquid. Dashed box: filtration. The % figures are mass percentages of the lignin introduced at the beginning of the fractionation.

5.3 Hansen solubility parameters make sense out of organic solvent solubility

This theory was developed by Hansen and coworkers [56] to ameliorate the Hildebrand theory of solubility [58], [59].The Hildebrand theory assigned a solubility parameter δ to every polymer and acomparing it with the δ of solvents. The theory states that the solubility of a polymer increases in solvents with similar δ. The Hildebrand theory only applied to strictly non-polar solvents. Hansen extended the theory by adding a parameter that would take into account polar interactions.

In Hansen solubility theory, each solvent and each polymer has three parameters: δ_D, δ_P and δ_H, that respectively symbolize dispersive interactions, dipole-dipole interactions and hydrogen bonding. Their unit is $(MPa)^{1/2}$. They are linked to the global parameter δ in one equation:

$$\delta^2 = \delta_D^2 + \delta_P^2 + \delta_H^2$$

Hansen parameters can be represented in the Hansen space, in which each axis is a parameter. The aim of the Hansen parameters is to allow comparison of multiple solvents or multiples polymers at once. The pieces of information that can be inferred from Hansen space are schemed in **fig. 29 and 30**. Let us take methanol as an example (orange dot in **fig. 29 and 30)**. If a lignin fraction is soluble in this solvent, it means that its Hansen parameters are spatially closer to the ones of the solvent. In the case of methanol, it clearly appears that the soluble lignin fraction must display lower dipole-dipole interactions, higher hydrogen bonding and lower dispersive interactions than pristine lignin. The Hansen spaces containing all solvents that have been used for analysis can be found in **Appendix III** [60]**.** The Hansen solubility parameters of mixtures are calculated by weighted average of the parameters of the pure solvents.
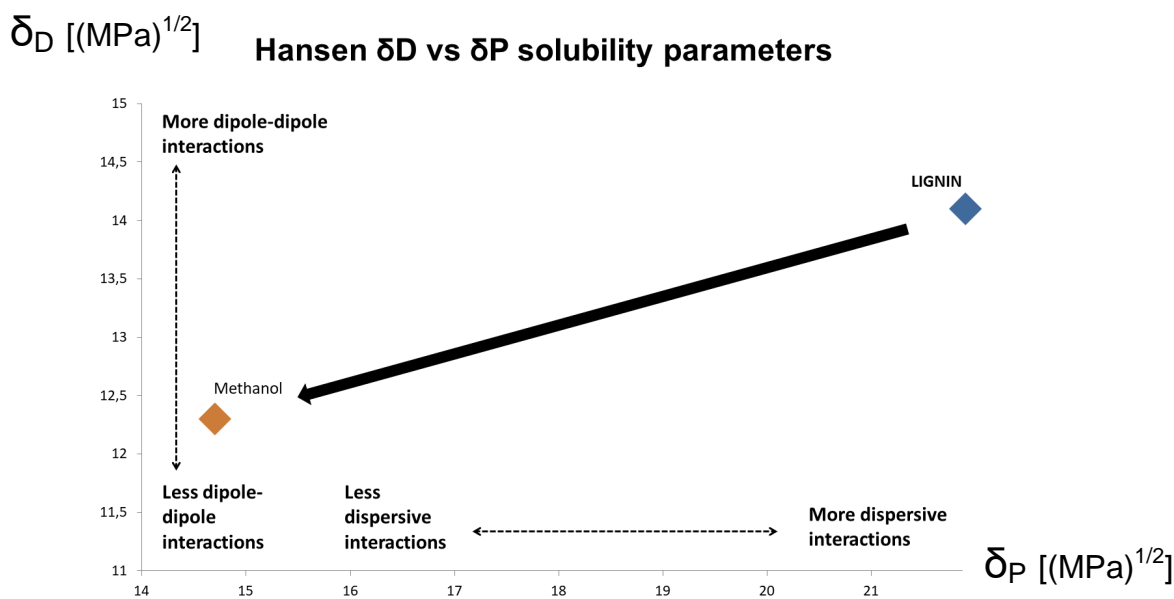
Figure 30 2D slice of the Hansen space. X-axis: dispersive interactions. Y-axis: dipolar interactions.
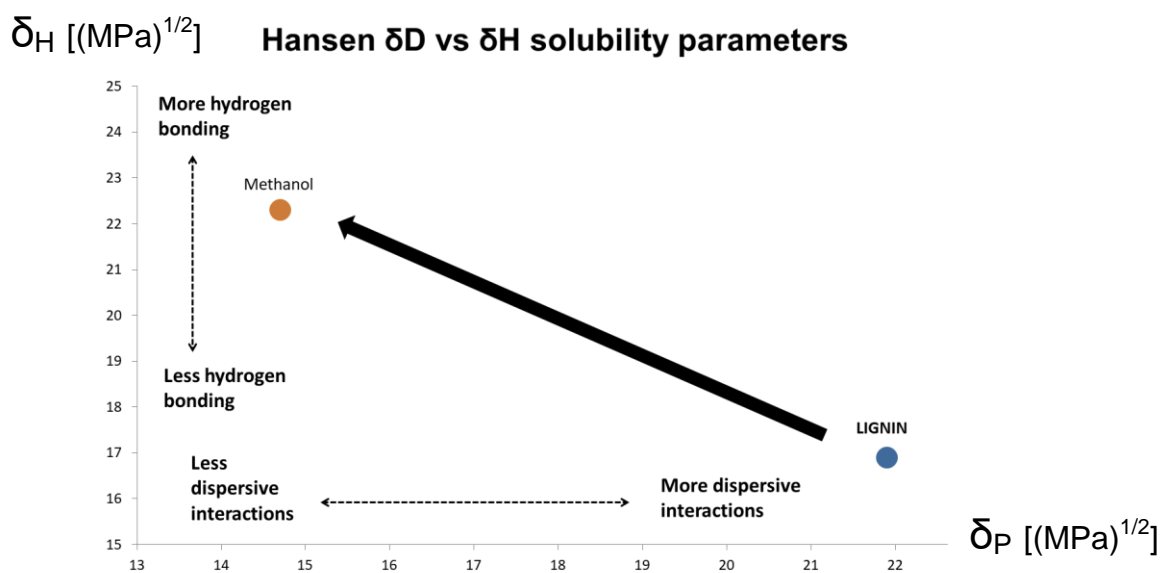
Figure 29 2D slice of the Hansen space. X-axis: dispersive interactions. Y-axis: hydrogen bonds.

Thus, the Hansen parameters of solvents can give us a general idea of what kind of functionalities they dissolve better, and in general, which solvents are adequate or not for different types of lignin. In **tab. 7**, we can see why DMSO and DMF are very good solvents for lignin: their distance to lignin is the smallest of all solvents.

The value that indicates the closeness of two molecules is R_a, which is calculated as such:

$$R_a{}^2 = 4(\delta D_1 - \delta D_2)^2 + (\delta P_1 - \delta P_2)^2 + (\delta H_1 - \delta H_2)^2$$

δD_1 being δD for molecule 1, δD_2 for molecule 2, and so forth. A list of R_a has been computed into **tab. 7.**

Hansen solubility parameters even allow solubility prediction. From a selection of organic solvents, the computations of their R_a to lignin are easily calculable if the parameters of the polymer are known. In the case of lignin, other good solvents should include: benzyl alcohol, m-cresol, dipropylene glycol and tetrahydrofurfuryl alcohol (green in **Appendix III**).

Table 7 Hansen parameters and relative distance to lignin of solvents used in this master thesis. δ_D: dispersive interactions. δ_P: dipolar interactions. δ_H: hydrogen bonding. R_a: relative distance to lignin parameters [59]. The unit of all parameters is $(MPa)^{1/2}$. In green, good lignin solvents and their low R_a value.

	δ_D	δ_P	δ_H	R_a
Lignin	**21.9**	**14.1**	**16.9**	**-**
Water	15.5	16	42.3	28.5
Acetone:water 30:70	15.5	14.3	31.7	19.6
Ethyl acetate	15.8	5.3	7.2	17.9
MEK	16	9	5.1	17.4
1,4-Dioxane	17.5	1.8	9	17.1
Acetone	15.5	10.4	7	16.6
Dioxane:water 95:5	17.4	2.5	10.7	15.9
Methanol	14.7	12.3	22.3	15.5
Acetone:water 60:40	15.5	12.6	21.1	13.6
DMF	17.4	13.7	11.3	10.6
DMSO	18.4	16.4	10.2	10

5.4 FTIR analysis points out general functionality content trends

5.4.1. Organic solvent fractionation

5.4.1.1. Successive fractionations

A band assignation chart was drawn from literature [3], [32], [61]–[63] and can be found in **appendix II**.

Spectra were recorded in between successive dissolutions, in order to compare soluble lignin to insoluble lignin at each step of the fractionation. In the following discussion, the soluble fraction of lignin in solvent 1 is called F1, and the solid residue is called F1C (for complementary); F2 and F2C for solvent 2, and so on.

DPL-F1 and BL-F1 showed similar band reductions and increases (**fig. 31**). DPL-F1C and BL-F1C did too. In F1, the 1030 cm^{-1}, and the 3300 cm^{-1} bands decreased; the 1115, 1200, 1500, 1850 and 2950 cm^{-1} bands increased. Complementarily, F1C showed an increase of the 3300 cm^{-1} band, and a decrease for the 1115, 1215, 2850 and 2950 cm^{-1} bands. Since the 1000-1100 cm^{-1} region was attributed to C-O stretching vibrations (ether, alcohol, carbonyl) and the 3300 cm^{-1} broad peak to O-H stretching, we hypothesized that ethyl acetate could less solubilize those kinds of oxygen-bearing functions. The intensity changes in the following complementary spectra (F2/F2C, F3/F3C) are summarized in **tab. 8**, and confirm this first hypothesis: low polarity, non-oxygenated parts of lignin seemed to have dissolved in ethyl acetate, while two characteristic bands of higher polarity ether and alcohol diminished. BL displays the same kind of behavior.

Table 8 Summary of increases and decreases for F1 to F3 for DPL. Upward arrow: increase in intensity. Downward arrow: decrease in intensity.

Band (cm⁻¹)	3300	2925	2850	1702	1500	1215	1115	1032
Attribution	O-H vibration	C-H stretching vibration	C-H of aromatics OCH3 stretching vibration	unconjugated C=O Stretching	Aromatic stretch	C-C alkane stretching	Aromatic stretch	C-O + O-H vibration
DPL-F1	↘	↗	↗	↗	-	↗	-	↘
DPL-F1C	↗	↘	↘	-	-	↘	↘	-
DPL-F2	-	↗	-	↗	↗	↗	-	↘
DPL-F2C	-	↘	↘	-	-	↘	-	-
DPL-F3	-	↗	↗	-	-	↗	↗	↘
DPL-F3C	↗	↘	-	↘	↘	↘	-	-

Figure 31 Comparative spectrum of DPL (in grey), F1 (in red) and F1C (in blue).

5.4.1.2. Total comparative spectra

The total comparative infrared analysis of the five fractions of **DPL** allowed us to highlight three experimental observations: (a) the increased 3200 cm-1 band, (b) the progressive diminution of the 1700 cm^{-1} band and (c) the pattern differences between the fractions in the 1000-1300 region cm^{-1} (those three points are illustrated in **fig. 32, fig. 33, fig. 34**).

(a) The INS fraction had a more intense 3200 cm^{-1} band than the four other fractions. This band was assigned to hydroxyl vibrations. The larger intensity of the alcohol band was exclusive to DPL. Comparative spectra of BL and HL (**Appendix II**) did not show this larger intensity. We inferred from this data that the organic solvents we used could not significantly dissolve hydroxyl-rich fractions.

(b) The relative intensity of the 1700 cm^{-1} band decreased with successive dissolutions. In other words, relative intensity went as such: F1 > F2 > F3=F4 > INS. We assigned the band to
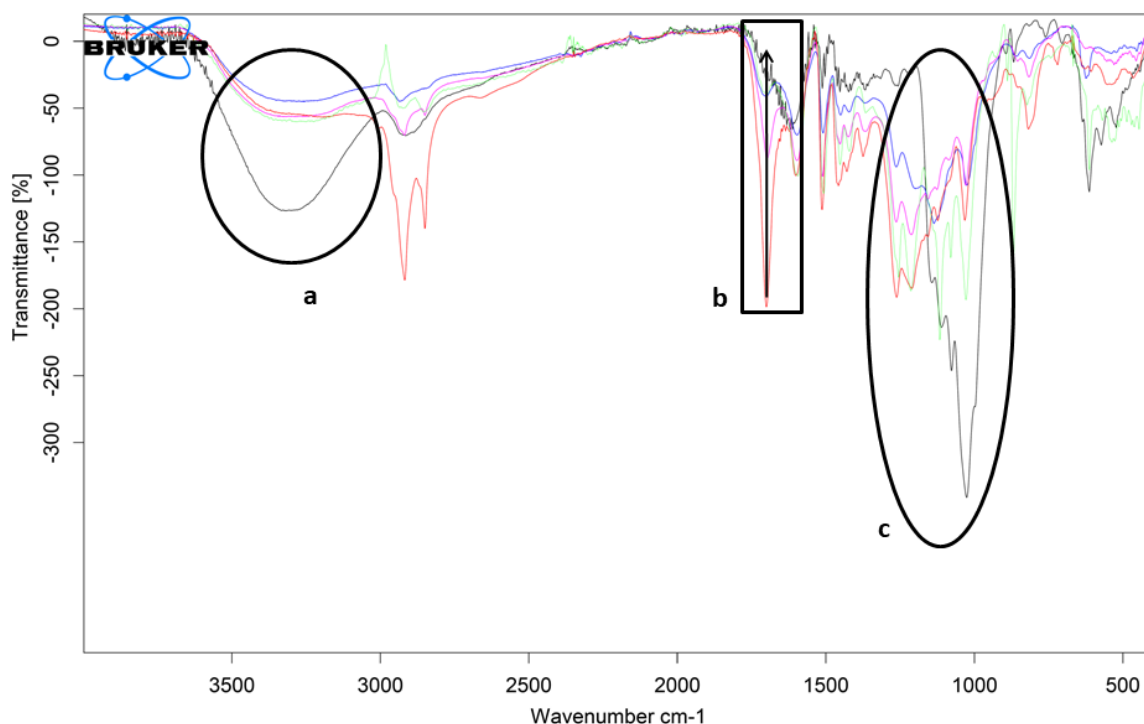
Figure 32 Comparative spectrum of the five soluble organic solvent fractions of DPL: F1 in red, F2 in pink, F3 in blue, F4 in green and INS in black.
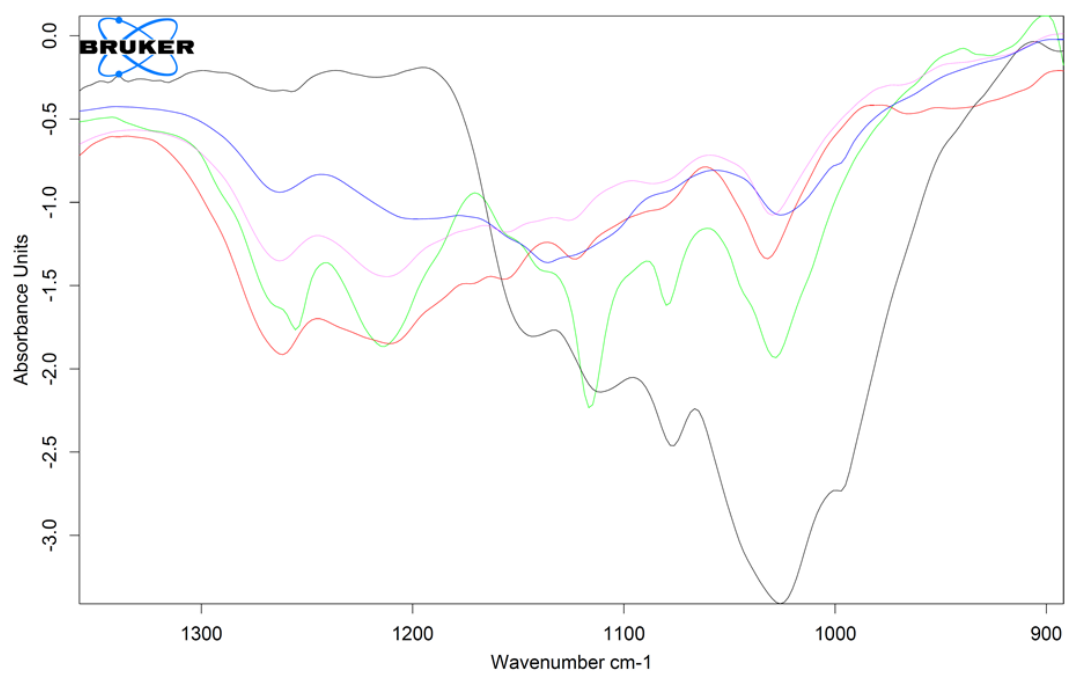
Figure 33 Zoom on zone « c » of **figure 32**. Comparative spectrum of the five soluble organic solvent fractions of DPL: F1 in red, F2 in pink, F3 in blue, F4 in green and INS in black.
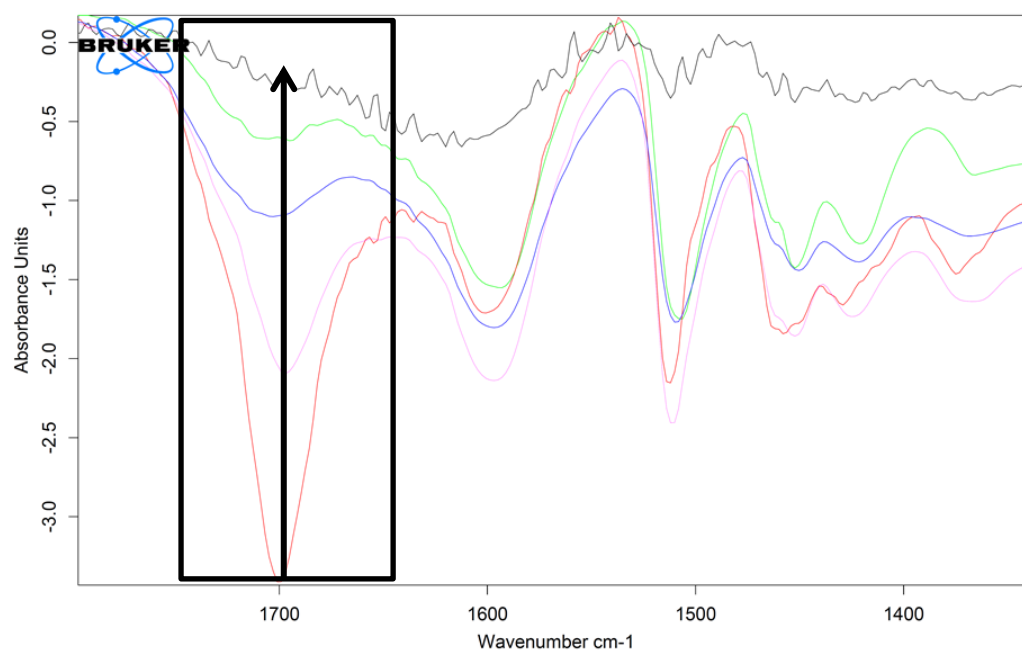
Figure 34 Zoom on zone « b » of **figure 32**. Comparative spectrum of the five soluble organic solvent fractions of DPL: F1 in red, F2 in pink, F3 in blue, F4 in green and INS in black. The arrow highlights the reduction of the 1700 cm^{-1} band.

unconjugated carbonyl stretching, which are mostly present in ester, ketone, aldehyde and carboxylic acid bonds. We had two hypotheses to explain this observation. First, we thought it might be that free aldehydes and aldehyde-rich lignins were selectively extracted from lignin by ethyl acetate and to a lesser extent by MEK. Since lignin monolignols are synthesized from aldehydes [7] and can sometimes polymerize under their aldehyde form [64], we found this explanation reasonable. To test this hypothesis, we did a Schiff test on all our lignin samples to specifically reveal the presence of aldehydes. All tests were negative, indicating the absence of aldehydes.

Our second hypothesis was that the presence of the 1700 cm^{-1} band, and its progressive diminution, was caused by the presence of numerous carboxylic acid moieties. We inferred this hypothesis from NMR data, which revealed that 33% of all hydroxyls in DPL-F1 were carboxylic acid hydroxyls. The NMR data also showed that the carboxylic acid proportion steadily diminished between F1 and F4, just as the 1700 cm^{-1} band steadily diminished in FTIR data between F1 and F4. The crosscheck between FTIR and NMR data suggests that this hypothesis is sounder than the aldehyde hypothesis.

(c) We noticed that the 1000-1200 cm^{-1} region contained very different band patterns for all fractions. F1, F2 and F3 did not have any intense absorbance in this region, except a medium intense band at 1030 cm-1. This last band appeared to be the most significant. We attributed it to C-O and O-H stretching, meaning the two last fractions, F4 and INS, should contain a lot of ether bonds and hydroxyls.

One possible explanation for the intensity of the 1030 cm^{-1} band of INS could be that we under evaluated the carbohydrate content by the Klason method. The NMR data of DPL-INS was not collected because the powder was not soluble enough in the NMR reaction mixture. Confirmation and quantification of ether and hydroxyl quantities in DPL-INS could be achieved in solid-state NMR (SSNMR) [65] since it does not require solubilization. In this NMR method, each carbon has a different chemical shift according to its type of bonding. Ether bonds could hence be directly observed.

In the **BL** total comparative spectrum (**Appendix II**), we noted the presence of a band at 1700 cm^{-1} for F1, F2, F3 and for its absence in INS. This furthers the point made for DPL that carbonyl-bearing lignins dissolve first in the fractionation sequence. To ensure that these large intensities for the 1700 cm^{-1} peaks of F1 in DPL and BL were not caused by solvent contamination, we compared the solution spectra with the solvent spectra. We observed that

ethyl acetate and MEK displayed a carbonyl peak at higher wave numbers, around 1750 cm^{-1}, suggesting our samples were not contaminated since their carbonyl band was displayed at 1700 cm^{-1}. The **HL** total comparative spectrum (**Appendix II**) had some similar features to BL and DPL: 1700 cm^{-1} band larger intensity for the first fractions, 1030 cm^{-1} band larger intensity for the last fractions.

5.4.1.2 Acetone/water mixtures fractionation

We noticed a feature on the comparative spectrum of the three fractions of **DPL** (**fig. 35**) which seemed to display an opposite trend to organic solvent fractionation. In SA1, the 1030 cm^{-1} band had increased intensity, while SA2 and SA3 had bands increase in the 1200-1500 cm^{-1} zone, as well as the 1700 cm^{-1}. **BL** showed another kind of intensity proportions for these two regions: SA1 had a more intense 1030 cm^{-1} band, SA2 a more intense 1200-1500 cm^{-1} region, and SA3 seemed to have the same intensity for the two (**fig. 36**). Using our
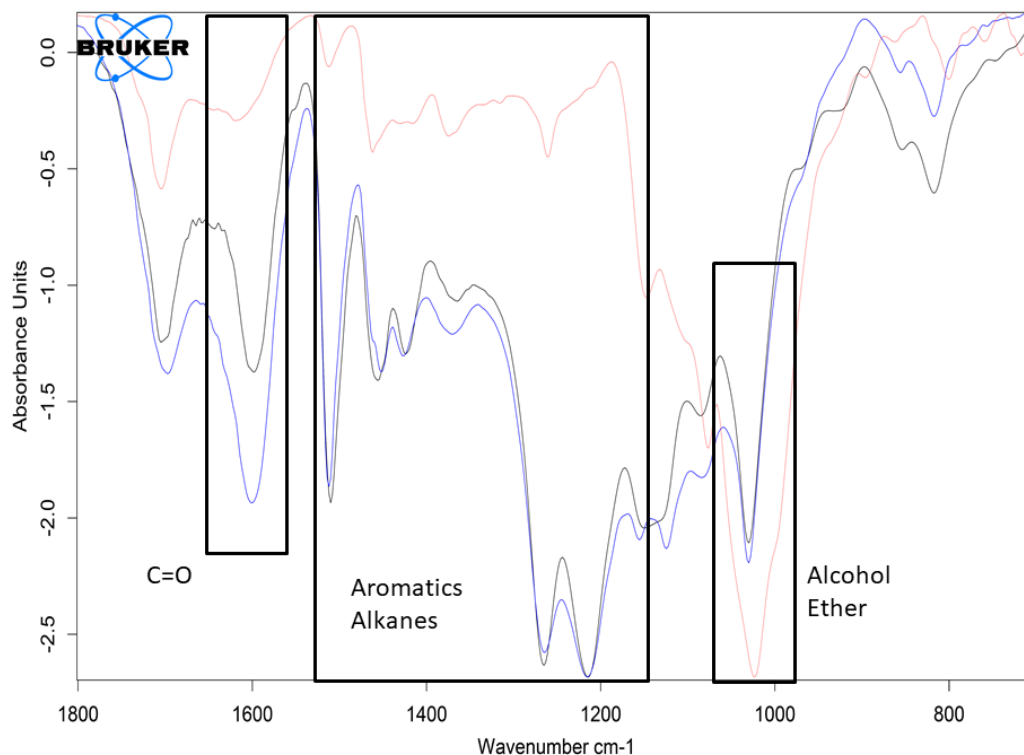
Figure 35 Comparative spectrum of the three acetone/water fractions of DPL: SA1 in red, SA2 in black and SA3 in blue.
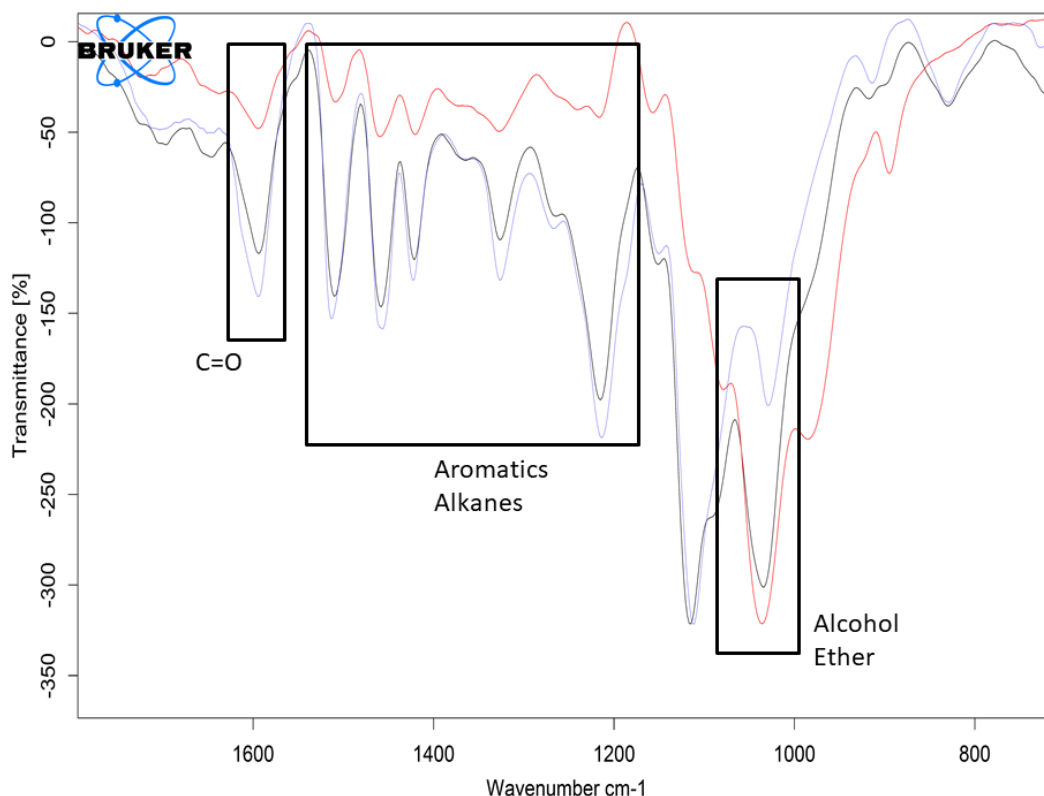
Figure 36 Comparative spectrum of the three acetone/water fractions of BL: SA1 in red, SA2 in black and SA3 in blue.

predefined assignations, we inferred that for DPL, SA1 contained larger amounts of ether/alcohol functions, while SA2 and SA3 contained more alkane/aromatics functions. For BL, the same observations were made, but we could also infer that SA3 contained intermediate proportions of ether/alcohol to alkane/aromatics between SA1 and SA2 because of the relative intermediate intensities of the bands. Compared with BL and DPL, **HL** acetone/water fractionation did not seem to work at all (**Appendix II**). There were no significant intensity increases or decreases. This non-discrimination was supported by fraction proportions: ~10% of HL dissolved in the first solvent, and ~10% in the second; 80% remained non dissolved. In terms of Hansen parameters, this probably meant that HL had more dispersive interactions, as, for example, if it was enriched in aromatics compared to oxygen-containing moieties. This crosschecked the NMR data that showed that 60% of HL detected hydroxyls were phenolic, versus 40% for DPL and 35% for HL.

5.4.1.3. pH fractionation

HL total comparative spectrum displayed three distinct features (**fig. 37**). First, SH1 showed an increased 3300 cm^{-1} hydroxyl band. Secondly, SH1, SH2 and SH3 showed a medium intense, a weak, and no band at 1700 cm^{-1} (assigned to carbonyls), respectively. Thirdly, the aromatic peaks between 1200 and 1500 cm^{-1} were very similar in intensity.

Assuming the third observation is correct, and that the aromatic content of the three fractions is the same, then we can conclude that the carboxylic acid content (proportional to the C=O 1700 cm^{-1} band intensity) decreased from SH3 to SH1; and that SH1 contained the majority of phenol-rich lignins. This hypothesis seemed correct because it was supported both by pKa considerations and by NMR data. The fraction that precipitated at pH = 8 (SH1) were the ones
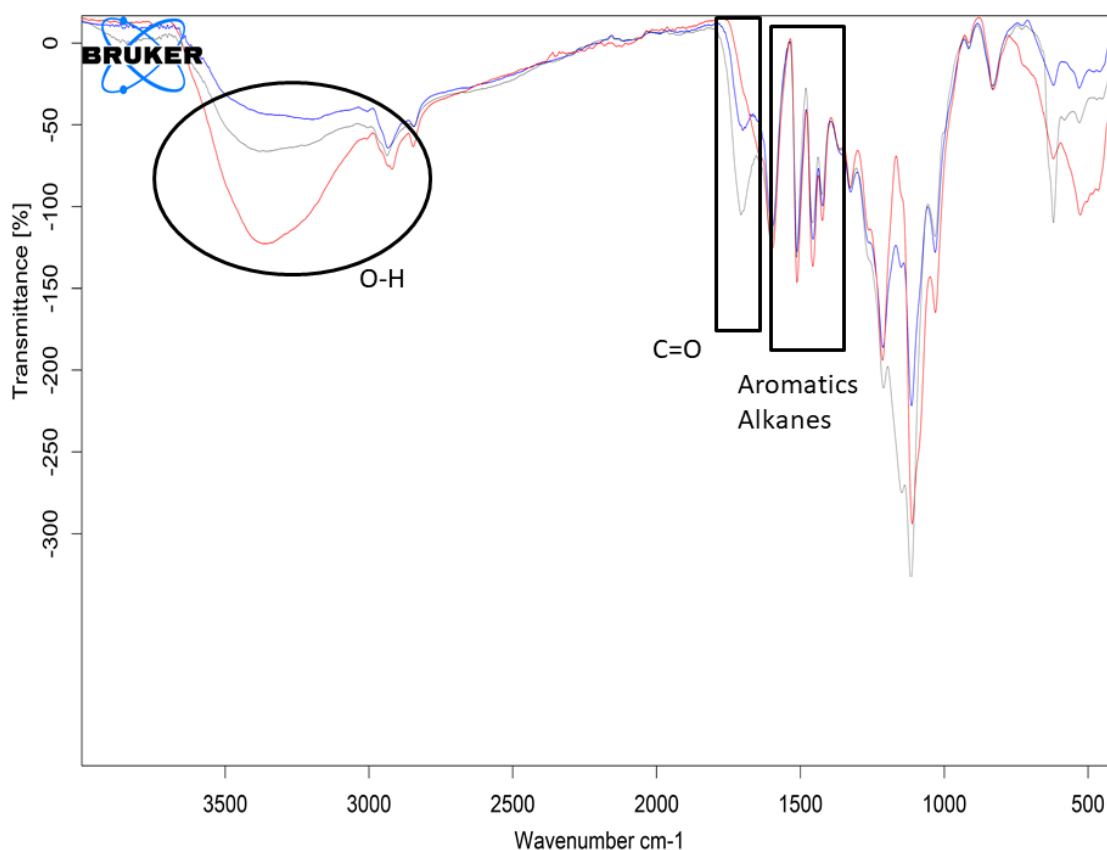
Figure 37 Comparative spectrum of the three pH fractions of HL: SH1 in red, SH2 in grey and SH3 in blue.

containing more phenols with a higher pKa, while the ones that precipitated at pH = 2 (SH3) were the ones containing more carboxylic acids which have a lower pKa. Moreover, in NMR, the phosphitylation of hydroxyl functionalities showed that COOH content increased from SH1 to SH3, corroborating this hypothesis.

As for the two other types of lignin, **BL** displayed exactly the same kind of behavior (not shown). **DPL** proportions of SH1 and SH2 (<1%) did not allow us to carry out FTIR measurements on them.

5.4.1.4. Sonication and ball-milling

Comparison of sonicated and non sonicated samples did not indicate any significant changes in the three samples **(Appendix II)**, which could mean that the sonication did not work. If it did work, we can affirm that it did not affect the functionalities of lignin. Since the polymerization of lignin demanded the condensation of a phenol moiety with an aromatic part or an alkene part of another lignin molecule, and that phenols do not have any specific IR band, polymerization could not be accurately assessed by FTIR. As for ball-milling, the samples did not show any significant changes **(Appendix II)**, whatever the ball-milling times. These negative results support the hypothesis that sonication and ball-milling do not affect the functionality content of the samples.

5.5. HPSEC analysis shows molecular weight fractionations did work

The HP-SEC technique is often used to characterize the molecular weight of polymers. It relies on a simple concept: the hydrodynamic volume, i.e. the average volume that the polymer takes up in a given solvent, is proportional to the molecular weight of the polymer. Therefore, when passed onto a size-excluding resin, large molecules are eluted first, and small molecules last.

This technique has two major hurdles: (a) it is not appropriate for lignin absolute molecular weight determination and (b) it is dependent on lignin solubility.

(a) There are no available and reliable lignin standards to calibrate the elution time-molecular weight relationship. Thus, we had to choose a similar standardized polymer. The polymer that had the most alike structure was polystyrene, because of its benzene rings. However, polystyrene is a linear, non-reticulated, carbonated homopolymer whereas lignin is an oxygen-bearing cross-linked heteropolymer: they are not comparable. The obtained results are thus expressed in polystyrene-equivalent; they are appropriate to compare the molecular weights of two samples of lignin, not to assess their absolute molecular weight.

(b) Alkaline-extracted lignin is a mixture of structurally different phenylpropane heteropolymers. Its solubility is thus unusual, some fractions being more soluble than others in some solvents. HPSEC only analyses soluble fractions. Therefore, if a lignin fraction is insoluble in the HPSEC solvent, it will not be observed; this is often the case for high molecular weight fractions. Therefore, we had to bear in mind that any insoluble fraction would not be observed by this technique.

Researchers often acetylate lignin in order to enhance solubility in HPLC solvents (DMF, THF or dimethylacetamide, DMAc) [66]. Since acetylation is a time-costly operation and that our samples seemed to solubilize well in DMF, we checked whether acetylation was necessary or not by comparing HPSEC-DMF spectra of DPL and acetylated DPL, as well as BL and acetylated BL. The spectra showed no differences in retention time. Thus, we analyzed all samples without acetylation.

Firs, we observed that in all tested samples, the measured polystyrene-equivalent molecular weights were higher in DMF than in water. Two reasons might explain this. First, DMF is a way better solvent than water for lignin. It allows lignin to be stable while spread out. The Hansen theory R_a of DMF is one of the smallest of organic solvents towards lignin. Secondly, in DMF, we added 0,5% (m:v) of LiCl. We could not add it in water, because it formed the corrosive salt LiOH that would have attacked the HPSEC column. LiCl was added to cancel the intra- and inter-molecular weak bonds such as hydrogen bonds or π-π stacking. This might be one of the factors that caused the larger values of M_n and M_w of lignin in DMF: the chains were much more spread out. **Tables 9, 10 and 11** (pp. 72-74) summarize all results.

For DPL (**tab. 9, fig. 38)** and BL (**tab. 10**), the **solvent fractionation** revealed a steady increase in molecular weight going from F1 to INS**.** The same experimental observations were noted for HL and BL, both in DMF and in alkaline water (**tab. 10, tab. 11**). The only odd results were DPL-INS in alkaline water and HL-INS in DMF: they did not follow the general trend and displayed lower polystyrene-equivalent molecular weights.
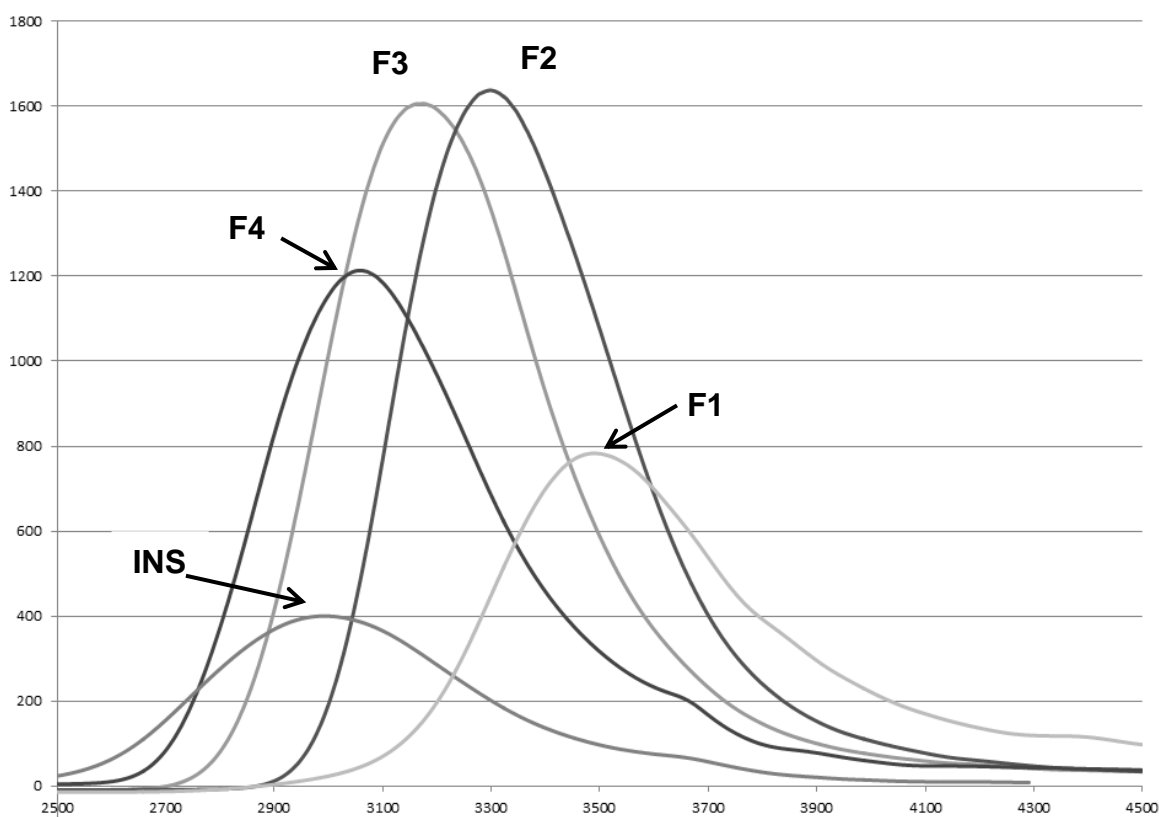
Figure 38 Comparative chromatogram of DPL fraction F1 to INS. X-axis: retention time, in 10^2 min. Y-axis: UV absorbance at 269 nm, arbitrary units.

The general trend could be explained by the simple fact that low molecular weight lignins are intrisically more soluble: their hydrodynamic volume is smaller, hence, their surface to bulk ratio is higher and they solubilize first, whatever the solvent. Given the Hansen solubility parameters of all our solvents, following no particular order, functionality-driven solubilization did not seem to be the prime factor. The oddity of the INS fraction could not be explained. It illustrated nicely the inherent problem cited in at the beginning of this section: HPSEC is not appropriate to analyze reticulate polymers, because their hydrodynamic volume varies greatly between solvents. The only pieces of information we can infer from this data is that the highest hydrodynamic volume of all DPL fractions is INS in DMF and F4 in water. Similarly, the highest hydrodynamic volume of all HL fractions in DMF is F4 and INS in water.

For **acetone/water mixtures fractionation**, we observed the same trend as for organic solvent fractionation (**tab. 9, 10, 11**): increase of M_n and M_w from DPL-SA1 to SA3, with a steady PDI. Lower molecular weight fractions hence dissolve first. Unlike organic solvent fractionation, we can here use the Hansen solubility parameters because they follow a clear trend: the two acetone/water solvents a have equivalent dispersive parameter values, and acetone:water 3:7 displays greater hydrogen bonding and dipole-dipole interactions parameters than acetone:water 6:4. Therefore, the acetone:water 3:7-soluble lignins must contain more hydrogen-bonding and polar functionalities, such as hydroxyls, acids, esters and ketones. This hypothesis is corroborated by FTIR data: comparative spectra of DPL and HL (**fig. 31 and Appendix II**) show higher C-O/aromatics and O-H/aromatics ratios for SA1 than for SA3 and SA3. For **pH fractionation**, we saw that M_n and M_w decreased with the decrease of pH. PDIs were comprised between 1.5 and 2.5, thus a little bit higher than in organic solvent fractionations.

We observed the same kind of low molecular weight solubility: the smaller molecules were more soluble, thus precipitated last (at the most acidic pH). This result seemed to show that molecular weight and functionality content were uncorrelated when it came to solubility. Fraction proportions, FTIR and NMR data showed that SH1, SH2 and SH3 for the three lignin samples contained significant amounts of hydroxyls and carboxylic acids. Those amounts determined when each type of fraction would precipitate (before pH =8, at pH = 5 or at pH = 2). Here, HPSEC results did not seem to be influenced by these functionalities: larger molecules, less soluble, precipitated first, independently from their acid/hydroxyls contents.

Sonication of an alkaline solution of lignin was tested because it allegedly repolymerized lignin. The cavitation induced by the sonic probe should have released enough energy in the solution to generate radicals, which would induce polymerization in lignin [67]. The results for BL and DPL, both in DMF and water, showed an increase of M_n and M_w of approximately 20-30%. This result seems to show that repolymerization is possible and that the method works. A technique that could corroborate this result is HSQC ^{13}C-^{1}H 2D-NMR: each carbon has a different signal according to its type of bonding [65]. Comparison of HSQC peaks from non- sonicated and sonicated samples could indicate if the number of linkages has increased, confirming repolymerization.

We tried **ball-milling** the lignin samples to determine if physical grinding could depolymerize lignin. No significant molecular weight changes were observed. 158h-ball-milled DPL lignin sample showed higher molecular weight, not lower. 36h-, 72h-, and 108h-ball-milled samples of HL and BL displayed diminished molecular weights (20-30% reduction) in DMF but no changes after 36h of ball-milling. In water, for BL, there was no change at all. We did not investigate the oddity of the DPL sample, because it seemed to have been contaminated with an unknown substance in FTIR. These results could be explained by grain thickness. Ball-milling might not have caused depolymerization, but rather a shrinking in lignin grain sizes, causing the lignin to be more impregnated with solvent, thus more unfolded in solution. Since the HPSEC method measures hydrodynamic volume, and not absolute molecular weight, this could be a reasonable explanation. Confirmation or invalidation could arise from molecular weight measurement techniques that do allow an estimation of the absolute M_n, such as viscosimetry [68], osmotic pressure measurement or light scattering [69].

Our polystyrene calibration curve can be found in **Appendix III**.

Table 9 Number average molecular weight (M_n), mass average molecular weight (M_w) and polydispersity index (PDI) for the fractions of DPL. n.a.: non acquired. Mp: multiple peaks.

	M_n		M_w		PDI	
	DMF	*H_2O*	*DMF*	*H_2O*	*DMF*	*H_2O*
DPL	30000	3300	74000	5100	2.44	1.53
DPL-F1	13000	2100	22000	3000	1.70	1.41
DPL-F2	25000	2600	34000	3500	1.4	1.37
DPL-F3	39000	4200	54000	6000	1.4	1.43
DPL-F4	54000	5400	78000	850	1.46	1.57
DPL-INS	76000	9900	127000	22000	1.67	2.19
DPL-SA1	21000	Mp	33000	Mp	1.57	Mp
DPL-SA2	30000	3500	50000	5400	1.64	1.54
DPL-SA3	38000	3800	58000	6200	1.54	1.63
DPL-SH1	60000	n.a.	130000	n.a.	2.19	n.a.
DPL-SH2	36000	n.a.	88000	n.a.	2.43	n.a.
DPL-SH3	44000	n.a.	68000	n.a.	1.56	n.a.
DPL-S45	38000	3702	104000	5700	2.75	1.53
DPL-BM156	58000	n.a.	103000	n.a.	1.77	n.a.
DPL-ACET	25000	n.a.	47000	n.a.	1.87	n.a.

Table 10 Number average molecular weight (M_n), mass average molecular weight (M_w) and polydispersity index (PDI) for the fractions of BL. n.a.: non acquired. Mp: multiple peaks.

	M_n		M_w		PDI	
	DMF	*H_2O*	*DMF*	*H_2O*	*DMF*	*H_2O*
BL	29000	3000	54000	4500	1.85	1.57
BL-F1	11000	n.a.	16000	n.a.	1.45	n.a.
BL-F2	21000	2000	30000	3200	1.42	1.56
BL-F3	33000	3000	45000	4500	1.38	1.49
BL-F4	53000	5000	74000	7900	1.41	1.53
BL-INS	74000	Mp	114000	Mp	1.55	Mp
BL-SA1	21000	n.a.	68000	n.a.	3.23	n.a.
BL-SA2	65000	n.a.	145000	n.a.	2.25	n.a.
BL-SA3	21000	n.a.	3500	n.a.	1.7	n.a.
BL-SH1	41000	n.a.	75000	n.a.	1.85	n.a.
BL-SH2	31000	n.a.	55000	n.a.	1.77	n.a.
BL-SH3	16000	n.a.	35000	n.a.	2.25	n.a.
BL-S45	36000	n.a.	62000	n.a.	1.74	n.a.
BL-BM36	20000	n.a.	35000	n.a.	1.75	n.a.
BL-BM72	23000	n.a.	45000	n.a.	1.97	n.a.
BL-BM108	21000	n.a.	35000	n.a.	1.69	n.a.
BL-ACET	31000	n.a.	51000	n.a.	1.63	n.a.

Table 11 Number average molecular weight (M_n), mass average molecular weight (M_w) and polydispersity index for the fractions of HL. n.a.: non acquired

	M_n		M_w		PDI	
	DMF	*H₂O*	*DMF*	*H₂O*	*DMF*	*H₂O*
HL	29000	2900	49000	5000	1.69	1.72
HL-F1	n.a.	1900	n.a.	3300	n.a.	1.7
HL-F2	n.a.	2400	n.a.	3400	n.a.	1.41
HL-F3	31000	3600	45000	5000	1.46	1.39
HL-F4	54000	5800	78000	9100	1.44	1.57
HL-INS	18000	7900	28000	14600	1.59	1.85
HL-SA1				n.a.		
HL-SA2				n.a.		
HL-SA3				n.a.		
HL-SH1	21000	3500	32000	5600	1.51	1.6
HL-SH2	13000	3200	17000	4600	1.30	1.43
HL-SH3	7500	2500	14000	3300	1.84	1.31
HL-S45				n.a.		
HL-BM36	17000	3000	32000	4700	1.92	1.57
HL-BM72	16000	3000	28000	4700	1.78	1.57
HL-BM108	16000	3000	28000	4700	1.81	1.57
HL-ACET				n.a.		

5.6. NMR analysis reports changes in oxygen-bearing moieties contents

The selective reaction between lignin hydroxyls and 2-chloro-4,4,5,5-tetramethyl-1,3,2-dioxaphospholane (TMDP) in $CDCl_3$/pyridine creates phosphite moieties. In these, the phosphorus atom has a different chemical shift depending on the kind of alcohol it reacted with: guaiacyl G, *p*-hydroxyphenyl H, syringyl S, aliphatic or carboxylic acid. The integration of the peaks (**fig. 39**), compared to an internal standard (cyclohexanol), gives us the relative proportions of each type of hydroxyl.

We emphasize the fact that the relative proportions of aliphatic, aromatic and carboxylic acid hydroxyls are biased, because the only detectable aromatic hydroxyls are the ones that have not polymerized, thus, the end-chain aromatic hydroxyls. Hence, the ratio aliphatic:acid is correct, but the aromatic units content is greatly underestimated. The "aromatic hydroxyls" described here should be understood as "end-chain aromatic hydroxyls". Still, the ratio G:H:S is correct, because it compares aromatic hydroxyls to other aromatic hydroxyls. **Fig. 40** shows the peak assignments.
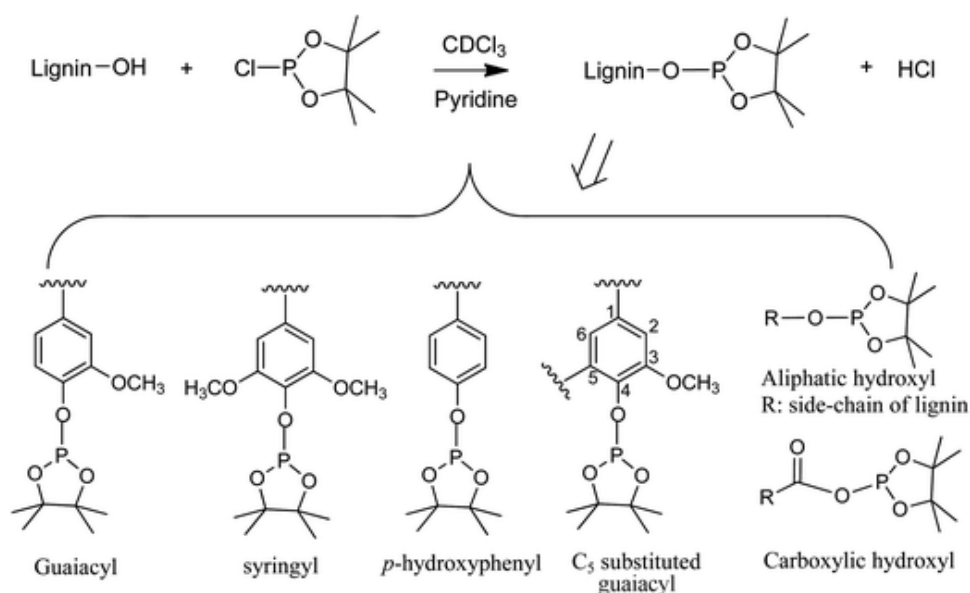
Figure 39 Reaction between a lignin hydroxyl and TMDP to generate a phosphityl moiety. The phosphorus atom linked to the hydroxyl hydrogen displays a different chemical shift depending on the type of hydroxyl it reacted with [76].
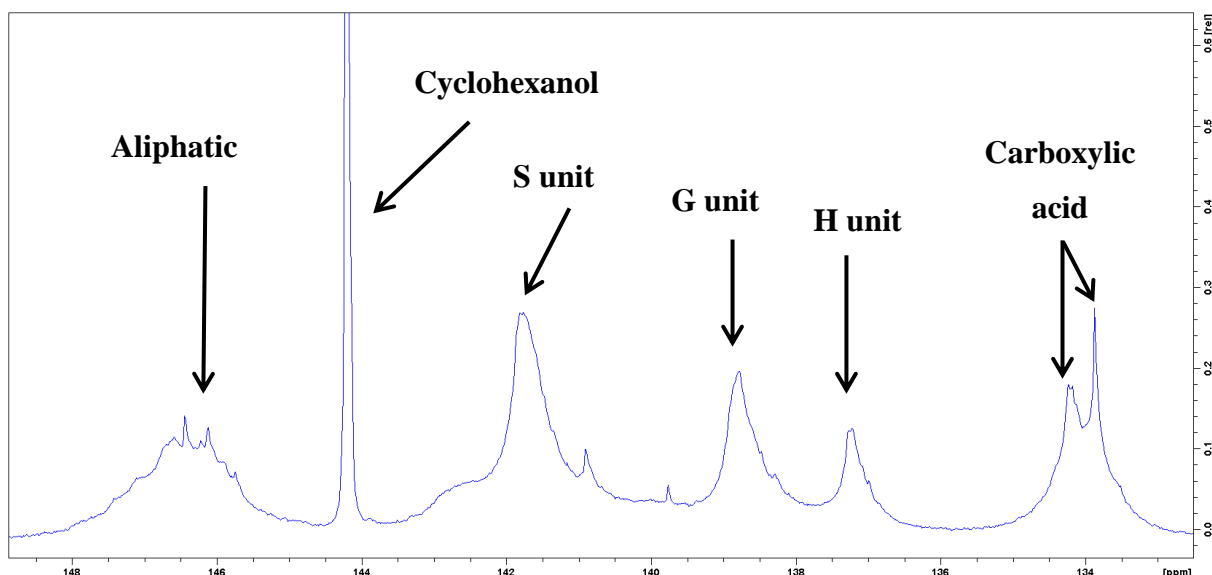
Figure 40 ^{31}P NMR spectrum of HL. Each peak is assigned to a type of hydroxyl. X-axis: chemical shift, in ppm. Y-axis: relative intensity, arbitrary units.

For **DPL**, as expected, we observed a major peak for G unit, and a minor peak for the H unit. The integration revealed a G:H 7:3 ratio. As for the aliphatic:aromatic:carboylic acid ratio, we found a 4:4:2 ratio (see **tab. 12** for percentages). During organic solvent fractionation, the relative quantity of aliphatic alcohol increased from 19% to 50% of the total, while the relative carboxylic acid hydroxyl quantity decreased from 33% to 10%. These changes could not be explained rationally by Hansen parameters: the chosen solvents did not display any logical sequence in any of the three Hansen spatial dimensions. They were chosen empirically to fractionate lignin according to molecular weight. Still, we inferred from the increase in aliphatic alcohol that the molecular weight increased, confirming HPSEC data. The aliphatic alcohols were mostly present in β-O-4 linkages. The relative proportion of aliphatic alcohol thus indicated that there were more bonds in DPL-F4 than in DPL-F1.

For BL, we could not measure SA1 because it was too insoluble in the reaction mixture. We witnessed that BL had a higher relative aliphatic hydroxyl content than DPL and HL, and lower carboxylic acid content. We hypothesized that aliphatic hydroxyls indicated a higher number of linkages, but that would not crosscheck with HPSEC data, which showed that the three types of lignin had roughly the same size. BL-SA1 data is needed for any further analysis. For HL, we saw that the relative abundances of aliphatic hydroxyls decreased between SH1 and SH3, whereas the carboxylic acid relative abundance increased. As we already crosschecked in the FTIR section, fractionation yields, FTIR and NMR data agree on

the functionality content of the SH1-SH2-SH3 fractions. SH1 was rich in hydroxyls and poor in acids, and SH3 was rich in acids, and poor in hydroxyls.

Since we had solubility problems for at least 20% of our samples, and that some did not dissolve at all, like BL-SA1, we tried a different method. The reaction mixture to analyze the lignin samples contains $CDCl_3$, pyridine and DMF in equivolume proportions. Pyridine is needed for the phosphitylation to occur. $CDCl_3$ provides the deuterated signal for the NMR machine to lock and shim (i.e. "calibrate") the magnets. DMF is added to help solubilize lignin. Since $CDCl_3$ is a poor lignin solvent (Hansen R_a = 17,7) and DMF a good lignin solvent (Hansen R_a = 10,2), we tried replacing $CDCl_3$ with deuterated DMF. The resulting spectra displayed peaks that had a higher S/N ratio, and were better resolved. A mixture of d7-DMF and pyridine thus seemed to be a better solvent for lignin analysis, and could be an alternative for low solubility samples. The disadvantage is that DMF-d7 (41$/g) [70] is way more expensive than $CDCl_3$ (<1$/g) [71].

Table 12 Relative proportions of aliphatic alcohol, H, G and S phenol, and carboxylic acid hydroxyls. The arrows show opposite increases between aliphatic and carboxylic hydroxyls.

	Aliphatic alcohol (%)	Phenol (%)				Carboxylic acid (%)
		S	G	H	Total	
DPL	40	0	71	29	40	19
DPL-F1	19	0	71	29	48	33
DPL-F2	30	0	66	34	51	18
DPI-F3	49	0	70	30	37	14
DPL-F4	50	0	70	30	40	10
BL	60	74	26	0	36	4
BL-SA1	-	-	-	-	-	-
BL-SA2	51	76	24	0	42	7
BL-SA3	58	93	7	0	37	5
HL	22	58	29	13	63	15
HL-SH1	23	59	29	12	69	8
HL-SH2	21	57	30	13	60	19
HL-SH3	15	56	30	14	59	26

5.7. SEM shows diverse structures in lignin fractions and inhomogeneity in electrode film

5.7.1. Lignin fractions show diverse microstructures

The microstructures of pristine lignin fractions were investigated by SEM. The aim was to collect pieces of information about the impact of the fractionation technique on the aggregation and structure of lignin particles.

First, we observed different microstructures between three organic solvent fractions of DPL. F4 and F2 (not shown) displayed aggregates with sizes ranging from 1 to 100 µm, with no preference for a certain size, while F3 showed smaller, 2-4 µm needle-shaped particles at the surface of the aggregates (**fig. 42**). F3 was the fraction soluble in methanol, and IR results showed that this fraction was enriched in aromatic units, and depleted in C-O bonds. This disparity might have caused the formation of needle-like structures. This last result could display enhanced electrochemical performances: other authors [49] showed the interest of fiber-like porous carbons to increase surface area, with success.

Second, sonication seemed to produce 10-100 µm agglomerates of 1-10 µm sheet-like particles. These sheet-like particles were also witnessed in HL pH-fractionated samples (**fig. 43**). It could mean that the acidic precipitation of lignin tends to produce sheet-like microstructures, which can be altered when the lignin was dissolved in organic solvents. A systematic SEM analysis of all the samples could confirm or invalidate this hypothesis.

Third, it appeared that, for HL, the SH3 fraction (**fig. 43**) was more porous than the SH1 fraction (**fig. 41**), which could result in higher electrochemical performances: carbon beads could be more inserted into the lignin particles, allowing better conductivity and increased pseudo-capacity.
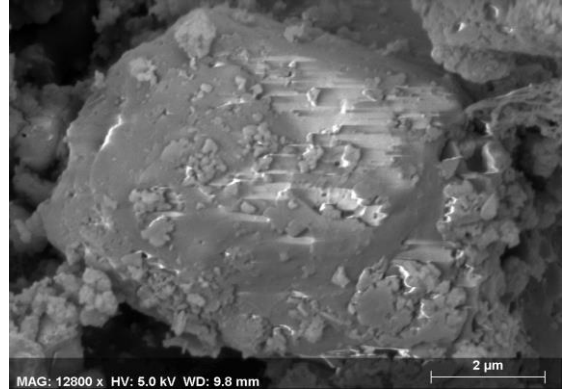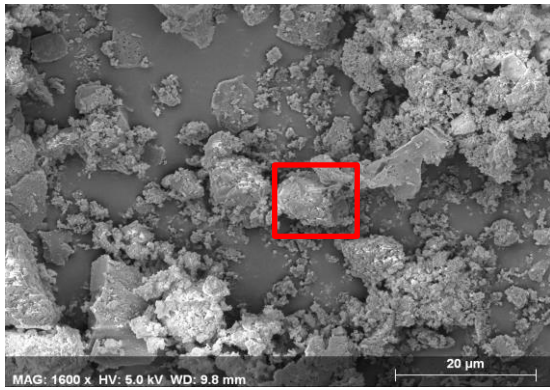
Figure 41 SEM pictures of HL-SH1. The picture on the right is a 10-fold zoom of the red rectangle in the left picture.
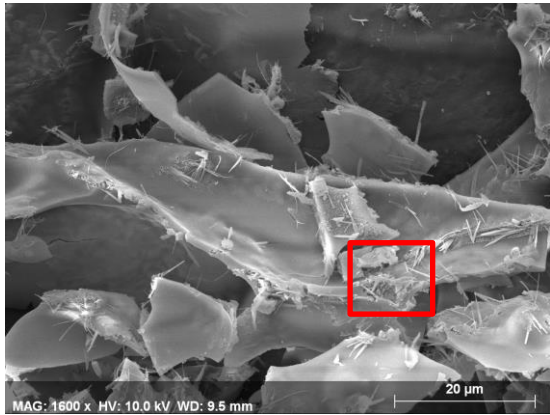
Figure 42 SEM pictures of DPL-F3. The picture on the right is a 10-fold zoom of the red rectangle in the left picture.
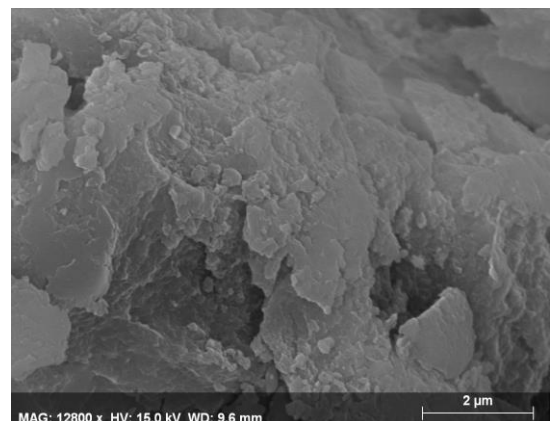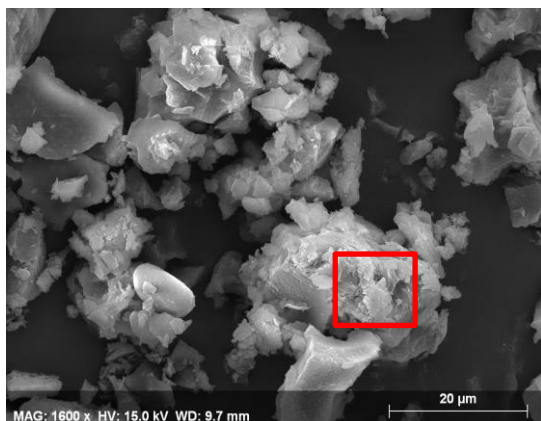
Figure 43 SEM pictures of HL-SH3. The picture on the right is a 10-fold zoom of the red rectangle in the left picture.

5.7.2. Lignin films are made of lignin particles embedded in carbon matrix

SEM pictures of lignin-carbon films were taken. Films (15% lignin, 75% carbon, 10% PVDF) were made from DPL, BL and HL, as well as repolymerized DPL, labelled DPL-S45, in order to witness the microstructure and compare any structural differences between the four samples. We observed lignin particles dispersed into a carbon matrix (**fig. 44**). The particles were either sitting on top of the matrix (**fig. 45**) or partially embedded in it. Lignin particle sizes ranged from 1 to 100 μm, without any preference for a certain size. We did not see any significant differences between the microstructures of DPL, BL, HL and DPL-S45.The lignin-carbon films that were described by Chalewaert-umpon and coworkers [9], [11] suggested that mixing the two powders with a binder (PVDF or glyoxal) in NMP would lead to the deposition of a thin film of lignin into the pores of activated carbon. The authors discussed the order in which the three reactants (lignin, carbon, binder) ought to be mixed (**fig. 47**) and concluded that the binder should be added after the mixing of lignin and carbon.

We did not observe the same kind of microstructure than Chalewaert-umpon's (**fig 46**) [9]; that is, <0,5 μm particles of lignin covered with a thin layer of carbon. Instead, we saw >5 μm particles of lignin, covered with beads of activated carbon or embedded in the carbon matrix. The major difference between their results and ours can probably be explained by the carbon used: we used carbon black with a surface area of 80 m²/g, while Chalewaert-umpon used >1500 m² carbons (that is, smaller carbon beads), allowing the covering of lignin particle with very thin carbon.

Other research teams [10], [17], [41], [46], [48] pointed out that the carbon microstructure, pore size and electrode thickness played a major role, and that the bigger the surface area, the better. Increasing surface area should thus be a priority for future works. When seeing the picture of our four samples, it appeared that no lignin had a tendency to form a film, or to preferentially form smaller particles, which would augment the surface area exposed to the electrolyte during electrochemical experiments. Therefore, as all tested samples exhibited the same kind of microstructure, we could assume that their electrochemical performances measured in cyclic voltammetry were not influenced by the microstructure, and that any performance difference could not be attributed to it.
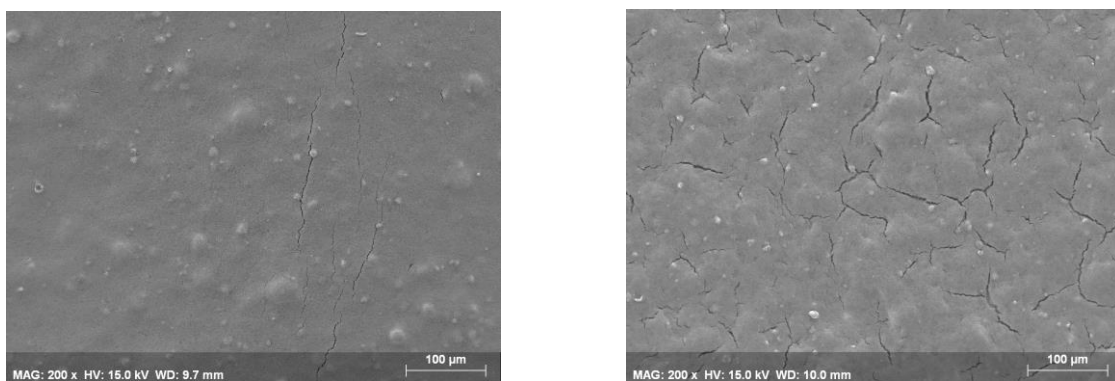
Figure 44 SEM picture of lignin-carbon films. On the left, HL film. On the right, DPL film. White dots are lignin aggregates. The black matrix is the carbon.

Figure 46 SEM picture of a particule of lignin (light grey) of DPL film sitting on top of carbon beads (dark grey).
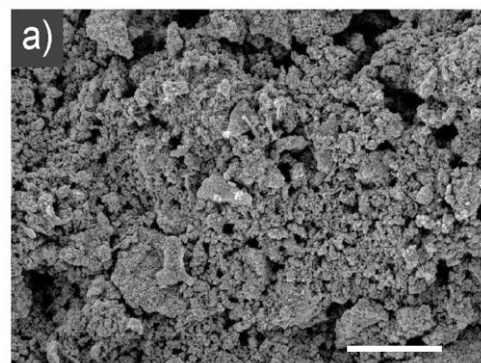
Figure 45 carbon-covered lignin particles from Chalewaert-umpon's article [ref 1]. Please note the difference with **fig. 46,** which is at the same scale . Scale: the white tick is 2 um [9].
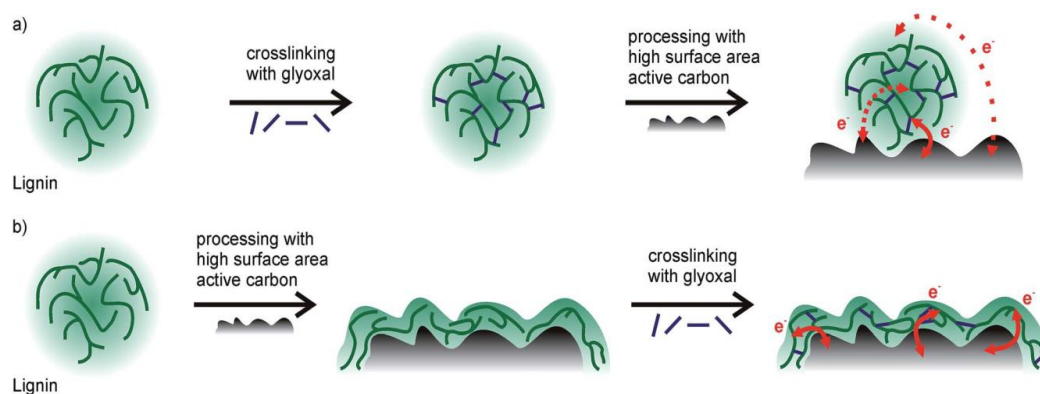
Figure 47 Schematic view of lignin-carbon mixing with glyoxal binder [ref 2]. (a) lignin is mixed with glyoxal then with carbon (b) lignin is mixed with carbon then glyoxal..

5.8. Cyclic voltammetry indicates DPL is much more capacitive than HL and BL

Cyclic voltammetry is a method that can be used to test out the specific capacity of a material. The lignin-carbon is used as the working electrode, with a counter electrode and a reference electrode, and a potential is applied between the two electrodes. The working and the reference electrodes potential is swept from a low value to a high value, then back down, creating a typical hysteretic curve in the measured voltammogram. The specific capacity of the material was obtained from the integral of the CV curve. Each peak in the curve is an indicator of a redox potential. In lignin, guaiacyl groups can be found in a hydroxyquinone or a quinone form. The reversible reaction between the two shows a redox potential [9], [11]. The results reported in this master thesis are a preliminary work that aims to highlight specific capacity difference between lignin sources and lignin fractions.

We chose to work with a H_2SO_4 1N (0,5 M) electrolyte. In the literature, three types of electrolytes have been used to test out lignin-sourced porous carbon electrodes: alkaline water, acidic water, and ionic liquids. Acidic electrolyte was favored for this work because we wanted to compare our results to the ones of Chalewaert-umpon and al. [9], [11]. H_2SO_4 was favored over HCl and $HClO_4$ because we wanted to ensure that the organic material would not degrade into the solution. We first tested films prepared on copper foil, which should have acted as substrate and current collector, but as suspected, the cyclic voltammetry curves showed that the copper immediately dissolved into the electrolyte and completely hid the carbon-lignin film response to the applied potential. We then opted for acidic-resistant fluorine tin oxide (FTO) glass, which did not display any influence on the curves and acted as current collector.
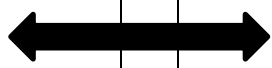
In **fig. 48,** we observed one distinct peak in all curves that varied between samples, ranging from 0.53 V in HL and BL to 0.65 V in DPL. This was comparable to the reference value of 0.55 V for Kraft lignin [9]. We attributed this peak to the reduction of G units (coniferyl alcohol). The peak shift to 0.65 V for DPL might be due to a greater abundance of G units. There was not the time necessary for the electrolyte to move through the film and transport charge to all G units. A slower scanning rate might display a lower value for the peak position.
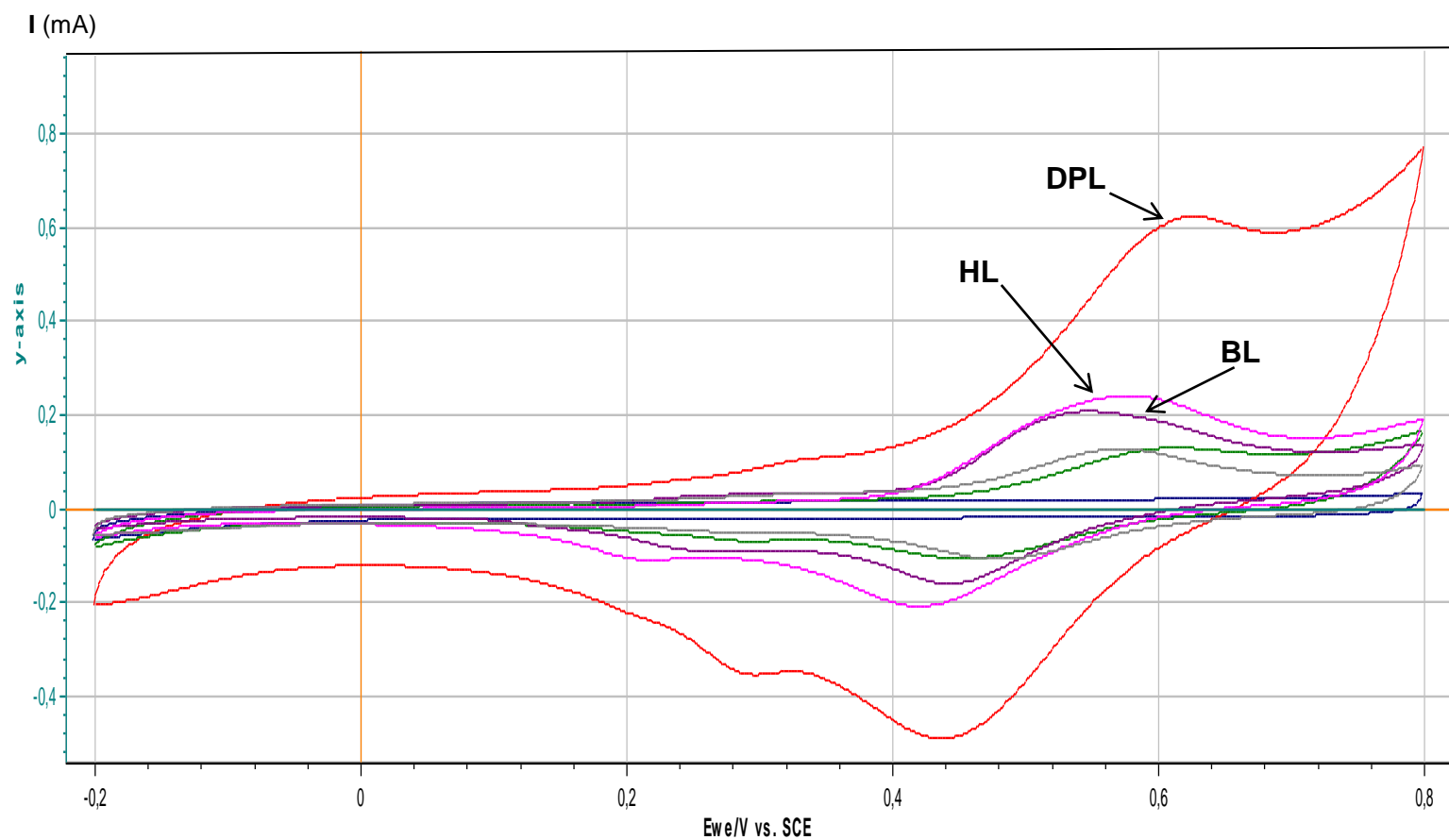
Figure 48 Cyclic voltametry curves for different lignin-carbon films at 5 mV/s in H_2SO_4 1N. The reference electrode is a calomel electrode. Legend: DPL (red), HL (pink), BL (brown), DPL-S45 (green) and DPL-INS (grey). X-axis is the working potential E against the standard calomel electrode (in V). Y-axis is the measured current (in mA).

The intensity of the current detected for pristine DPL seemed much larger than the ones of all the other samples. We thought this increased electron storage capacity was caused by the natural abundance of quinone-like G units in DPL, whereas HL and BL contained proportionally less G units, hence the lower specific capacity. The calculated specific capacities were calculated and displayed in **table 13**. From these preliminary results (no repetitions), we saw that DPL was 3 times more capacitive than HL and 8 times more capacitive than BL. We also noticed that DPL-S45 and DPL-INS had negative contributions to the overall specific capacity, i.e. their presence worsened the specific capacity of pristine porous carbon. We hypothesized that their contribution was sufficiently small that film inhomogeneity or statistical fluctuations made it look like they had a negative contribution; repetition of the experiments should allow one to confirm or invalidate this hypothesis. The pseudocapacitive contribution of our lignin in specific capacity measurements is almost identical (~16 mAh/g) to the results of Chalewaert-umpon [9]. The higher value of 80 mAh/g reported by the research team was caused by higher capacity carbon, not by lignin enhanced pseudocapacity. The pioneering work of Chalewaert-umpon is thus partly confirmed. Also, they used softwood Kraft lignin, and we found identical results for softwood soda lignin, pointing towards the fact that the lignin type (softwood, hardwood, herbaceous) is a major factor, much more than the pretreatment method.

Table 13 CV specific capacity results for different lignins and lignin fractions. The third column is the substraction of the value of the second column by the carbon blank capacitive value (4.1 mAh/g). DPL displays a close value to our reference value [9].

	Total capacity (mAh/g)	Lignin pseudocapacitive contribution (mAh/g)	Reference Value for lignin pseudocapacitive contribution (mAh/g) [9]
DPL	20.3	**16.1**	**16.6**
BL	5.6	1.5	
HL	7.7	3.6	
Carbon blank	4.1	/	
FTO blank	0.004	/	

5.9. Summarized overview: NMR, HPSEC and FTIR agree on molecular weight determination

In **tab 14** and **tab. 15**, we summarize our observations for the characterization of some chosen fractions of DPL and HL, to witness any pattern, complementarity or disagreements between techniques.

We observe that HPSEC-DMF and HPSEC-H_2O agree: increase of M_w from F1 to INS for DPL, decrease from SH1 to SH3 for HL. In almost all HPSEC results, though the absolute value was different, the relative molecular weight increases and decreases were the same in the two solvents. The fractionation methods we used in this master thesis were taken from literature for their ability to discriminate molecular weight [38]. That objective seems achieved for the three methods, though the mechanism that underlies the fractionation remains unclear. The simplest explanation is simple volume to surface ratio: the small molecules dissolved first, whatever the solvent, then the medium ones, then the large ones. However, this hypothesis seems at best incomplete when we look at FTIR and NMR data. FTIR and NMR data agreed on the aliphatic OH:COOH (aOH:COOH) relative proportions, showing an interesting crosscheck between the two techniques. When compared with the molecular weight, we observe that the aOH:COOH ratio and molecular weight appear to be correlated: the higher the molecular weight, the higher the aOH:COOH ratio. As already mentioned in **section 5.5**, we can hypothesize that aliphatic OH are mostly present in β-O-4 linkages and COOH in end-chain units. Then the data makes sense: high molecular weight lignins have a high ratio of linkages to end-chains, thus a high aOH:COOH ratio, and low molecular weight lignins display the opposite. In summary, it looks as if HPSEC, NMR and FTIR data point to the same piece of information: the molecular weight. HPSEC, via hydrodynamic volume and NMR/FTIR, by the ratio aOH:COOH which is directly linked to molecular weight. Therefore, the three analytical techniques support and crosscheck each other.

Finally, SEM pictures show that the molecular weight and the functionality content influenced the microstructure, in pore size and in morphology: some samples displayed micrometric sheets, others needles, and some, particles. It does not look like there are any links between molecular weight, oxygenated moieties, and apparent microstructure.

Table 14 Summarized overview of all characterization results concerning DPL, DPL-F1, DPL-F3 and DPL-F4, in order to highlight crosschecks and converging trends. In the framed boxes, "OH" means "aliphatic OH".

	DPL-F1	DPL-F2	DPL-F3	DPL-F4	DPL-INS	DPL
FP	21%	26.2%	29.3%	8.7%	14.8%	-
FTIR	Rich in COOH / Poor in OH	C=O band decreases → C-O and O-H band increase			Rich in OH / Poor in COOH	Major bands: O-H, C=O, Aromatics, C-O
NMR	Rich in COOH / Poor in OH	→	Rich in OH / Poor in COOH		-	Aromatics: 70% G, 30% H
HPSEC	22000 g/mol ○ 3000 g/mol	PDI constant at ~1.5 →			127000 g/mol ○ 8500 g/mol	74000 g/mol / *5100 g/mol* / Higher PDI in DMF (2.45) than water (1.53)
SEM	-	10-100 µm sheets	10-100 µm sheets / 2 µm « needles »	1-10 µm sheets aggregated in 10-30 µm particles	-	-

Table 15 Summarized overview of all characterization results concerning HL, HL-SH1, HL-SH2 and HL-SH3, in order to highlight crosschecks and converging trends. In the framed boxes, "OH" means "aliphatic OH".

	HL-SH1	HL-SH2	HL-SH3	HL
FP	70.6%	23.9%	5.5%	/
FTIR	Rich in OH / Poor in COOH	C=O band increases → / C-O and O-H band decrease	Rich in COOH / Poor in OH	Major bands O-H C=O Aromatics C-O
NMR	Rich in OH / Poor in COOH	→	Rich in COOH / Poor in OH	Aromatics 60% S 30% G 10% H
HPSEC	32000 g/mol / 5600 g/mol	→	14000 g/mol / 3300 g/mol	74000 g/mol 5100 g/mol / Higher PDI in DMF (2.45) than water (1.53)
SEM	10-50 µm aggregates of 1-10 µm sheets	-	10-100 µm particles	-

6. Conclusion and perspectives

The characterization techniques used in this master thesis were fraction proportions, Klason dosage of carbohydrates, FTIR, HPSEC, NMR, and SEM. Fraction proportions showed equivalent repartition of lignin for most of organic fractions, and drastic differences in pH fractions. These differences were used to infer carboxylic acid and phenol relative contents. Klason lignin and carbohydrate dosage showed the lignin samples purity was >97%. It assured that inorganic salt content would not interfere with electrochemical measurements. FTIR spectroscopy indicated general moieties content trends, such as C=O increase/O-H decrease between F1 and INS of DPL, or the aromatics and C-O content of some fractions. HPSEC was performed in DMF and in water, and the molecular weights trends almost always agreed in both solvents. M_n and M_w increased between F1 and INS and between SA1 and SA3 for all three lignins. M_n and M_w decreased between SH1 and SH3 for all three lignins **(tab. 16)**. NMR showed expected H:G:S ratios. It also exhibited the evolutions in aliphatic OH:COOH ratios, that were correlated with molecular weight, as explained in the summarized **section 5.9**. SEM pictures showed different microstructures, but without suggesting a link between microstructure and molecular weight or functionality content.

Table 16 List of highlights of this master thesis, ordered by topic.

Topic	Highlights
Fractionation method	Organic solvents fractionate lignin from smallest to largest pH fractionates lignin from largest to smallest
Characterization	NMR and FTIR, through aliphatic OH:COOH ratio, agree with HPSEC on molecular weights
Electrochemical results	Softwood lignin is much more capacitive than hardwood or and herbaceous lignins
Others	Hansen solubility parameters rationalize solubility observations

Table 17 List of minor hurdles met during this master thesis. On the right, the perspectives of improvement for these problems.

Hurdles	Perspectives
HPSEC calibration curve	Osmometry, viscosimetry, light scattering
Poor film homogeneity	Ball-milling, optimization
NMR insolubility	Replace $CDCl_3$ by DMF-d7
Organic solvent sequence has no trend	Create a new sequence based on Hansen solubility parameters
Aromatics and C-O too complex FTIR	2D-NMR
Stepwise fractionation	Parallel fractionation

The three fractionation methods did work, according to HPSEC, NMR and FTIR data. pH fractionation was the most simple, but it did not work on DPL. Sonication did show an increase of M_w in HPSEC, between 20 and 30%. Still, no changes were observed in FTIR data. The collection of ^{31}P or 2D NMR data could confirm or invalidate the method as efficient or inefficient for repolymerization. We also showed that ball-milling had little effect on lignin molecular weight and none on functionality content.

Finally, preliminary CV measurement were performed on DPL, HL and BL. DPL had similar values to the reference value [9], i.e. ~16 mAh/g. BL and HL displayed 8 and 4 times lower capacity values, respectively. These results highlighted the fact that the type of lignin, with a high G content, had a major impact, while the difference in pretreatment (alkaline vs Kraft) did not seem to have impacted the result.

Minor hurdles (**tab. 17**) include the dependence of HPSEC values on a non-related polymer to calibrate the retention time-molecular weight relationship, because we assumed polystyrene does not behave like lignin in solution, and thus is not reliable for a reference hydrodynamic volume. Perspectives include osmometry, which relies on colligative properties, and not hydrodynamic volume, viscosimetry, which relies on friction, and light scattering, which relies on colloidal diffusion.

The poor lignin-carbon film homogeneity we observe in SEM could probably be bettered by grain size reduction in dry ball-milling, or ball-milling in NMP, even more so since we showed in this master thesis that it did not affect functionality content.

The organic sequence we tested (EtOAc, MEK, MeOH, dioxane:water 95:5) worked empirically, but did not follow any trend, preventing solubility interpretations. Using Hansen solubility parameters, we could create rationalized sequences that would fractionate and highlight certain functionalities. For example, using the table in **Appendix III**, we could test the sequence: methyl iso-amyl ketone, n-butyl propionate, ethyl acetate, isopentyl alcohol and 2-butanol, which have similar δ_D (~16) and δ_P (~5) while their δ_H value varies: 4.1, 5.9, 7.2, 13.3 and 14.5, respectively.

As we discussed in **section 5.6**, DMF-d7, expensive but more performing than CDCl$_3$, could be used to help solubilize some fractions in NMR. Also, hard-to-analyze FTIR bands could be supported by HSQC NMR data. In these, the second dimension allows for identification and dosage of each linkage, thus of aromatics and ethers, for example.

With stepwise fractionation, we were not able to observe some of the lignin-organic solvent interactions. If a molecule had dissolved in solvent 1, then we were not allowed to see its interactions with solvent 2 or any of the following solvents. Consequently, we think a parallel fractionation, i.e. the dissolution of pristine lignin in all solvents, would bring complementary and important pieces of data to stepwise fractionation.

Finally, we think DPL-F1 and DPL-SH3, low molecular weight fractions, should give better results in CV than DPL alone. The reasoning is: DPL-INS shows a null specific capacity, and it makes up 15% of DPL. It contains all the highest molecular weight molecules. Therefore, smaller lignin fractions should be the most redox-active. Once rid of non-redox-active, high molecular weight molecules, small molecular weight lignins should, per gram, be more performing. Further investigation of small molecular weight is thus needed and advised.

If the small molecular weight lignin molecules happen to be more capacitive than large molecular weight lignin, then their valorization should go through fractionation. We showed that acetone/water 6:4 and ethyl acetate preferentially extracted small lignins. Therefore, in a biorefinery perspective, we would advise to choose acetone/water, since water is harmless and acetone can be bio-sourced. The other fractions could then be valorized in other electrochemical applications (binder, insulator, carbonized in porous carbon) or in lower value applications (cement, fertilizer, low-grade fuel), paving the way for the complete valorization of lignin.

7. Bibliography

[1]   V. Menon and M. Rao, "Trends in bioconversion of lignocellulose: Biofuels, platform chemicals & biorefinery concept," *Prog. Energy Combust. Sci.*, vol. 38, no. 4, pp. 522–550, 2012.

[2]   W. Tang *et al.*, "Natural biomass-derived carbons for electrochemical energy storage," *Mater. Res. Bull.*, vol. 88, pp. 234–241, 2017.

[3]   D. M. Le, A. D. Nielsen, H. R. Sørensen, and A. S. Meyer, "Characterisation of Authentic Lignin Biorefinery Samples by Fourier Transform Infrared Spectroscopy and Determination of the Chemical Formula for Lignin," *Bioenergy Res.*, vol. 10, no. 4, pp. 1025–1035, 2017.

[4]   S. Admassie, F. N. Ajjan, A. Elfwing, and O. Inganäs, "Biopolymer hybrid electrodes for scalable electricity storage," *Mater. Horiz.*, vol. 3, no. 3, pp. 174–185, 2016.

[5]   Z. Strassberger, S. Tanase, and G. Rothenberg, "The pros and cons of lignin valorisation in an integrated biorefinery," *RSC Adv.*, vol. 4, no. 48, pp. 25310–25318, 2014.

[6]   V. Natalis, "Utilisation de solvants eutectiques profonds (DEP) et de solvants commutables comme méthodologie verte pour l ' extraction et la valorisation de la biomasse lignocellulosique et de ses composants apparentés Introduction," no. figure 1, 2017.

[7]   W. Boerjan, J. Ralph, and M. Baucher, "LIGNIN BIOSYNTHESIS," *Annu. Rev. Plant Biol.*, vol. 54, no. 1, pp. 519–546, 2003.

[8]   W. Liu *et al.*, "Lignin-derived carbon nanosheets for high-capacitance supercapacitors," *RSC Adv.*, vol. 7, no. 77, pp. 48537–48543, 2017.

[9]   S. Chaleawlert-umpon, T. Berthold, X. Wang, M. Antonietti, and C. Liedel, "Kraft Lignin as Electrode Material for Sustainable Electrochemical Energy Storage," *Adv. Mater. Interfaces*, vol. 1700698, pp. 1–7, 2017.

[10] H. Wang, Y. Yang, and L. Guo, "Renewable-Biomolecule-Based Electrochemical Energy-Storage Materials," *Adv. Energy Mater.*, vol. 1700663, pp. 1–6, 2017.

[11] S. Chaleawlert-umpon and C. Liedel, "More sustainable energy storage: lignin based electrodes with glyoxal crosslinking," *J. Mater. Chem. A*, pp. 24344–24352, 2017.

[12] A. Mukhopadhyay, Y. Jiao, R. Katahira, P. N. Ciesielski, M. Himmel, and H. Zhu, "Heavy Metal-Free Tannin from Bark for Sustainable Energy Storage," *Nano Lett.*, vol. 17, no. 12, pp. 7897–7907, 2017.

[13] A. J. Ragauskas *et al.*, "Lignin valorization: Improving lignin processing in the biorefinery," *Science (80-.).*, vol. 344, no. 6185, 2014.

[14] H. Zhang *et al.*, "Alkaline lignin derived porous carbon as an efficient scaffold for lithium-selenium battery cathode," *Carbon N. Y.*, vol. 122, pp. 547–555, 2017.

[15] F. N. Ajjan *et al.*, "High performance PEDOT/lignin biopolymer composites for electrochemical supercapacitors," *J. Mater. Chem. A*, vol. 4, no. 5, pp. 1838–1847, 2016.

[16] A. K. Kumar and B. S. Parikh, "Natural deep eutectic solvent mediated pretreatment of rice straw : bioanalytical characterization of lignin extract and enzymatic hydrolysis of pretreated biomass residue," *Environ. Sci. Pollut. Res.*, pp. 9265–9275, 2016.

[17] M. J. Uddin, P. K. Alaboina, L. Zhang, and S. J. Cho, "A low-cost, environment-friendly lignin-polyvinyl alcohol nanofiber separator using a water-based method for safer and faster lithium-ion batteries," *Mater. Sci. Eng. B Solid-State Mater. Adv. Technol.*, vol. 223, pp. 84–90, 2017.

[18] A. K. Kumar and S. Sharma, "Recent updates on different methods of pretreatment of lignocellulosic feedstocks: a review," *Bioresour. Bioprocess.*, vol. 4, no. 1, p. 7, 2017.

[19] R. Rinaldi *et al.*, "Paving the Way for Lignin Valorisation: Recent Advances in Bioengineering, Biorefining and Catalysis," *Angew. Chemie - Int. Ed.*, vol. 55, no. 29, pp. 8164–8215, 2016.

[20] G. D. Mcglnnls, W. W. Wllson, and C. I. M. E. Mullen, "Biomass Pretreatment with Water and High-pressure Oxygen . The Wet-Oxidation Process," pp. 352–357, 1983.

[21] C. Mart, H. B. Klinke, and A. Belinda, "Wet oxidation as a pretreatment method for enhancing the enzymatic convertibility of sugarcane bagasse," vol. 40, pp. 426–432, 2007.

[22] C.-J. Wei and C.-Y. Cheng, "Effect of hydrogen peroxide pretreatment on the structural features and the enzymatic hydrolysis of rice straw," *Biotechnol. Bioeng.*, vol. 27, no. 10, pp. 1418–1426, 1985.

[23] C. J. Chuck, H. J. Parker, R. W. Jenkins, and J. Donnelly, "Renewable biofuel additives from the ozonolysis of lignin," *Bioresour. Technol.*, vol. 143, pp. 549–554, 2013.

[24] Y. Zhao, Y. Wang, J. Y. Zhu, A. Ragauskas, and Y. Deng, "Enhanced enzymatic hydrolysis of spruce by alkaline pretreatment at low temperature," *Biotechnol. Bioeng.*, vol. 99, no. 6, pp. 1320–1328, 2008.

[25] X. Zhao, K. Cheng, and D. Liu, "Organosolv pretreatment of lignocellulosic biomass for enzymatic hydrolysis," *Appl. Microbiol. Biotechnol.*, vol. 82, no. 5, pp. 815–827, 2009.

[26] Z. Wu and Y. Y. Lee, "Ammonia recycled percolation as a complementary pretreatment to the dilute-acid process.," *Appl. Biochem. Biotechnol.*, vol. 63–65, pp. 21–34, 1997.

[27] F. F. De Menezes *et al.*, "Alkaline Pretreatment Severity Leads to Different Lignin Applications in Sugar Cane Biorefineries," *ACS Sustain. Chem. Eng.*, vol. 5, no. 7, pp. 5702–5712, 2017.

[28] F. Cotana, M. Barbanera, D. Foschini, E. Lascaro, and C. Buratti, "Preliminary optimization of alkaline pretreatment for ethanol production from vineyard pruning," *Energy Procedia*, vol. 82, pp. 389–394, 2015.

[29] W. Palz, D. Pirrwitz, and C. of the E. Communities, "Energy from Biomass," pp. 1–4, 1984.

[30] S. Xie *et al.*, "Advanced Chemical Design for Efficient Lignin Bioconversion," *ACS Sustain. Chem. Eng.*, vol. 5, no. 3, pp. 2215–2223, 2017.

[31] R. J. A. Gosselink, *Lignin as a renewable aromatic resource for the chemical industry,*

no. December. 2011.

[32] C. G. Boeriu, D. Bravo, R. J. A. Gosselink, and J. E. G. Van Dam, "Characterisation of structure-dependent functional properties of lignin with infrared spectroscopy," *Ind. Crops Prod.*, vol. 20, no. 2, pp. 205–218, 2004.

[33] "Phenol price."

[34] J. S. Lupoi, S. Singh, R. Parthasarathi, B. A. Simmons, and R. J. Henry, "Recent innovations in analytical methods for the qualitative and quantitative assessment of lignin," *Renew. Sustain. Energy Rev.*, vol. 49, pp. 871–906, 2015.

[35] E. A. B. da Silva *et al.*, "An integrated process to produce vanillin and lignin-based polyurethanes from Kraft lignin," *Chem. Eng. Res. Des.*, vol. 87, no. 9, pp. 1276–1292, 2009.

[36] X. H. Li and S. Bin Wu, "Chemical structure and pyrolysis characteristics of the soda-alkali lignin fractions," *BioResources*, vol. 9, no. 4, pp. 6277–6289, 2014.

[37] A. Ang, Z. Ashaari, E. S. Bakar, and N. A. Ibrahim, "Characterisation of sequential solvent fractionation and base-catalysed depolymerisation of treated alkali lignin," *BioResources*, vol. 10, no. 3, pp. 4137–4151, 2015.

[38] J. Domínguez-Robles, T. Tamminen, T. Liitiä, M. S. Peresin, A. Rodríguez, and A. S. Jääskeläinen, "Aqueous acetone fractionation of kraft, organosolv and soda lignins," *Int. J. Biol. Macromol.*, vol. 106, pp. 979–987, 2018.

[39] D. P. Dubal, O. Ayyad, V. Ruiz, and P. Gómez-Romero, "Hybrid energy storage: the merging of battery and supercapacitor chemistries," *Chem. Soc. Rev.*, vol. 44, no. 7, pp. 1777–1790, 2015.

[40] E. J. Son, J. H. Kim, K. Kim, and C. B. Park, "Quinone and its derivatives for energy harvesting and storage materials," *J. Mater. Chem. A*, vol. 4, no. 29, pp. 11179–11202, 2016.

[41] N. Guo, M. Li, X. Sun, F. Wang, and R. Yang, "Enzymatic hydrolysis lignin derived hierarchical porous carbon for supercapacitors in ionic liquids with high power and energy densities," *Green Chem.*, vol. 19, no. 11, pp. 2595–2602, 2017.

[42] D. Yoon, J. Hwang, W. Chang, and J. Kim, "Carbon with Expanded and Well-Developed Graphene Planes Derived Directly from Condensed Lignin as a High-Performance Anode for Sodium-Ion Batteries," *ACS Appl. Mater. Interfaces*, vol. 10, no. 1, pp. 569–581, 2018.

[43] R. Pucciariello, M. D'Auria, V. Villani, G. Giammarino, G. Gorrasi, and G. Shulga, "Lignin/Poly(ε-Caprolactone) blends with tuneable mechanical properties prepared by high energy ball-milling," *J. Polym. Environ.*, vol. 18, no. 3, pp. 326–334, 2010.

[44] C. D. Tran, H. C. Ho, J. K. Keum, J. Chen, N. C. Gallego, and A. K. Naskar, "Sustainable Energy-Storage Materials from Lignin–Graphene Nanocomposite-Derived Porous Carbon Film," *Energy Technol.*, vol. 5, no. 11, pp. 1927–1935, 2017.

[45] K. Ojha, B. Kumar, and A. K. Ganguli, "Biomass derived graphene-like activated and non-activated porous carbon for advanced supercapacitors," *J. Chem. Sci.*, vol. 129, no. 3, pp. 397–404, 2017.

[46] M. Klose *et al.*, "Softwood Lignin as a Sustainable Feedstock for Porous Carbons as Active Material for Supercapacitors Using an Ionic Liquid Electrolyte," *ACS Sustain. Chem. Eng.*, vol. 5, no. 5, pp. 4094–4102, 2017.

[47] L. Zhu, F. Shen, R. L. Smith, L. Yan, L. Li, and X. Qi, "Black liquor-derived porous carbons from rice straw for high-performance supercapacitors," *Chem. Eng. J.*, vol. 316, pp. 770–777, 2017.

[48] S. Hu and Y.-L. Hsieh, "Lignin derived activated carbon particulates as an electric supercapacitor: carbonization and activation on porous structures and microstructures," *RSC Adv.*, vol. 7, no. 48, pp. 30459–30468, 2017.

[49] S. Hu, S. Zhang, N. Pan, and Y. Lo Hsieh, "High energy density supercapacitors from lignin derived submicron activated carbon fibers in aqueous electrolytes," *J. Power Sources*, vol. 270, no. x, pp. 106–112, 2014.

[50] C. Lai *et al.*, "Free-standing and mechanically flexible mats consisting of electrospun carbon nanofibers made from a natural product of alkali lignin as binder-free electrodes for high-performance supercapacitors," *J. Power Sources*, vol. 247, pp. 134–141, 2014.

[51] D. Saha *et al.*, "Studies on supercapacitor electrode material from activated lignin-

derived mesoporous carbon," *Langmuir*, vol. 30, pp. 900–910, 2014.

[52]   F. Chen *et al.*, "Self-assembly of NiO nanoparticles in lignin-derived mesoporous carbons for supercapacitor applications," *Green Chem.*, vol. 15, no. 11, p. 3057, 2013.

[53]   W. E. Tenhaeff, O. Rios, K. More, and M. A. McGuire, "Highly robust lithium ion battery anodes from lignin: An abundant, renewable, and low-cost material," *Adv. Funct. Mater.*, vol. 24, no. 1, pp. 86–94, 2014.

[54]   T. Chen, J. Hu, L. Zhang, J. Pan, Y. Liu, and Y. T. Cheng, "High performance binder-free SiOx/C composite LIB electrode made of SiOxand lignin," *J. Power Sources*, vol. 362, pp. 236–242, 2017.

[55]   X. Geng *et al.*, "Bioinspired Ultrastable Lignin Cathode via Graphene Reconfiguration for Energy Storage," *ACS Sustain. Chem. Eng.*, vol. 5, no. 4, pp. 3553–3561, 2017.

[56]   J. Sameni, S. Krigstin, and M. Sain, "Solubility of Lignin and Acetylated Lignin in Organic Solvents," *BioResources*, vol. 12, no. 1, pp. 1548–1565, 2017.

[57]   "Table de pKa." [Online]. Available: http://ccchemteach.com/?page_id=64.

[58]   E. I. Evstigneev, "Factors affecting lignin solubility," *Russ. J. Appl. Chem.*, vol. 84, no. 6, pp. 1040–1045, 2011.

[59]   T. B. Nielsen and C. M. Hansen, "Elastomer swelling and Hansen solubility parameters," *Polym. Test.*, vol. 24, no. 8, pp. 1054–1061, 2005.

[60]   "Hansen Parameters Table." [Online]. Available: https://www.hansen-solubility.com/downloads.php.

[61]   O. Y. Abdelaziz and C. P. Hulteberg, "Physicochemical Characterisation of Technical Lignins for Their Potential Valorisation," *Waste and Biomass Valorization*, vol. 8, no. 3, pp. 859–869, 2017.

[62]   A. Casas, M. V. Alonso, M. Oliet, E. Rojo, and F. Rodríguez, "FTIR analysis of lignin regenerated from Pinus radiata and Eucalyptus globulus woods dissolved in imidazolium-based ionic liquids," *J. Chem. Technol. Biotechnol.*, vol. 87, no. 4, pp. 472–480, 2012.

[63] M. Konstantopoulou *et al.*, "Variation in susceptibility to microbial lignin oxidation in a set of wheat straw cultivars : influence of genetic , seasonal and environmental factors," vol. 32, no. 4, 2017.

[64] H. Kim, J. Ralph, N. Yahiaoui, M. Pean, and A. M. Boudet, "Cross-coupling of hydroxycinnamyl aldehydes into lignins," *Org. Lett.*, vol. 2, no. 15, pp. 2197–2200, 2000.

[65] G. Hatfield, G. Maciel, O. Erbatur, and G. Erbatur, "Qualitative and Quantitative Analysis of Solid Lignin Samples by Carbon- 13 Nuclear Magnetic Resonance Spectrometry," *Anal. Chem.*, vol. 59, pp. 172–179, 1987.

[66] A. Guerra, A. R. Gaspar, S. Contreras, L. A. Lucia, C. Crestini, and D. S. Argyropoulos, "On the propensity of lignin to associate: A size exclusion chromatography study with lignin derivatives isolated from different plant species," *Phytochemistry*, vol. 68, no. 20, pp. 2570–2583, 2007.

[67] T. Wells, M. Kosa, and A. J. Ragauskas, "Polymerization of Kraft lignin via ultrasonication for high-molecular- weight applications," *Ultrason. Sonochem.*, vol. 20, no. 6, pp. 1463–1469, 2013.

[68] D. Dong and A. Fricke, "Intrinsic viscosity and the molecular weight of kraft lignin," *Polymer (Guildf).*, vol. 36, no. 10, pp. 2075–2078, 1995.

[69] M. G. Neira-Velázquez, M. T. Rodríguez-Hernández, E. Hernández-Hernández, and A. R. Y. Ruiz-Martínez, "Polymer Molecular Weight Measurement," *Handb. Polym. Synth. Charact. Process.*, pp. 355–366, 2013.

[70] "Price DMF-d7." [Online]. Available: https://www.sigmaaldrich.com/catalog/product/aldrich/189979?lang=fr&region=BE

[71] "Price CDCl3." [Online]. Available: https://www.sigmaaldrich.com/catalog/product/aldrich/151823?lang=fr&region=BE&g clid=CjwKCAjwpIjZBRBsEiwA0TN1r1DOMBrVRSy45OPvtWcdMA1QnyGEgd5rhz wQqkCG80KdNt6vgqH31hoCnTMQAvD_BwE

[72] "Hardwood symbol." [Online]. Available: https://visualpharm.com/free-icons/oak tree-595b40b75ba036ed117d7c11.

[73]   "Softwood   symbol."   [Online].   Available:
        https://www.pinterest.com/pin/280138039300249796/.

[74]   "Grass   symbol."   [Online].   Available: https://icon-icons.com/es/icono/alta-
        hierba/38534.

[75]   "Lignin   scheme."   [Online].   Available: https://www.nrel.gov/research/gregg-
        beckham.html.

[76]   Y. Pu, S. Cao, and A. J. Ragauskas, "Application of quantitative 31P NMR in biomass
        lignin and biofuel precursors characterization," *Energy Environ. Sci.*, vol. 4, no. 9, p.
        3154, 2011.

8. Appendixes

Appendix I : Klason calculations

Table 18 Ashes (inorganic salts) calculation for Douglas Pine lignin, given as an exemple. The ashes are weighted by difference after carbonization of acid insoluble lignin.

N° sample	sample mass (g)	dry matter (%)	dry crucible mass (g)	crucible mass + dry matter (g)	crucible + ashes (g)	dry solid residue (g)	ashes (%)	ashes average (%)
1	0.1002	95.10	49.0468	49.1276	49.0473	0.0808	0.52	
2	0.1025	95.30	50.3547	50.4360	50,.3581	0.0813	3.48	1.92
3	0.1020	95.10	50.3401	50.4222	50,.3418	0.0821	1.75	

Table 19bis Acid soluble lignin determination of Douglas Pine lignin by UV absorption at 280 nm.

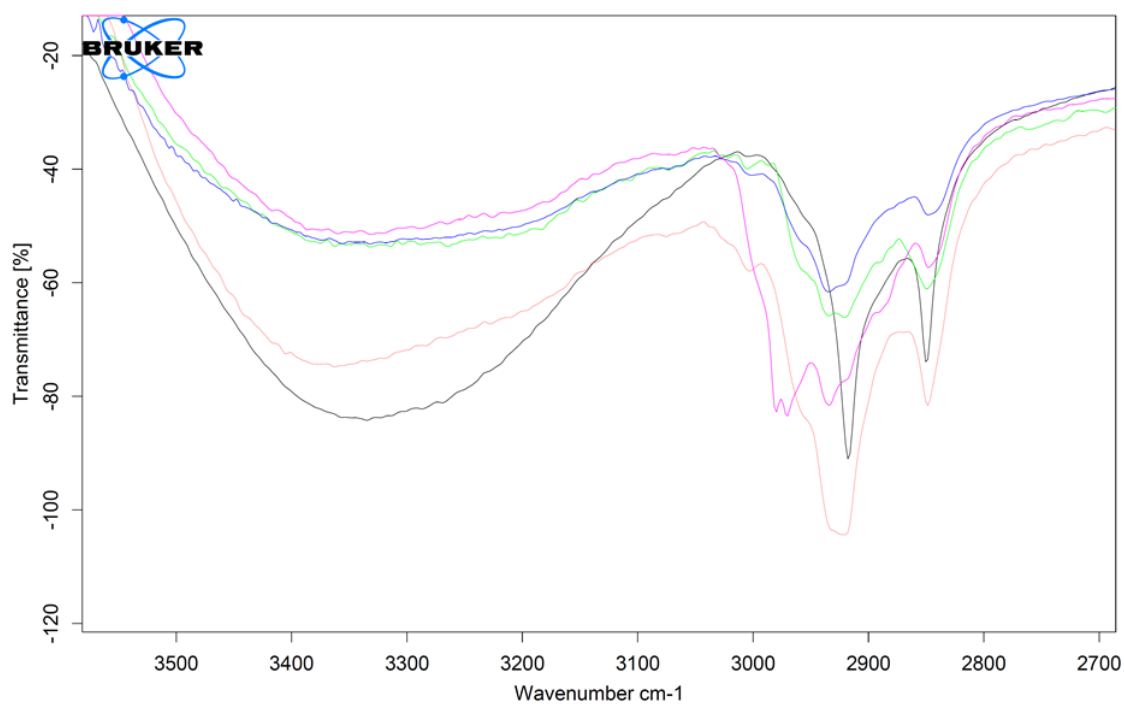| N° sample	Dilution (x times)	Absorbance average (AU)	Acid soluble lignin (%)	Acid soluble lignin (mg/g)	Acid soluble lignin average	Standard deviation acid soluble lignin (%)
1	50	0.3327	13.76	137.63		
2	50	0.3423	13.82	138.16	15.15	2.36
3	50	0.4400	17.88	178.82		

Appendix II : FTIR data

Table 20 FTIR assignation table, drawn and summarized from literature. Region 1270-810 cm^{-1}. Black: at least two sources. Grey: one source. Sources: [3], [32], [61]–[63]

		1270-1265	1220	1220-1215	1215-1210	1190	1150-1140	1130	1125	1115	1085-1080	1035-1030	860-855	845-835	820-810
alcohols	phenol		■												
	primary		■									■			
	secondary		■				░				■				
alcane	CH														
	CH2														
	CH3														
	Ar-OCH3														
	Aromatic skeleton					■		■							
	C=C														
	C-C			■											
Carbonyl	unconjugated		■												
	conjugated		■				░								
	COOH														
Ether	aromatic		■									■			
	aliphatic		■							■	■	■			
S unit	(G contamination)														
	no contamination									■					■
G unit	C-H deformation	■					■		■			■	■	■	
	C-O stretch				■										

100

Table 21 FTIR assignation table, drawn and summarized from literature. Region 3460-1325 cm^{-1}. Black: at least two sources. Grey: one source. Sources: [3], [32], [61]–[63]

		3460-3100	2960-2925	2850-2840	3000-2500	1735-1700	1660-1650	1600-1585	1515-1500	1425-1417	1375-1365	1330-1325
alcohols	phenol	■									■	
	primary	■										
	secondary	■										
alcane	CH		■									
	CH2		■									
	CH3		■									
	Ar-OCH3			■								
	Aromatic skeleton							■	■	■		
	C=C								▦			
	C-C											
Carbonyl	unconjugated					■						
	conjugated						■					
	COOH				▦							
Ether	aromatic											
	aliphatic											
S unit	(G contamination)											■
	no contamination											■
G unit	C-H deformation											▏
	C-O stretch											

Figure 50 Comparative spectrum of BL, zoom on the 3600-2700 cm^{-1} region. F1 in red, F2 in pink, F3 in blue, F4 in green and INS in black.
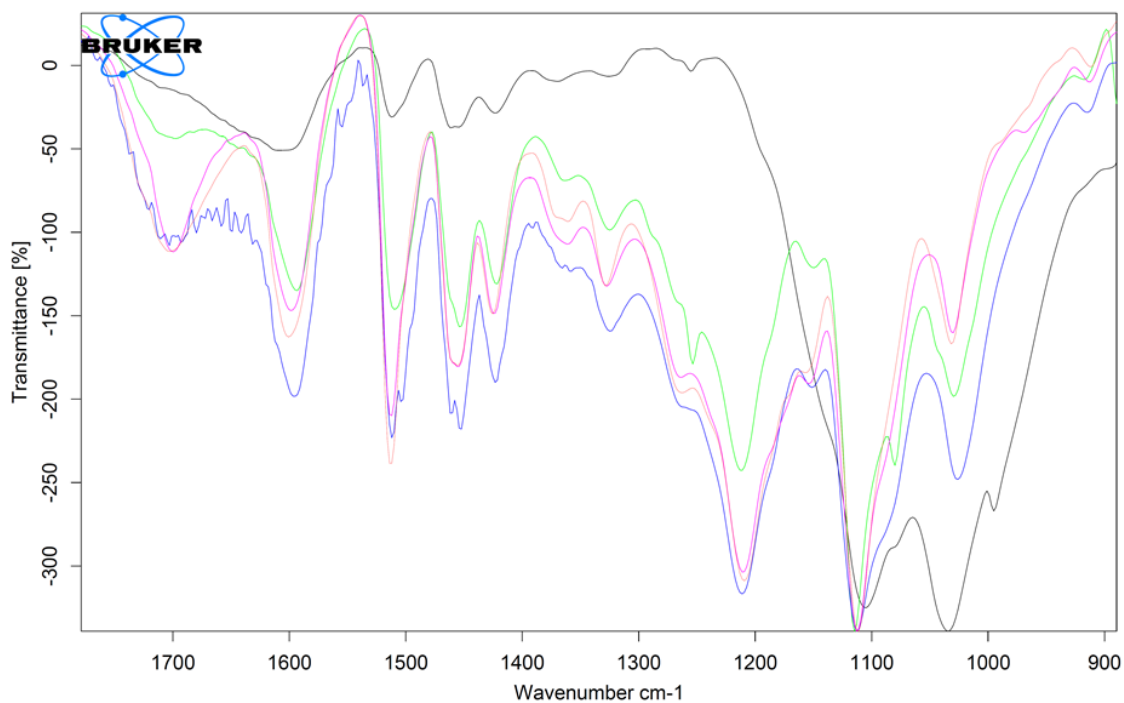
Figure 49 Comparative spectrum of BL, zoom on the 1800-900 cm^{-1} region. F1 in red, F2 in pink, F3 in blue, F4 in green and INS in black.
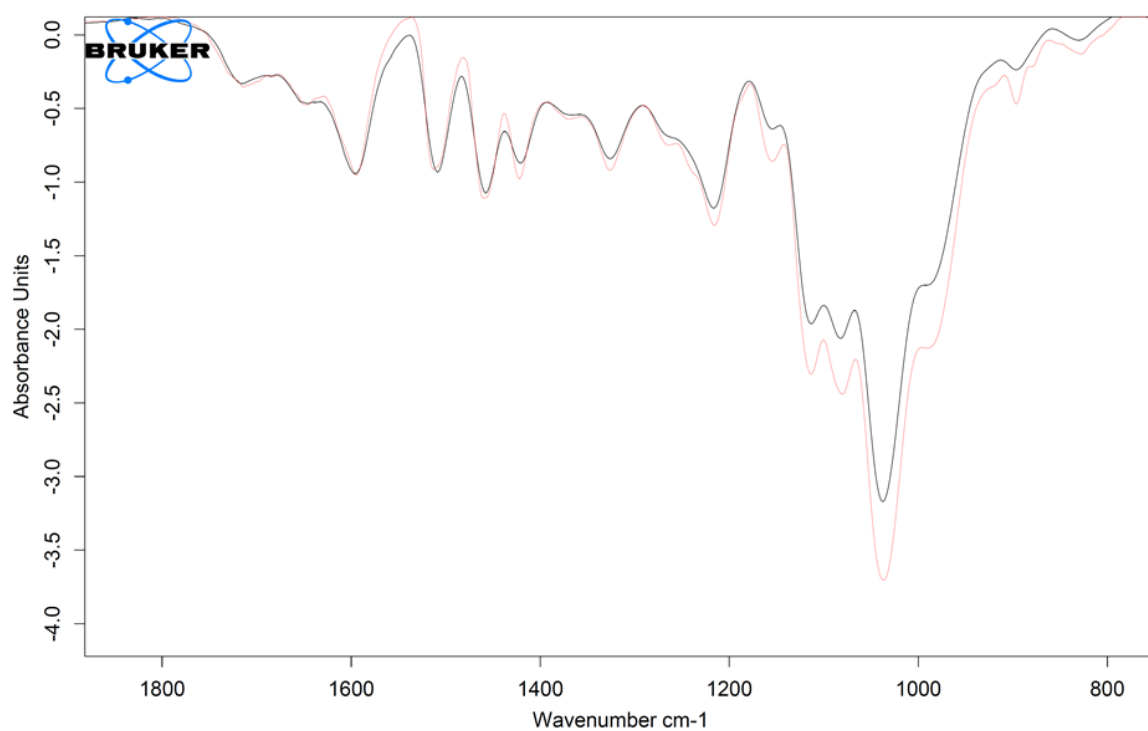
Figure 51 Comparative spectrum of BL-BM 36h (black) and BL-BM-108 (red)

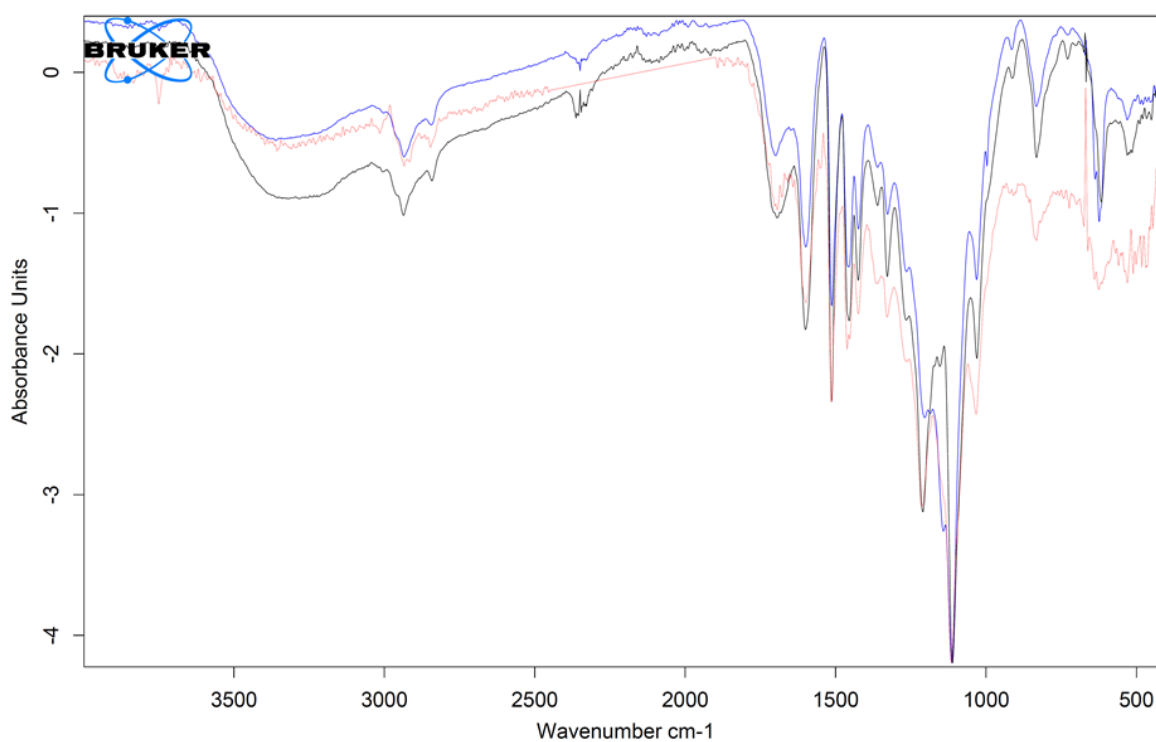**Figure 52** Comparative spectrum of the acetone/water fractions of HL: SA1 (red), SA2 (black) and SA3 (blue)

F**igure 53** Comparative spectrum of HL, zoom on the 3600-2700 cm^{-1} region. F1 in red, F2 in pink, F3 in blue, F4 in green and INS in black.

Figure 54 Comparative spectrum of BL, zoom on the 1800-900 cm^{-1} region. F1 in red, F2 in pink, F3 in blue, F4 in green and INS in black.
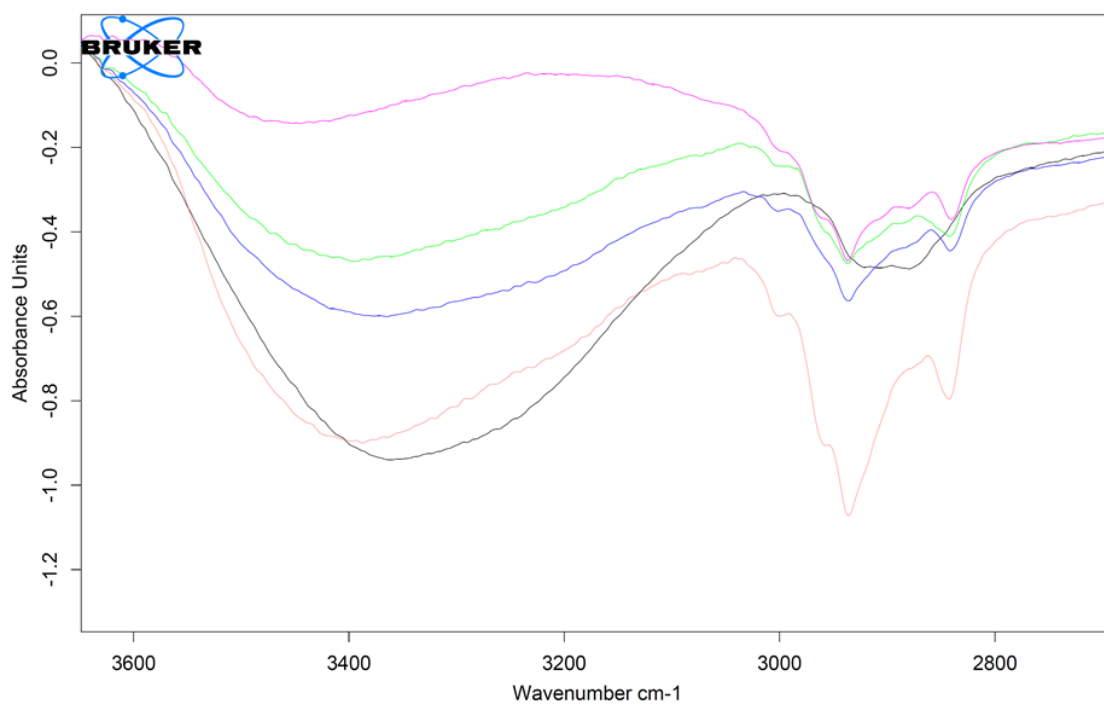
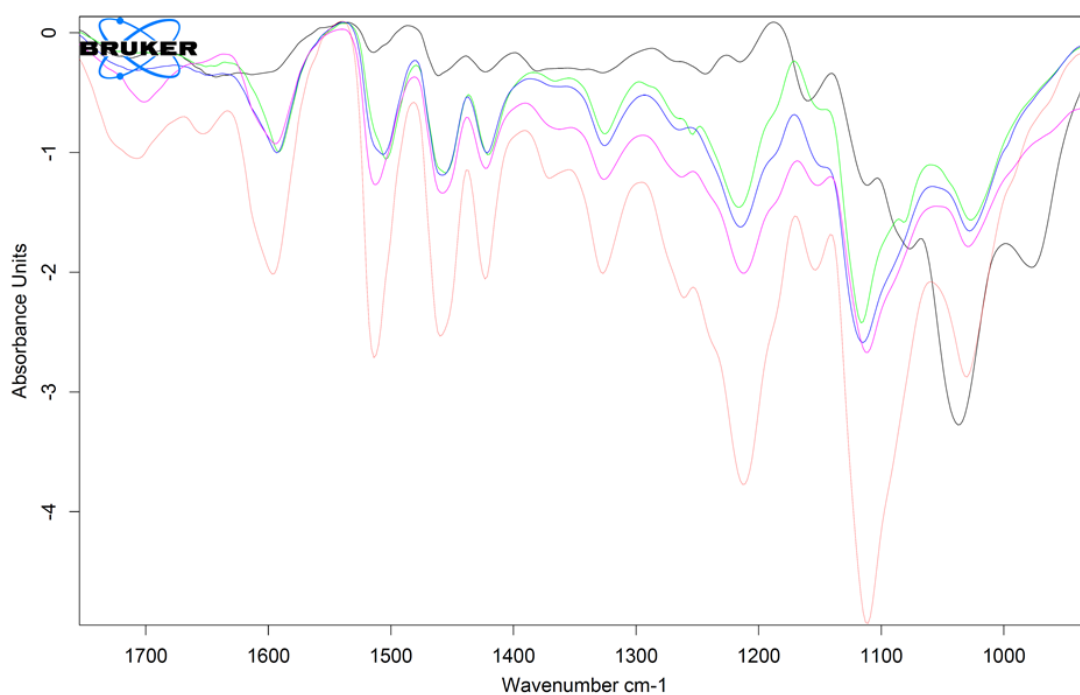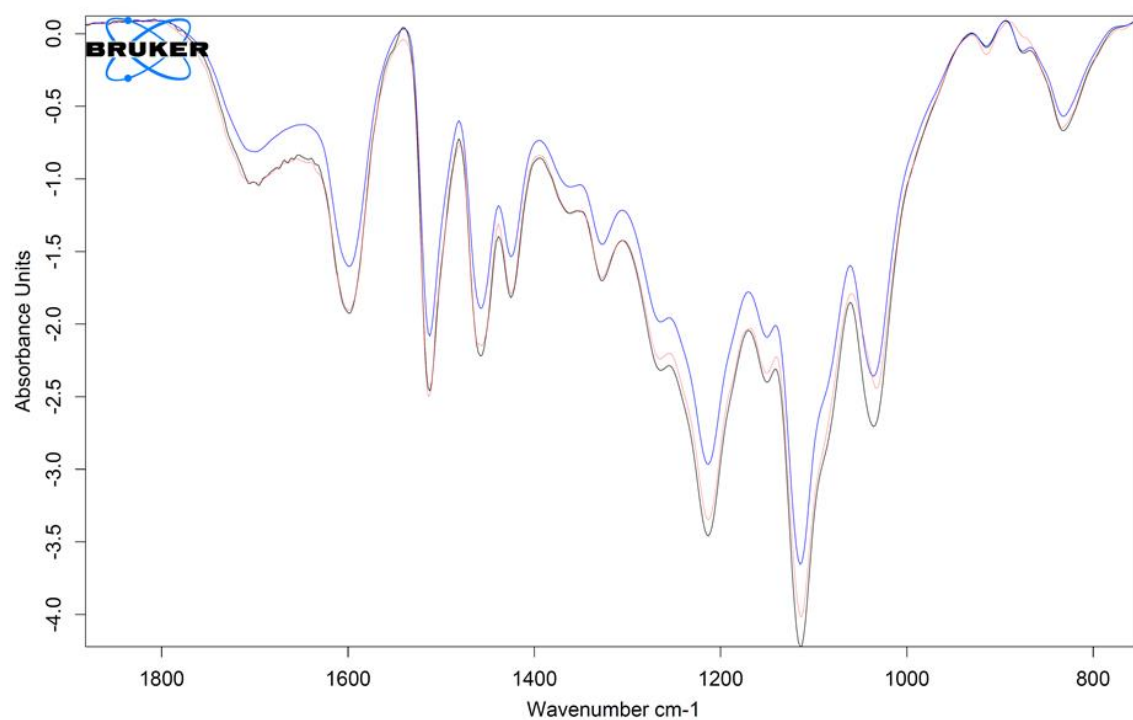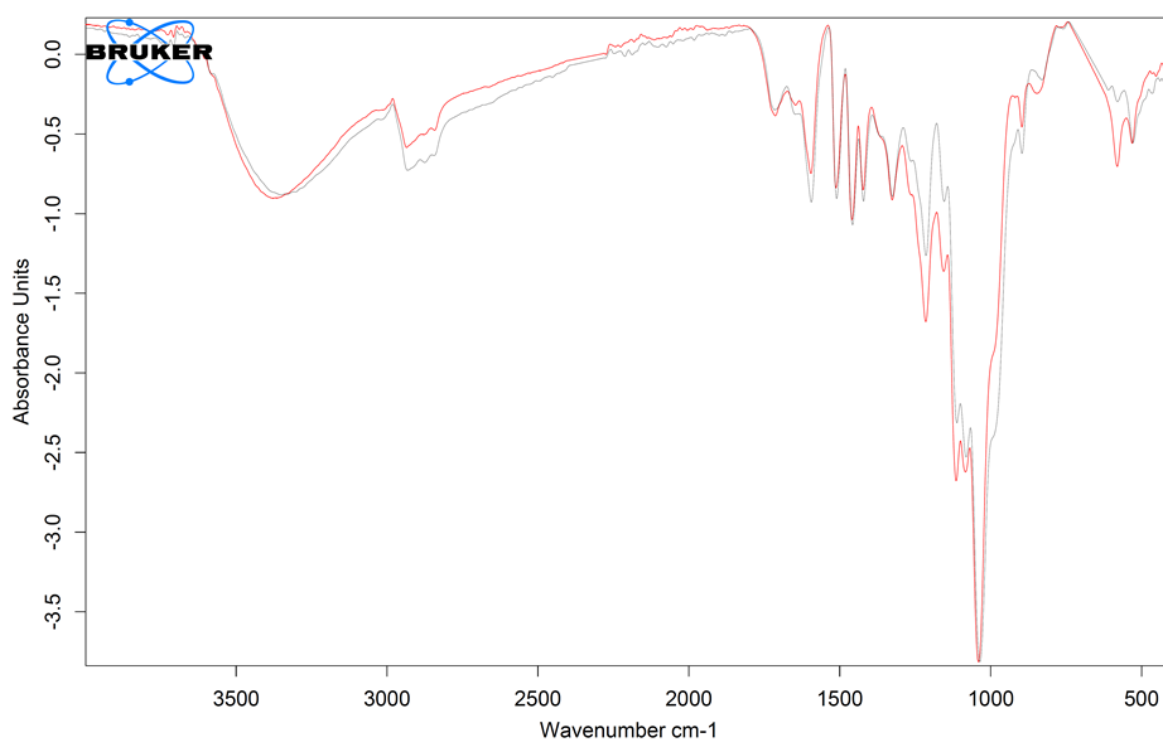**Figure 55** Comparative spectrum of HL-BM 36 (red), HL-BM72 (black) and BL-BM108 (blue)

Figure 56 Comparative spectrum of HL (black) and HL-S45 (red)

APPENDIX III : Hansen parameters

Table 22 Table of Hansen parameters for common solvents and polymers. The Ra was computed from the Hansen parameters of lignin. In green, solvents with Ra < 11,5 [60].

Solvents	dD	dP	dH	Ra
Acetone	15,5	10,4	7	16,6
Acetonitrile	15,3	18	6,1	17,5
n-Amyl Acetate	15,8	3,3	6,1	19,5
n-Amyl Alcohol	15,9	5,9	13,9	14,8
Benzene	18,4	0	2	21,7
Benzyl Alcohol	18,4	6,3	13,7	11,0
Benzyl Benzoate	20	5,1	5,2	15,2
1-Butanol	16	5,7	15,8	14,5
2-Butanol	15,8	5,7	14,5	15,0
n-Butyl Acetate	15,8	3,7	6,3	19,2
t-Butyl Acetate	15	3,7	6	20,4
t-Butyl Alcohol	15,2	5,1	14,7	16,3
Butyl Benzoate	18,3	5,6	5,5	15,9
Butyl Diglycol Acetate	16	4,1	8,2	17,7
Butyl Glycol Acetate	15,3	7,5	6,8	17,9
n-Butyl Propionate	15,7	5,5	5,9	18,7
Caprolactone (Epsilon)	19,7	15	7,4	10,5
Chloroform	17,8	3,1	5,7	17,7
m-Cresol	18,5	6,5	13,7	10,7
Cyclohexane	16,8	0	0,2	24,1
Cyclohexanol	17,4	4,1	13,5	13,9
Cyclohexanone	17,8	8,4	5,1	15,5
Di-isoButyl Ketone	16	3,7	4,1	20,3
Diacetone Alcohol	15,8	8,2	10,8	14,9
Diethyl Ether	14,5	2,9	4,6	22,3
Diethylene Glycol Monobutyl Ether	16	7	10,6	15,1
Dimethyl Cyclohexane	16,1	0	1,1	24,1
Dimethyl Sulfoxide (DMSO)	18,4	16,4	10,2	10,0
1,4-Dioxane	17,5	1,8	9	17,1
1,3-Dioxolane	18,1	6,6	9,3	13,1
Dipropylene Glycol	16,5	10,6	17,7	11,4
Dipropylene Glycol Methyl Ether	15,5	5,7	11,2	16,3
Dipropylene Glycol Mono n-Butyl Ether	15,7	6,5	10	16,1
Ethanol	15,8	8,8	19,4	13,5
Ethyl Acetate	15,8	5,3	7,2	17,9
Ethyl Benzene	17,8	0,6	1,4	22,1
Ethyl Lactate	16	7,6	12,5	14,2

Ethylene Carbonate	18	21,7	5,1	16,1
Ethylene Glycol	17	11	26	13,7
Ethylene Glycol Monobutyl Ether	16	5,1	12,3	15,5
Ethylene Glycol Monomethyl Ether	16	8,2	15	13,3
gamma-Butyrolactone (GBL)	18	16,6	7,4	12,5
Glycerol Carbonate	17,9	25,5	17,4	13,9
Heptane	15,3	0	0	25,7
Hexane	14,9	0	0	26,1
Iso-Butanol	15,1	5,7	15,9	16,0
Iso-Butyl Isobutyrate	15,1	2,8	5,8	20,9
Iso-Pentyl Acetate	15,3	3,1	7	19,8
iso-Pentyl Alcohol	15,8	5,2	13,3	15,5
Iso-Propyl Acetate	14,9	4,5	8,2	19,1
Iso-Propyl Ether	15,1	3,2	3,2	22,2
Isophorone	17	8	5	16,6
d-Limonene	17,2	1,8	4,3	20,0
Methanol	14,7	12,3	22,3	15,5
Methyl Acetate	15,5	7,2	7,6	17,3
Methyl Carbitol	16,2	7,8	12,6	13,7
Methyl Cellosolve	16	8,2	15	13,3
Methyl Cyclohexane	16	0	1	24,3
Methyl Ethyl Ketone (MEK)	16	9	5,1	17,4
Methyl iso-Amyl Ketone	16	5,7	4,1	19,3
Methyl iso-Butyl Carbinol	15,4	3,3	12,3	17,5
Methyl Iso-Butyl Ketone (MIBK)	15,3	6,1	4,1	20,1
Methyl Oleate	16,2	3,8	4,5	19,7
Methyl Propyl Ketone	16	7,6	4,7	18,2
N-Methyl-2-Pyrrolidone (NMP)	18	12,3	7,2	12,6
Methylene Chloride	17	7,3	7,1	15,4
N,N-Dimethyl Acetamide	16,8	11,5	10,2	12,5
N,N-Dimethyl Formamide (DMF)	**17,4**	**13,7**	**11,3**	**10,6**
1-Nitropropane	16,6	12,3	5,5	15,7
2-Phenoxy Ethanol	17,8	5,7	14,3	12,0
2-Propanol	15,8	6,1	16,4	14,6
1-Propanol	16	6,8	17,4	13,9
n-Propyl Acetate	15,3	4,3	7,6	18,9
n-Propyl Propanoate	15,5	5,6	5,7	19,0
Propylene Carbonate	20	18	4,1	13,9
Propylene Glycol Phenyl Ether	17,4	5,3	11,5	13,7
sec-Butyl Acetate	15	3,7	7,6	19,6
Sulfolane (Tetramethylene Sulfone)	**18**	**18**	**9,9**	**11,2**
Tetrahydrofuran (THF)	16,8	5,7	8	15,9
Tetrahydrofurfuryl Alcohol	**17,8**	**8,2**	**12,9**	**10,9**
Toluene	18	1,4	2	21,1
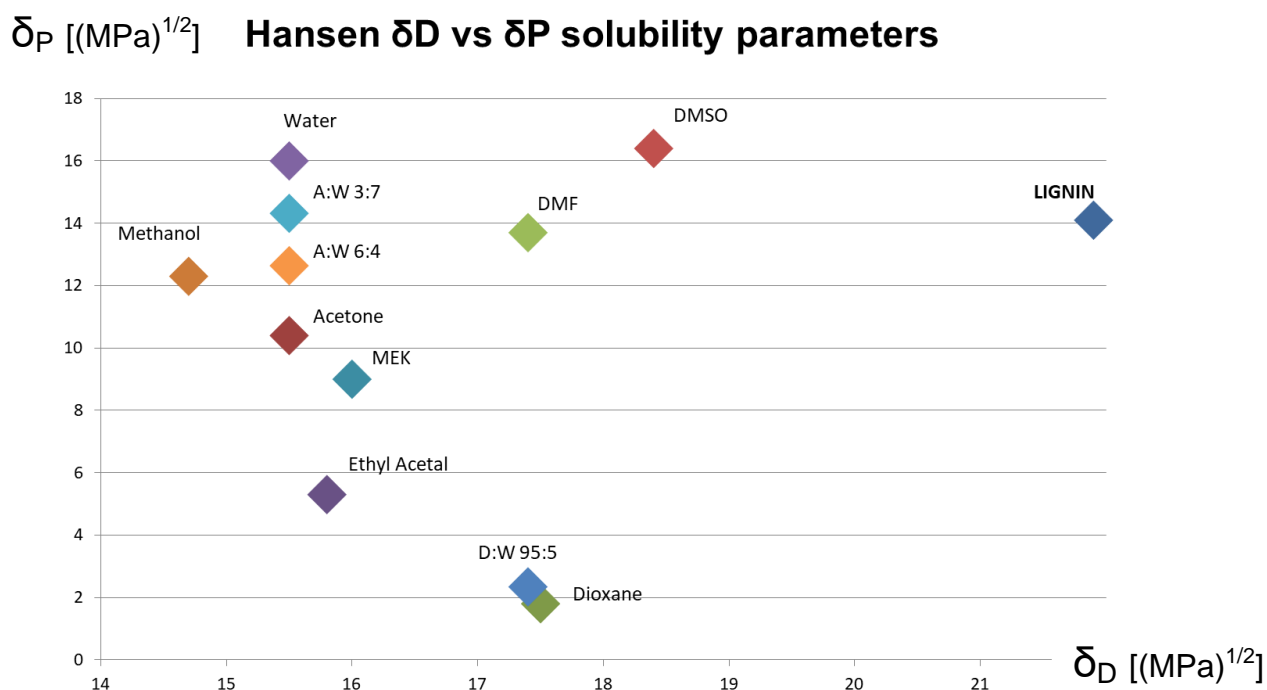
Figure 57 2D slice of Hansen space. All dots represent one solvent that was used in this master thesis. On the right, in blue, lignin.
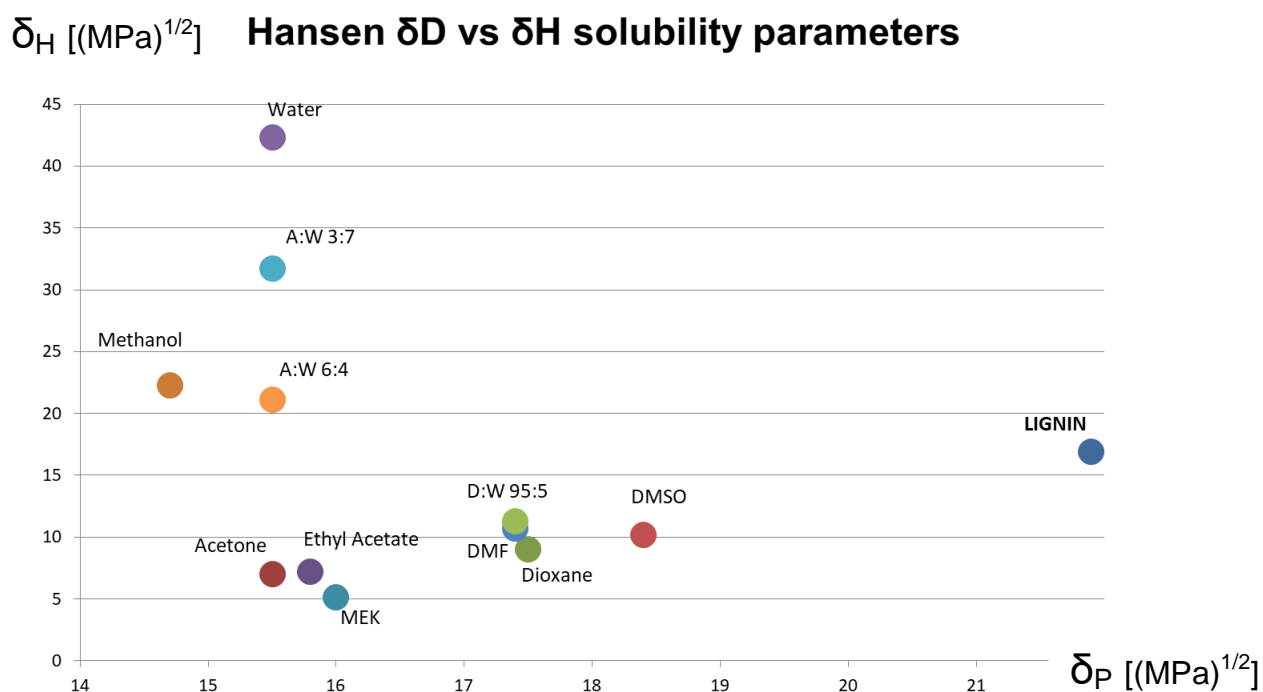

Figure 58 2D slice of Hansen space. All dots represent one solvent that was used in this master thesis. On the right, in blue, lignin.

Appendix IV : HPSEC polystyrene calibration curve

Table 23 Polystyrene retention times and mass average molecular weights. The relationship between log (M_w) and t_r is linear and can be used to transform one into the other

Calibration curve		
Polystyrene molecular weight M_W (Da)	log (M_W)	Retention time (min)
1000	3.00	29.016
2000	3.30	27.693
3000	3.48	26.646
4000	3.60	26.152
10000	4.00	24.106
20000	4.30	22.704
30000	4.48	21.781

y = -4.9196x + 43.827
R² = 0.9994
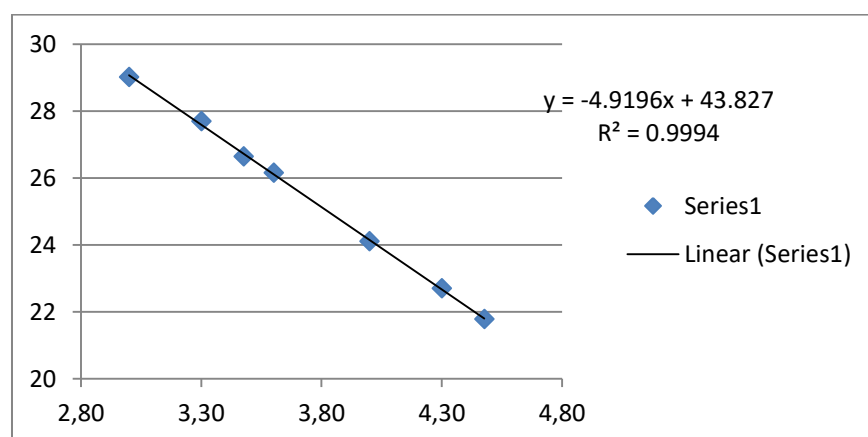
Figure 59 Calibration curve of polystyrene for HPSEC, coming from the data in **table 22**

j